

728217

DATE ISSUED JUN 22 1982

ORNL/TM-6539

**ornl**

**OAK  
RIDGE  
NATIONAL  
LABORATORY**



**ORNL  
MASTER COPY**

**An Experimental Investigation  
of the Distribution of Krypton  
During the Removal and Fixation  
of CO<sub>2</sub> from Simulated HTGR Fuel  
Reprocessing Off-Gas by the  
CO<sub>2</sub>-Ca(OH)<sub>2</sub> Slurry Reaction**

D. W. Holladay <sup>DN</sup>

**OPERATED BY  
UNION CARBIDE CORPORATION  
FOR THE UNITED STATES  
DEPARTMENT OF ENERGY**

Printed in the United States of America. Available from  
National Technical Information Service  
U.S. Department of Commerce  
5285 Port Royal Road, Springfield, Virginia 22161  
NTIS price codes—Printed Copy: A06 Microfiche A01

This report was prepared as an account of work sponsored by an agency of the United States Government. Neither the United States Government nor any agency thereof, nor any of their employees, makes any warranty, express or implied, or assumes any legal liability or responsibility for the accuracy, completeness, or usefulness of any information, apparatus, product, or process disclosed, or represents that its use would not infringe privately owned rights. Reference herein to any specific commercial product, process, or service by trade name, trademark, manufacturer, or otherwise, does not necessarily constitute or imply its endorsement, recommendation, or favoring by the United States Government or any agency thereof. The views and opinions of authors expressed herein do not necessarily state or reflect those of the United States Government or any agency thereof.

Contract No. W-7405-eng-26  
CHEMICAL TECHNOLOGY DIVISION

AN EXPERIMENTAL INVESTIGATION OF THE DISTRIBUTION OF KRYPTON  
DURING THE REMOVAL AND FIXATION OF CO<sub>2</sub> FROM SIMULATED  
HTGR FUEL REPROCESSING OFF-GAS BY THE CO<sub>2</sub>-Ca(OH)<sub>2</sub>  
SLURRY REACTION

D. W. Holladay

Date Published: June 1982

**NOTICE** This document contains information of a preliminary nature.  
It is subject to revision or correction and therefore does not represent a  
final report.

OAK RIDGE NATIONAL LABORATORY  
Oak Ridge, Tennessee 37830  
operated by  
UNION CARBIDE CORPORATION  
for the  
DEPARTMENT OF ENERGY

•

•

•

•

•

•

## CONTENTS

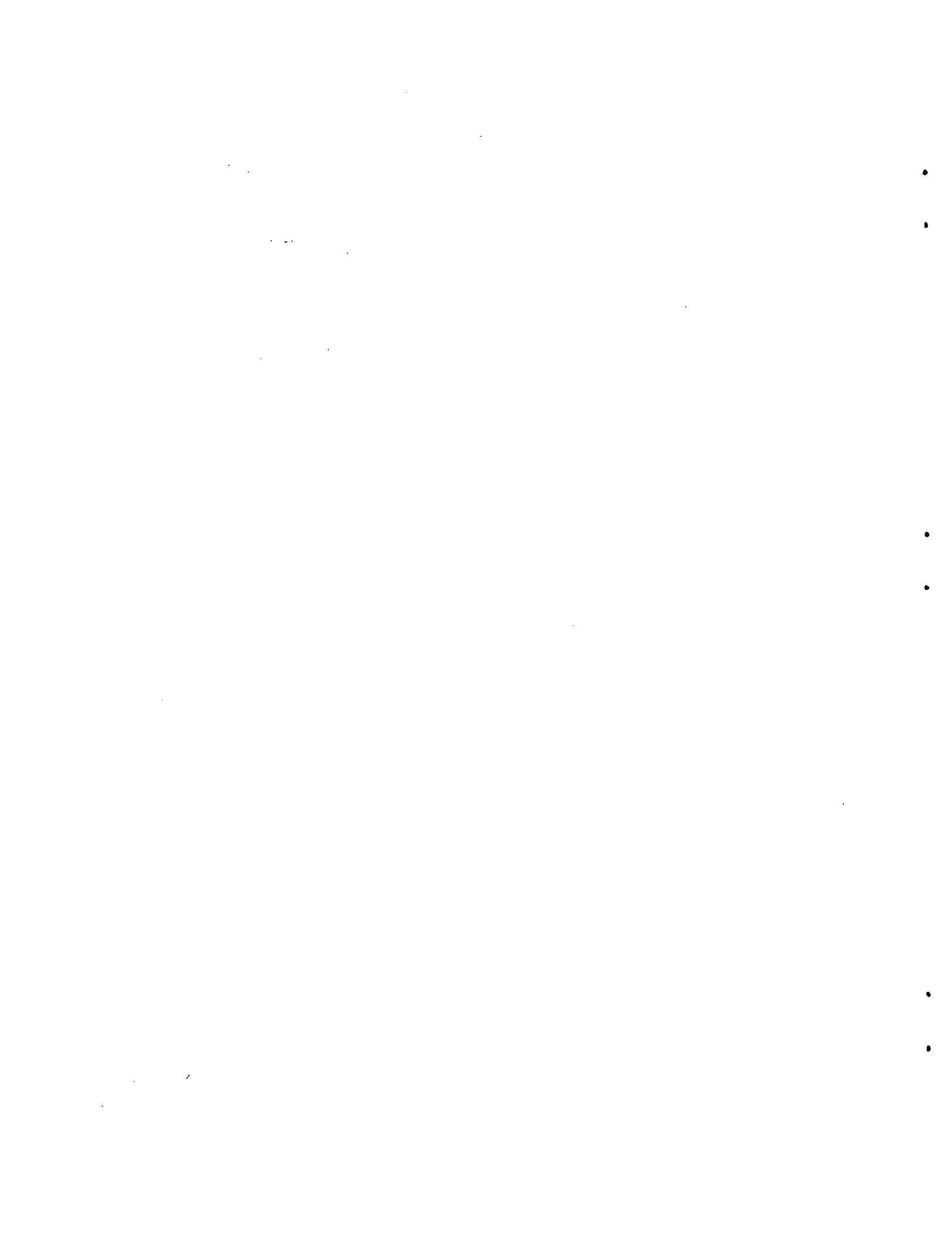
	<u>PAGE</u>
NOMENCLATURE . . . . .	vii
ABSTRACT . . . . .	1
1. INTRODUCTION . . . . .	1
2. EXPERIMENTAL EQUIPMENT AND ANALYTICAL TECHNIQUES . . . . .	7
2.1 Experimental Apparatus . . . . .	7
2.2 Background on the Radiation Problems Associated with Inclusion of $^{85}\text{Kr}$ in $\text{CaCO}_3$ Solids Containing $^{14}\text{C}$ . . . . .	12
2.3 Advantages and Disadvantages of Beta and Gamma Counting . . . . .	13
2.4 Feed Gas Analysis . . . . .	16
2.4.1 Determination of $^{85}\text{Kr}$ content in the feed gases . . . . .	16
2.4.2 Determination of $\text{CO}_2$ and total krypton in the feed gases . . . . .	16
3. THEORY OF CARBONATION OF LIME SLURRIES . . . . .	16
4. DISCUSSION OF RESULTS . . . . .	18
4.1 Determination of the Distribution of Krypton from the Feed Gas to the Product $\text{CaCO}_3$ Slurry . . . . .	18
4.2 Dependency of DFs for $\text{CO}_2$ and Krypton on Operating Parameters . . . . .	21
4.2.1 Types of contactor operation . . . . .	23
4.2.2 Dependency of DFs for $\text{CO}_2$ and krypton on gas superficial velocity . . . . .	23
4.2.3 Krypton distribution in dynamic contactor operation . . . . .	27
4.2.4 Dependency of DFs for krypton and $\text{CO}_2$ on slurry molality . . . . .	31
4.2.5 Dependency of DFs for krypton and $\text{CO}_2$ on the $\text{CO}_2$ concentration in the feed . . . . .	31
4.2.6 Dependency of DFs for krypton and $\text{CO}_2$ on temperature . . . . .	32
4.2.7 Dependency of DFs for krypton and $\text{CO}_2$ on impeller speed . . . . .	34
4.2.8 Dependency of DFs for krypton and $\text{CO}_2$ on multiple contactor operation . . . . .	35

CONTENTS (continued)

	<u>PAGE</u>
4.2.9 Dependency of DFs for krypton and CO <sub>2</sub> on $d_i$ , $\text{OH}_s^-$ , H, $D_{cd}$ , $k_2$ , $\sigma$ , and $\mu$ and correlations for those parameters . . . . .	38
5. DEVELOPMENT OF MODELS TO DESCRIBE THE DFs FOR SIMULTANEOUS CO <sub>2</sub> AND KRYPTON DISTRIBUTION TO A Ca(OH) <sub>2</sub> SLURRY . . . . .	39
5.1 Rate Expression for Carbonation of Lime Slurries and Models for Process Scale-Up . . . . .	40
5.1.1 Possible rate expressions . . . . .	40
5.1.2 Forms of models used for calculating scale-up contactor dimensions . . . . .	43
5.1.3 Expressions for predicting DFs for krypton . . . . .	44
6. SUMMARY AND CONCLUSIONS . . . . .	45
APPENDIX A: METHODS OF ANALYZING THE DISTRIBUTION OF KRYPTON BETWEEN THE FEED GAS AND THE SOLID AND LIQUID PHASES OF THE CaCO <sub>3</sub> SLURRY . . . . .	49
A.1 General Comments on Beta and Gamma Counting . . . . .	49
A.2 Procedure for Obtaining Beta and Gamma Counts . . . . .	50
A.3 Distribution of Krypton in the Solid and Liquid Phases of the Slurry . . . . .	57
A.4 Definitions of DFs for Krypton . . . . .	61
APPENDIX B: DEVELOPMENT OF THEORETICAL EQUATIONS TO CALCULATE DFs FOR KRYPTON ( $DF_k$ ) AND FOR CO <sub>2</sub> ( $DF_{cd}$ ) AND TO SHOW THE DEPENDENCY OF $DF_k$ ON $DF_{cd}$ . . . . .	63
B.1 An Expression for $DF_{cd}$ . . . . .	63
B.2 Relationship between $DF_k$ and $DF_{cd}$ . . . . .	65
APPENDIX C: DEVELOPMENT OF MASS TRANSFER MODELS FOR DESCRIBING FIXATION OF CO <sub>2</sub> IN Ca(OH) <sub>2</sub> SLURRIES . . . . .	69
C.1 Considerations of Rate Expressions . . . . .	69
C.2 Mass Transfer Rate as a Function of Superficial Velocity. . . . .	71
C.3 Prediction of the Effect of Temperature on the DF for CO <sub>2</sub> . . . . .	72
C.4 Gas-Side Mass Transfer Resistance . . . . .	74
C.5 Conditions for Utilization of Rate Expressions . . . . .	75

CONTENTS (continued)

	<u>PAGE</u>
APPENDIX D: UTILIZATION OF MODELS FOR PREDICTION OF SCALE-UP . .	79
D.1 Rearrangement of Eq. (C-10) . . . . .	79
D.2 Method 1 for Estimating Interfacial Areas and Large- Scale Tank Diameters . . . . .	80
D.3 Method 2 for Estimating Interfacial Areas and Scaled-Up Tank Dimensions . . . . .	84
D.4 A General Modeling Approach . . . . .	87
D.5 Prediction of DFs for Krypton Utilizing Empirical DFs for CO <sub>2</sub> . . . . .	91
7. REFERENCES . . . . .	94

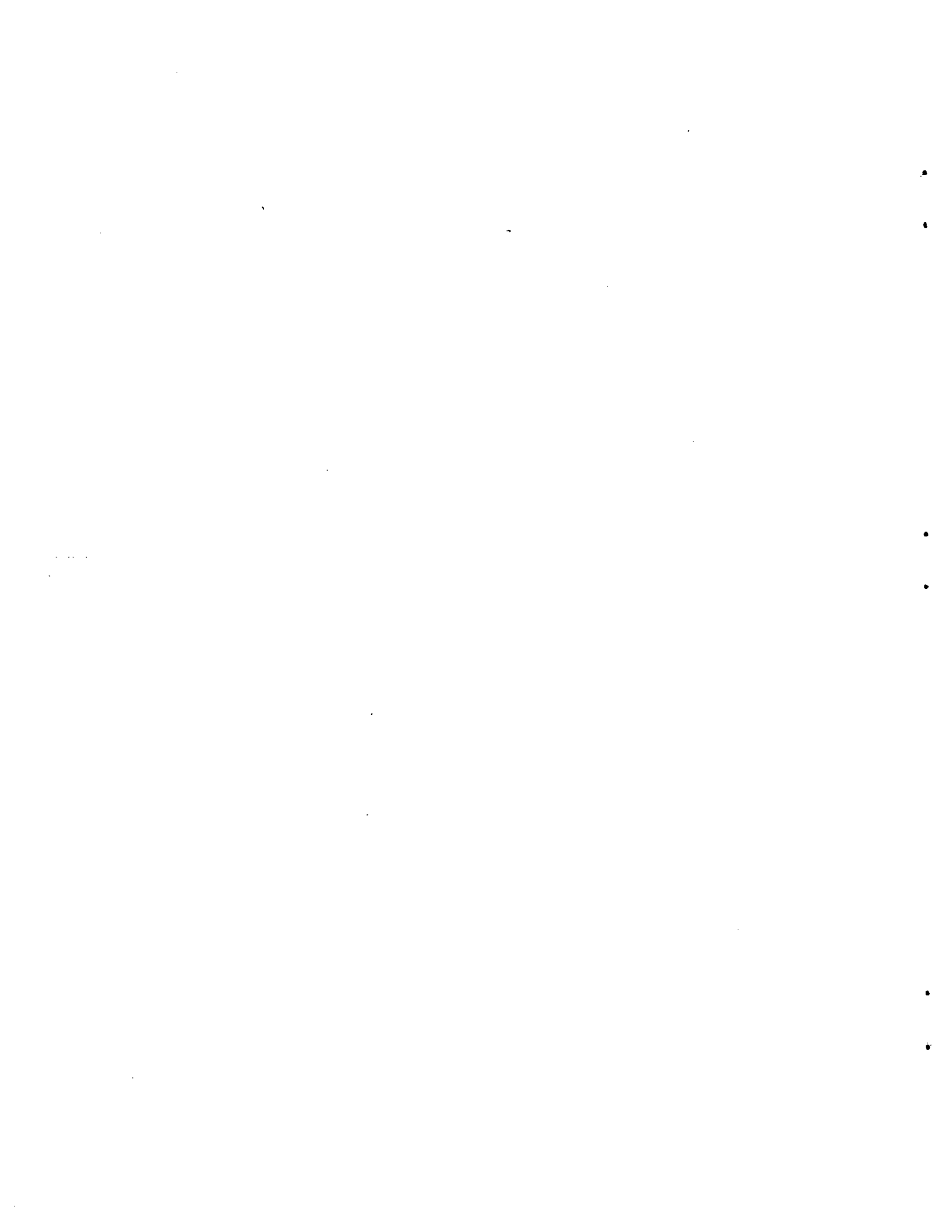


## NOMENCLATURE

A	Cross-sectional area of the contactor.
A*	Concentration of dissolved CO <sub>2</sub> at the liquid-gas interface which is in equilibrium with the gas, g-mole/liter.
a	Effective interfacial area for mass transfer, cm <sup>2</sup> /cm <sup>3</sup> .
[B]	Molar concentration of anion reacting with gas, g-mole/liter.
C	Moles of H <sub>2</sub> O out of reactor per mole of CO <sub>2</sub> reacted.
C <sub>1</sub> , C <sub>2</sub>	Factors in Eqs. (23) and (24).
D <sub>cd</sub>	Diffusivity of the CO <sub>2</sub> in aqueous solution, cm <sup>2</sup> /sec.
d <sub>i</sub>	Impeller diameter, m.
DF <sub>cd</sub>	Decontamination factor for CO <sub>2</sub> . (moles CO <sub>2</sub> /time) <sub>in</sub> /(moles CO <sub>2</sub> /time) <sub>out</sub> .
DF <sub>k</sub>	Decontamination factor for krypton, moles krypton in the gasified stream/moles krypton in slurry effluent, single contactor.
DF <sub>k,2</sub>	Decontamination factor for krypton, contactors in series.
DF <sub>ks</sub>	Decontamination factor for krypton, moles krypton in feed gas/moles krypton in solids of the slurry, single contactor.
DF <sub>kt</sub>	Total decontamination factor of krypton, primary contactor operation and appropriate add-on processes. (DF <sub>kt,1</sub> -single contactor, DF <sub>kt,2</sub> -contactor in series).
D <sub>OH</sub>	Diffusivity of hydroxyl ion in aqueous solution, cm <sup>2</sup> /sec.
d <sub>t</sub>	Contactor diameter, m.
e <sub>1</sub> , e <sub>2</sub> , e <sub>3</sub> , e <sub>4</sub> , e <sub>5</sub> , e <sub>6</sub> , e <sub>7</sub> , e <sub>8</sub> , e <sub>9</sub> , e <sub>10</sub>	Exponents in Eq. (D-19).
f	Power number for Rushton agitator power characteristics.

$F_{cd}$	Molar flow rate of $CO_2$ , g-moles/sec.
$F_n$	Molar flow rate of inert gases, g-mole/sec.
$F_r$	Fraction of feed gas converted.
$F_t$	Total molar gas flow rate, g-moles/sec.
$H$	Solubility of $CO_2$ in the slurry, g-mole/( $cm^3$ -atm).
$h$	Height in the contactor.
$K$	Distribution coefficient for krypton in $H_2O$ .
$k_2$	Second-order reaction rate constant, liter/(g-mole-sec).
$k_G$	Gas-side mass transfer coefficient, g-mole/( $cm^2$ dispersion-sec-atm).
$k_L$	True liquid-side mass transfer coefficient, cm/sec.
$L_o$	Total molar liquid flow rate, g-moles/sec.
$N_{cd}$	Overall mass transfer rates, g-mole/time.
$n$	Impeller speed, rpm.
$n_1$	Impeller speed for small-scale contactor, rpm.
$n_2$	Impeller speed for scaled-up contactor 2, rpm.
$[OH_s^-]$	Saturation concentration of $OH^-$ ions in aqueous solutions in equilibrium with solid $Ca(OH)_2$ , g-ion/ $cm^3$ .
$P_{cd}$	Partial pressure of $CO_2$ , atm.
$P_{df}$	Pressure driving force for mass transfer, atm.
$P_i$	Pressure at the interface, atm.
$P_k$	Partial pressure of krypton in feed gas, atm.
$P_n$	Partial pressure of inerts in the feed gas, atm.
$P_t$	Total gas pressure, atm.
$P_e$	Effective power input, hp or $kg\text{-m}^2/\text{sec}^3$ .
$P_m$	Aerated power input by mechanical agitation, hp or $kg\text{-m}^2/\text{sec}^3$ .

$Q_t$	Total volumetric gas flow rate, std liters/min.
$R$	Mass transfer rate per unit interfacial area, g-mole/(cm <sup>2</sup> -sec).
$R_1$	Mole fraction of the gas feed which reacts in contactor 1.
$S$	Contactor cross-sectional area, cm <sup>2</sup> .
STP	Standard temperature and pressure, which for all our data were 70°F and 1 atm.
$t$	Time.
$T$	Temperature.
$U_s$	Gas superficial velocity, cm/sec.
$U_t$	Terminal bubble rise velocity, cm/sec.
$V$	Volume of liquid in slurry, cm <sup>3</sup> .
$V_d$	Volume of dispersion (gas + slurry), cm <sup>3</sup> .
$V_L$	Clear liquid volume, m <sup>3</sup> .
$V_o$	Volume of krypton absorbed at STP in H <sub>2</sub> O.
$x_k$	Mole fraction of krypton in the liquid phase.
$y_{cd}$	CO <sub>2</sub> mole fraction in gas phase.
$y_k$	Mole fraction of krypton in gas.
$y_n$	Inert gas mole fraction in gas phase.
$z$	Moles of anion reacting per mole of CO <sub>2</sub> .
$\rho_s$	Density of slurry, kg/m <sup>3</sup> .
$\sigma$	Surface tension, kg/sec <sup>2</sup> .
$\mu$	Viscosity of slurry, kg/(m-sec).
$i$	Influent stream.
$o$	Effluent stream.
$\phi$	Enhancement factor, ratio of the liquid-side mass transfer coefficient with reaction to that in the absence of chemical reaction.



AN EXPERIMENTAL INVESTIGATION OF THE DISTRIBUTION OF KRYPTON  
DURING THE REMOVAL AND FIXATION OF CO<sub>2</sub> FROM SIMULATED  
HTGR FUEL REPROCESSING OFF-GAS BY THE CO<sub>2</sub>-Ca(OH)<sub>2</sub>  
SLURRY REACTION

D. W. Holladay

ABSTRACT

An experimental investigation was conducted to determine the behavior of krypton during the removal and fixation of CO<sub>2</sub> from simulated HTGR fuel reprocessing off-gas in a mechanically agitated gas-Ca(OH)<sub>2</sub> slurry contactor. For CO<sub>2</sub> removal, decontamination factors (DFs) in the range of 10<sup>2</sup> to 10<sup>3</sup> were obtained with a single contactor; DFs for CO<sub>2</sub> of 10<sup>3</sup> to 10<sup>4</sup> were obtained during operation of two contactors in series. For the primary CO<sub>2</sub> removal step in a single contactor, 0.5 to 1% of the krypton in the feed gas was retained in the slurry. Additional treatment resulted in further reduction of the slurry krypton content by a factor of 10<sup>2</sup>. (Overall, evacuation of the product slurry during agitation was the most desirable add-on process.) Thus, the quantity of krypton in the feed that was retained in the product CaCO<sub>3</sub> slurry could be restricted to 0.01 to 0.001% by using a combination of primary processes and add-on treatments. Models are presented that predict the distributions of both CO<sub>2</sub> and krypton during gas treatment in Ca(OH)<sub>2</sub> slurries for both single-contactor and contactors-in-series operation.

---

1. INTRODUCTION

In the reprocessing of High-Temperature Gas-Cooled Reactor (HTGR) fuel, a large quantity of CO<sub>2</sub> is produced during the burning of the graphite fuel elements. The normal <sup>12</sup>CO<sub>2</sub> formed from this burning process constitutes the bulk of the reprocessing off-gas. However, the total off-gas stream, including dissolver off-gas (DOG) and vessel off-gas (VOG), would contain isotopes of iodine (~20 ppm total iodine as both <sup>127</sup>I and <sup>129</sup>I), krypton (~1.0 ppm <sup>85</sup>Kr and 15 ppm <sup>84</sup>Kr), and <sup>14</sup>CO<sub>2</sub> (100 to 500 ppb <sup>14</sup>CO, depending on fuel composition). In terms of radioactivity,

the total available quantities of these radionuclides in a model plant processing 450 metric tons of heavy metal (MTHM) of fuel annually would be  $\sim 7000$  Ci  $^{14}\text{C}$ ,  $2.7 \times 10^7$  Ci  $^{85}\text{Kr}$ , and 54 Ci  $^{129}\text{I}$ .<sup>1,2</sup> The U.S. Environmental Protection Agency (EPA) has already established that processes must be added to the fuel reprocessing plant to remove the iodine and krypton radionuclides. Estimates of the  $^{14}\text{CO}_2$  released during HTGR fuel reprocessing have been made by Bonka et al.<sup>3</sup> Croff,<sup>4</sup> and Davis.<sup>5</sup> The scope of the  $^{14}\text{CO}_2$  problem as it relates to human dosage in the vicinity of a fuel reprocessing plant has been discussed by Magno et al.<sup>6</sup> Machta,<sup>7</sup> Killough, et al.<sup>8,9</sup> and Snider and Kaye.<sup>10</sup> Because of the possible biohazards associated with  $^{14}\text{C}$  release, it now appears that the EPA will probably also require the removal of  $^{14}\text{CO}_2$  from the off-gas. In anticipation of this requirement, an experimental program was established in the Chemical Technology Division to not only develop a process to efficiently remove  $\text{CO}_2$  from HTGR fuel reprocessing off-gas, but also to determine the optimum location for that process in the off-gas treatment scheme.

For the off-gas processing treatment scheme as presently designed,<sup>2</sup> iodine removal (by processes such as sorption on zeolite-type solid bed or reaction with hyperazeotropic  $\text{HNO}_3$ , as in Iodox) would be followed by the KALC process to remove krypton from the liquefied  $\text{CO}_2$  in a high-pressure, low-temperature operation. The  $^{14}\text{C}$ -contaminated  $\text{CO}_2$  would then be removed by some process that would produce a solid with characteristics which would allow it to remain stable during the long-term burial necessary to contain the radiation during the very long half-life (5730 years) of  $^{14}\text{C}$ . In an initial evaluation of options concerning the isolation and disposal of  $^{14}\text{C}$ -contaminated  $\text{CO}_2$ , Croff<sup>3</sup> proposed that all of the  $\text{CO}_2$  could be fixed as  $\text{CaCO}_3$  by direct reaction of the HTGR off-gas, following the KALC process, with a  $\text{Ca}(\text{OH})_2$  slurry. The feasibility of this process for achieving DFs for the removal of  $\text{CO}_2$  of  $10^2$  to  $10^4$  from the KALC-type off-gas has previously been shown.<sup>11</sup> Croff<sup>3</sup> calculated that even if a DF for  $^{85}\text{Kr}$  of 100 was achieved in KALC, the radioactivity level of the  $\text{CaCO}_3$  product formed during  $\text{CO}_2$  fixation would be controlled by the included krypton. This calculation was based on

the worst-case assumption that all of the krypton would be trapped in the  $\text{CaCO}_3$  solid. Croff also calculated that 99.8% (DF = 500) of the krypton would have to be removed from the slurry product before Department of Transportation (DOT) regulations would permit transportation in bulk. Therefore, reducing the quantity of the krypton in the solid product by factors of  $10^2$ ,  $10^3$ , or greater would certainly allow for a considerable reduction in the cost of transporting the product.

Forsberg<sup>12</sup> conducted experiments to develop a process to further concentrate the krypton-rich product stream produced by the KALC operation when applied to the HTGR fuel reprocessing off-gas. The resulting KALC product gas has an approximate composition of >90%  $\text{CO}_2$ , 1 to 1.5% krypton, and various amounts of  $\text{O}_2$ ,  $\text{N}_2$ , and xenon as the balance. The presence of the  $\text{CO}_2$  and  $\text{O}_2$  in the krypton product is undesirable because there is a potential explosion hazard which may result from unstable intermediate compounds produced from radiolysis of those gaseous components. Also, because krypton is generally a more difficult radionuclide to handle<sup>13</sup> (requiring more shielding) than  $^{14}\text{C}$ , it would be more efficient to separate the  $\text{CO}_2$  (containing  $^{14}\text{C}$ ) from the krypton and then to prepare each isotope individually for appropriate shipment and storage. Utilizing Linde 5A molecular sieves, Forsberg<sup>12</sup> obtained a krypton-oxygen product that contained  $<10^{-3}\%$  (10 ppm)  $\text{CO}_2$  and >50% krypton. Forsberg's<sup>12</sup> initial study is relevant to this experimental program because it delineates one method of further purifying krypton from an off-gas containing primarily krypton,  $\text{O}_2$ , and  $\text{N}_2$ . Such a stream could be obtained as the product when a  $\text{CO}_2$ -krypton- $\text{O}_2$ - $\text{N}_2$  stream is treated in a  $\text{Ca(OH)}_2$  slurry.

Forsberg<sup>13</sup> initiated the investigation into the feasibility of locating the  $\text{CO}_2$  removal process prior to krypton removal during the processing of HTGR fuel reprocessing off-gas. His study, which was primarily theoretical, was supported by simple bench-scale experiments. A feed gas containing 93%  $\text{CO}_2$ , 5.4%  $\text{O}_2$ , and 1.5% krypton (with  $^{85}\text{Kr}$  tracer) was sorbed in 250 ml of  $\text{Ca(OH)}_2$  slurry. If  $\text{CO}_2$  removal by  $\text{Ca(OH)}_2$  slurry could be achieved while minimizing the effect of the krypton on the activity level of the solid  $\text{CaCO}_3$  product, the following advantages would be realized:

1. The size of the krypton removal system could be reduced because the bulk  $\text{CO}_2$  would be removed (for example, the flow rate for a 90%  $\text{CO}_2$  feed with a nominal DF for  $\text{CO}_2$  of 100 would be reduced by a factor of 20.
2. Molecular sieve sorption or the Freon Absorption System for Treatment of Effluents from Reprocessors (FASTER) process (with final krypton purification by molecular sieves) could be utilized for krypton removal, instead of KALC.
3. If the FASTER process were utilized, the overall treatment flow train would be more immune to process interruption.

Although most of the study was devoted to theoretical development, there were two basic conclusions drawn from the preliminary experimental data: (1) most of the krypton found in the  $\text{CaCO}_3$  slurry was dissolved in the water, rather than in the solid; (2) it was possible to remove most of the krypton from the  $\text{CaCO}_3$  slurry by purging with an inert gas or by applying a vacuum during slurry agitation. Based on these preliminary studies, Forsberg suggested that it might be feasible to remove  $^{14}\text{C}$ -contaminated  $\text{CO}_2$  from HTGR fuel reprocessing off-gas prior to krypton removal with operating conditions such that the bulk of the krypton could be recovered separately from the  $\text{Ca}^{14}\text{CO}_3$  product. However, it was further evident that additional studies should be conducted with larger engineering-scale equipment and improved analytical techniques to firmly establish the distribution of krypton to the product  $\text{CaCO}_3$  slurry.

The primary objective of this study was to accurately determine the distribution of the krypton during removal and fixation of  $\text{CO}_2$  from a simulated HTGR fuel reprocessing off-gas by reaction with a  $\text{Ca}(\text{OH})_2$  slurry. To accomplish the objective, it was necessary to show the feasibility of removing  $\text{CO}_2$  from HTGR fuel reprocessing off-gas prior to krypton removal. Operating conditions were developed to minimize any additional hazard that the krypton, which is included in the  $\text{CaCO}_3$  slurry, might pose to the handling of the  $^{14}\text{C}$ -contaminated  $\text{CaCO}_3$  product. In particular, careful measurements of the residual krypton in the solid portion of the slurry were made because that portion would require

considerable handling during processing, immobilization into concrete, and burial. The two most desirable distributions of krypton would be either (1) that all of the krypton remain in the  $\text{Ca}^{14}\text{CO}_3$  solid so that it could be permanently bound in concrete, or (2) that none of the krypton remain in the slurry so that it would pass through the  $\text{CO}_2$  removal process and thus could be concentrated relatively simply. The basic question was as follows: In the treatment of HTGR fuel reprocessing off-gas, if it is mandated that most of the  $\text{CO}_2$  be removed to prevent long-term environmental hazards of small quantities of included  $^{14}\text{CO}_2$ , can the  $\text{CO}_2$  removal step be placed before the krypton removal step so that the need for the expensive and difficult-to-operate KALC process can be eliminated?

Basically, two experimental facts had to be established in order to answer this question. First, it had to be shown that the presence of krypton and xenon in the feed gas to the  $\text{CO}_2$ - $\text{Ca}(\text{OH})_2$  slurry process did not interfere with the DFs for  $\text{CO}_2$ . Second, the amount of krypton included in the slurry had to be low enough so that any extra cost incurred for the disposal of the  $\text{Ca}^{14}\text{CO}_3$ -krypton-concrete waste would be less expensive than the cost of the KALC- $\text{CO}_2$  removal process.

The following clarification of the options available for  $\text{CO}_2$  and krypton removal in HTGR reprocessing can be made. The sequence for option 1, with krypton removal by KALC followed by  $\text{CO}_2$  removal, is as follows: (1) KALC equipment, (2) molecular sieves, (3)  $\text{CO}_2$  fixation process equipment, (4) bottling or encapsulation and transportation of virtually all the krypton, and (5) immobilization of  $\text{CaCO}_3$  (containing  $^{14}\text{C}$  and traces of  $^{85}\text{Kr}$ ) in concrete and transportation to the disposal site. The sequence for option 2, with  $\text{CO}_2$  removal before krypton removal, is: (1)  $\text{CO}_2$  fixation process equipment, (2) molecular sieves (70 to 100 times more capacity than option 1) or FASTER, (3) bottling or encapsulation and transportation of virtually all the krypton, (4) add-on vacuum equipment to remove the necessary amount of krypton from  $\text{CaCO}_3$ , and (5) immobilization of  $\text{CaCO}_3$  (containing  $^{14}\text{C}$  and traces of  $^{85}\text{Kr}$ ) in concrete and transportation of the product to the disposal site (see Fig. 1).

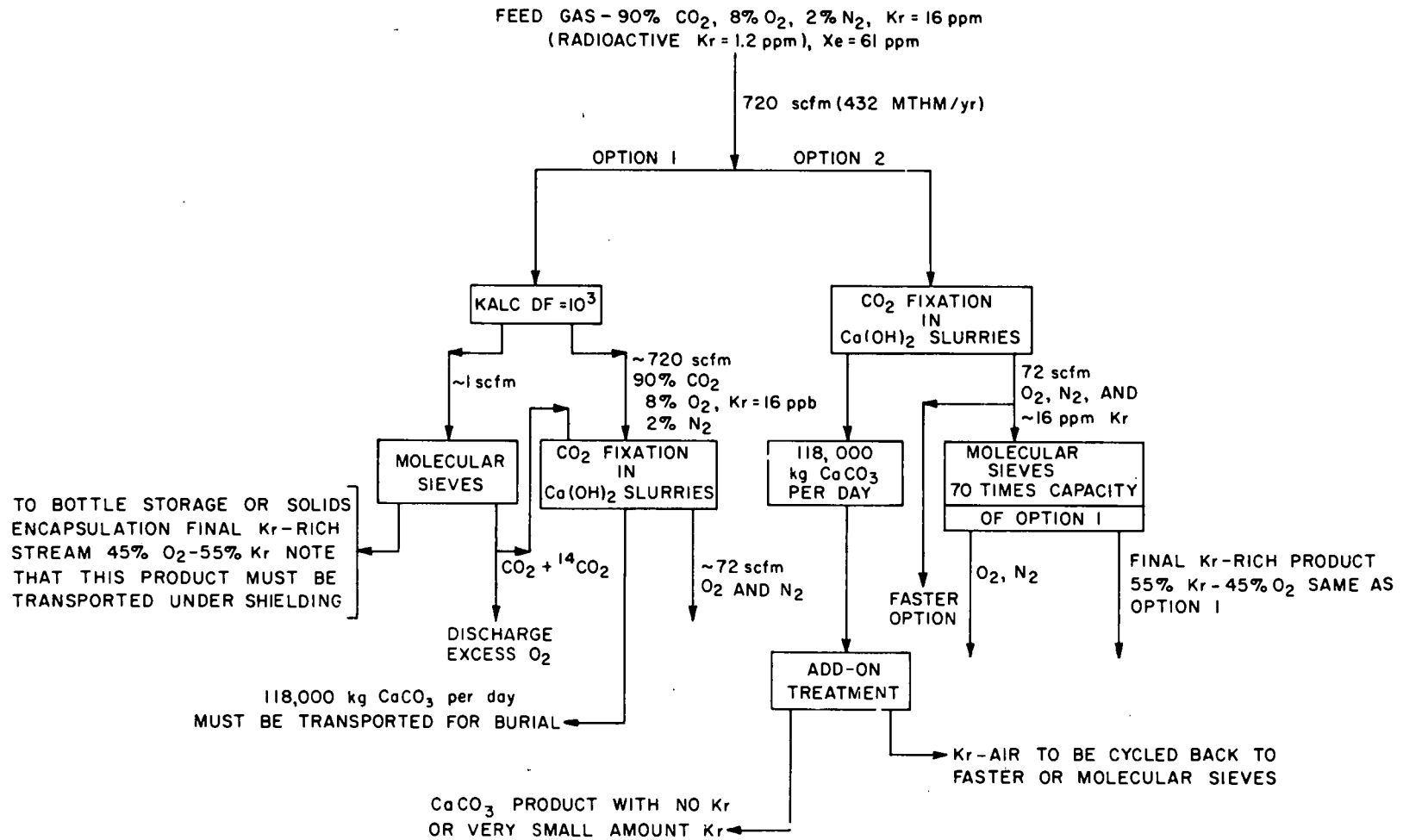


Fig. 1. Process options for treatment of HTGR fuel reprocessing off-gas.

Hence, the basic difference between the two options in that option 1 includes the KALC operation and a small-scale molecular sieve operation. Option 2 includes either larger-scale ( $\sim 100$  times that of option 1) molecular sieve equipment or FASTER to concentrate krypton in the effluent from the carbonation reactor. Option 2 also includes equipment to improve the removal of krypton included in the  $\text{CaCO}_3$  slurry. Thus, if the add-on treatment could be vacuum equipment and provide sufficient krypton removal so that the additional costs of transporting  $\text{CaCO}_3$  containing  $^{14}\text{C}$  and  $^{85}\text{Kr}$  would be feasible, then option 2 would appear to be at least as efficient as option 1 and economically more attractive than option 1.

A list of nomenclature has been included in the report for the reader's convenience (see p. vii).

## 2. EXPERIMENTAL EQUIPMENT AND ANALYTICAL TECHNIQUES

### 2.1 Experimental Apparatus

In these experiments, runs were conducted for both semibatch (no slurry flow) and continuous slurry flow in the agitated contactors. All of the continuous runs were conducted with the gas-slurry system in the standard countercurrent method of contact. Schematics for the experimental setups for operation of a single contactor in continuous slurry flow and for operation of two contactors in series with continuous slurry flow are shown in Figs. 2 and 3, respectively.

Three stirred-tank contactors were utilized in the studies for  $\text{CO}_2$  removal from simulated HTGR fuel reprocessing off-gas. The 20.3-cm-ID Rushton-type contactor has been previously described in detail,<sup>10</sup> whereas the 27.3-cm-ID contactors were designed to be geometrically similar, scaled-up versions, by about a factor of 2, of the smaller contactor. A schematic of a standard-design Rushton-type contactor is shown in Fig. 4.

Improvements to the original contactor included substitution of a dependable mechanical seal for the original unreliable shaft seal, which consisted of pressure rings and a packing gland. These mechanical

ORNL-DWG 78-4945R

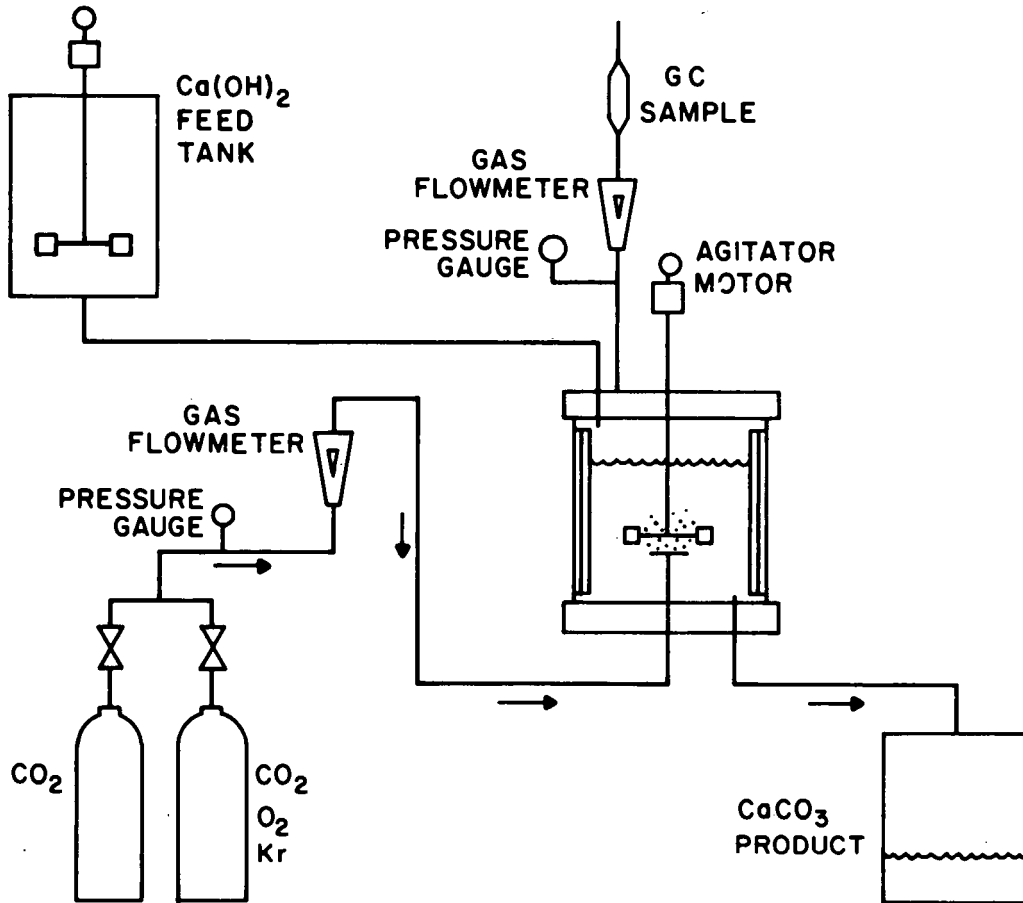


Fig. 2. Schematic of layout of a single agitated contactor for continuous flow of slurry and feed gas.

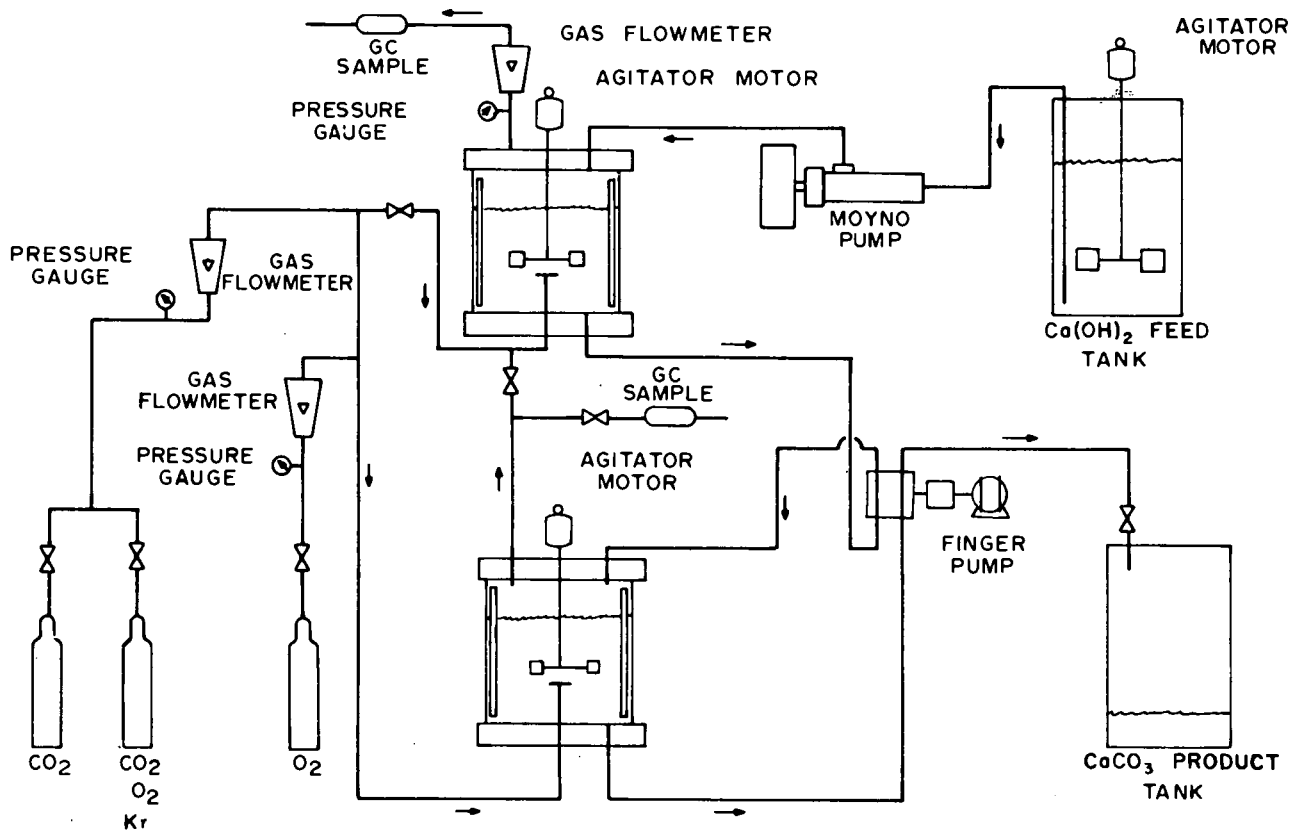


Fig. 3. Schematic of countercurrent layout for two agitated contactors.

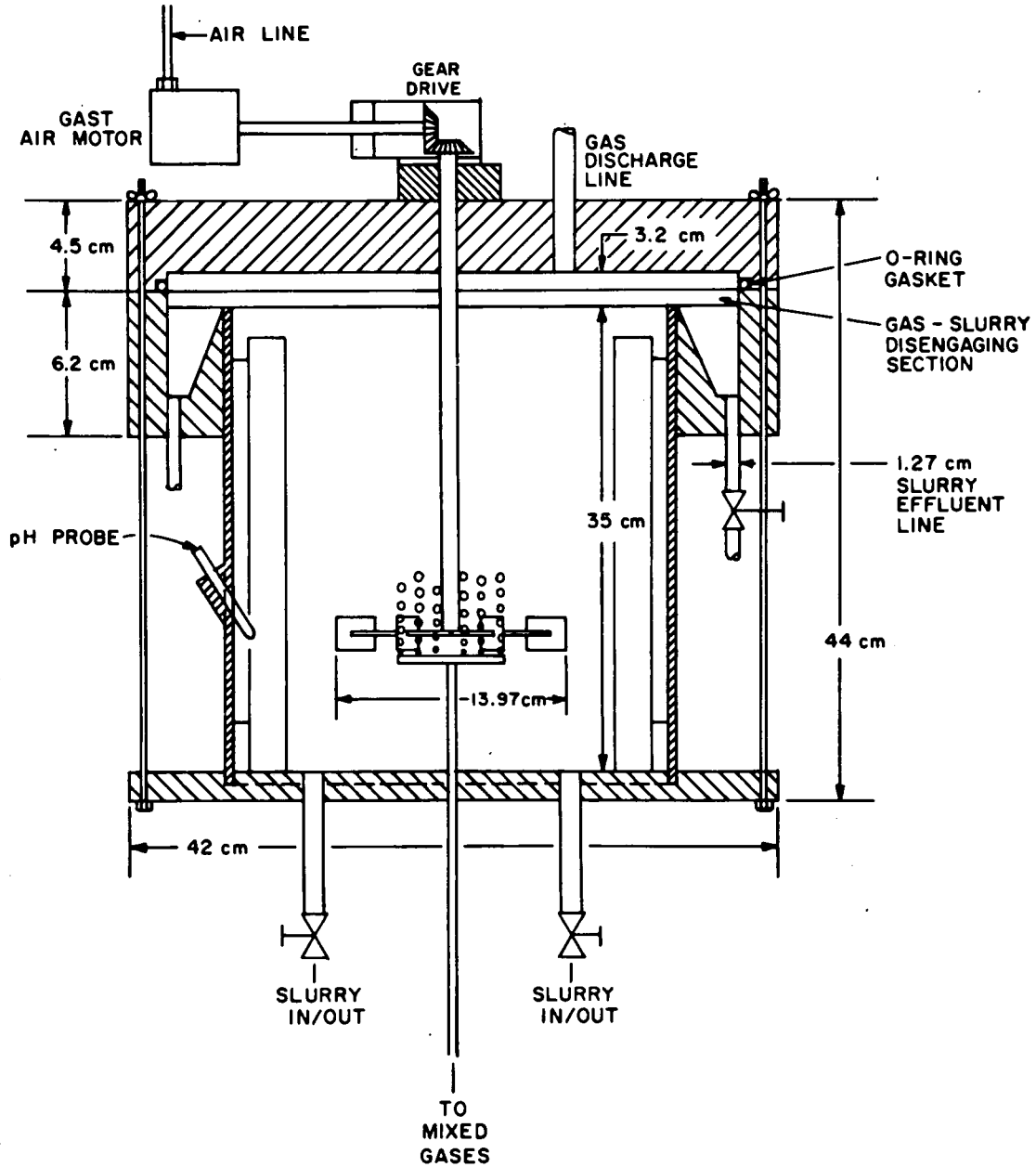


Fig. 4. Cutaway view of stirred-cell contactor.

seals were taken from the water pumps of Chevrolet automobiles. The seals were very reliable for long periods of operating time at impeller speeds of 500 to 1000 rpm. They did tend to run hot, however, when the operating time exceeded 30 min, resulting in a small elevation in temperature of the slurries.

Another improvement to the contactor design was replacement of the original plexiglass baffles, which had been attached to the plexiglass contactors by chemical bonding, with stainless steel baffles bolted to the contactor wall. Slow erosion of the chemical bonding for the plexiglass baffles had necessitated periodic shutdowns of operation for baffle repair.

Special pumps were necessary to transport the highly abrasive  $\text{Ca(OH)}_2\text{-CaCO}_3$  slurries. Two pumps were required when data were taken for operation of two contactors in series. Two different types of slurry pumps were used; one was a Moyno-type progressive cavity pump, and the other was a peristaltic-type finger pump.

The progressive cavity Midland Model E2H400 pump was manufactured by the Fluids Control Division of LFE Corp. (Hamden, Conn.). For processing lime slurries, the pump was fitted with a BUNA N stator and chrome-plated tool steel rotor. The transmission was a Carter hydrostatic variable-speed-drive Model 4A with a No. 5 SFRD Ritespeed gear with handwheel control. A maximum output speed of 297 rpm was obtained when the pump was powered by a top-mounted, 7.5-hp, 1800-rpm motor. The pump could deliver flow rates ranging from 0.5 to 113 liters/min (0.13 to 30 gal/min) against a head of 40 psig.

The second pump was a Sigma Motor Model 6KC40J, consisting of an explosion-proof 0.75-hp motor connected to a Vickers TR3 reversible-drive transmission. Motor speed was adjustable with a flow rate ranging from 50 ml/min to 16 liters/min.

2.2 Background on the Radiation Problems Associated  
with Inclusion of  $^{85}\text{Kr}$  in  $\text{CaCO}_3$  Solids  
Containing  $^{14}\text{C}$

To be classified as LSA (low-specific-activity) waste, the  $\text{CaCO}_3$  product (taken here as moist filter cake, 60 wt % solids and 40 wt %  $\text{H}_2\text{O}$ ) would have to contain  $<0.01 \text{ Ci } ^{14}\text{C/g}$  and  $<0.1 \text{ Ci } ^{85}\text{Kr/g}$ .<sup>4</sup> For a model plant processing 450 MTHM (Th + U) of HTGR fuel per year,<sup>2</sup>  $\sim 10^7 \text{ Ci } ^{85}\text{Kr}$  and  $10^4 \text{ Ci } ^{14}\text{C}$  would be present in the plant annually. If these quantities of  $^{85}\text{Kr}$  and  $^{14}\text{C}$  appeared in the off-gas, the amount of  $\text{CaCO}_3$  formed in fixation of the  $\text{CO}_2$  would be enough (without any removal method for krypton) to dilute the  $^{85}\text{Kr}$  level sufficiently to satisfy the above concentration restrictions. For inclusion of all the krypton in the  $\text{CaCO}_3$  product, maximum concentration would be only  $3.71 \times 10^{-4} \text{ Ci } ^{85}\text{Kr/g}$ . However, if the  $\text{CaCO}_3$  product containing  $^{14}\text{C}$  and  $^{85}\text{Kr}$  is to be transported in bulk, the resulting activity must be below 0.1 Ci per gram of concentrated krypton. For bulk transportation of radioactive material, IAEA restrictions require allowance for the possibility of concentration of all the  $^{85}\text{Kr}$  in a bulk shipment into one large "bubble." For that contingency, the presence of 50 Ci of krypton in one truck shipment could exceed the 0.1-Ci  $^{85}\text{Kr/g}$  limit.

Croff<sup>4</sup> pointed out that bulk shipment of the unpackaged, unsolidified  $\text{Ca}^{14}\text{CO}_3$  is favored because of the very large savings in transportation cost for the  $\text{Ca}^{14}\text{CO}_3$  product (total disposal cost, \$13.55/kg heavy metal; transportation cost, \$4/kg heavy metal). The cost for the most extensive case of product protection, which included the fixation of  $\text{CO}_2$  to  $\text{CaCO}_3$ , packaging, solidification, transportation, and disposal, was \$86/kg heavy metal (transportation cost was \$26.80/kg heavy metal). In general, about half of the cost was due to transporting  $\sim 3$  in. of iron shielding on the waste containers. If the krypton activity level were reduced by a factor of 100, about half the total shielding weight (only 0.12 in. of iron shielding would be required) could be deducted.

Croff calculated that in order to completely avoid any possibility of exceeding the IAEA regulations for  $^{85}\text{Kr}$ -contaminated  $\text{CaCO}_3$  in bulk shipment, no more than  $2 \times 10^{-5}\%$  of the krypton in the feed to the slurry

could be retained in the slurry. For the fixation of  $\text{CO}_2$  in a  $\text{Ca}(\text{OH})_2$  slurry in the presence of krypton, it appears that a good target fraction of inclusion for  $^{85}\text{Kr}$  is 0.1% (maximum). Forsberg showed that for this fraction the radiation dose at the surface of a drum containing  $\text{CaCO}_3$  product with  $^{14}\text{C}$  and  $^{85}\text{Kr}$  was 2 to 5 mrem/hr (Fig. 5). The maximum dose rate at a distance of 6 ft from the external surface of the transport vehicle carrying the drum must be <10 mrem/hr. Thus, operation of the  $\text{CO}_2$ - $\text{Ca}(\text{OH})_2$  slurry reaction so that <0.001 of the krypton is included in the solids would satisfy the most general and least stringent case for shielded bulk transportation. If an additional 99.9% of the krypton in the  $\text{CaCO}_3$  product could be evolved, even the most stringent requirement for unshielded bulk transportation, including the accounting for concentrations of all the krypton in one location, could be met.

### 2.3 Advantages and Disadvantages of Beta and Gamma Counting

Krypton-85\* decays predominantly by the emission of beta particles of 0.67-MeV maximum energy. A low-yield (0.41%), 0.51-MeV gamma ray is also emitted. Analysis of krypton activity by gamma counting offers the best technique for accurately measuring the true radiation level in the  $\text{CaCO}_3$  solids due to the residual krypton remaining after  $\text{CO}_2$  fixation in  $\text{Ca}(\text{OH})_2$ , sparging or vacuum treatment of the  $\text{CaCO}_3$  slurry, and centrifugation to recover the net solid precipitate. In analyzing a particular slurry for contained krypton by gamma counting, a complete balance for the krypton in the off-gas can be obtained as follows:

1. A known amount of krypton in the feed gas is fed to the agitated contactor in semibatch operation.
2. The fraction taken up in the slurry must then be analyzed because such a large fraction (>99%) of the krypton passes through the slurry that the slight difference in influent/effluent beta counts cannot be readily detected in an in-line beta detector.
3. The slurry is counted first in a Searle gamma counter.
4. The liquid is carefully separated from the solid (by centrifugation) and then counted for gamma content.

---

\* Half-life = 10.7 years.

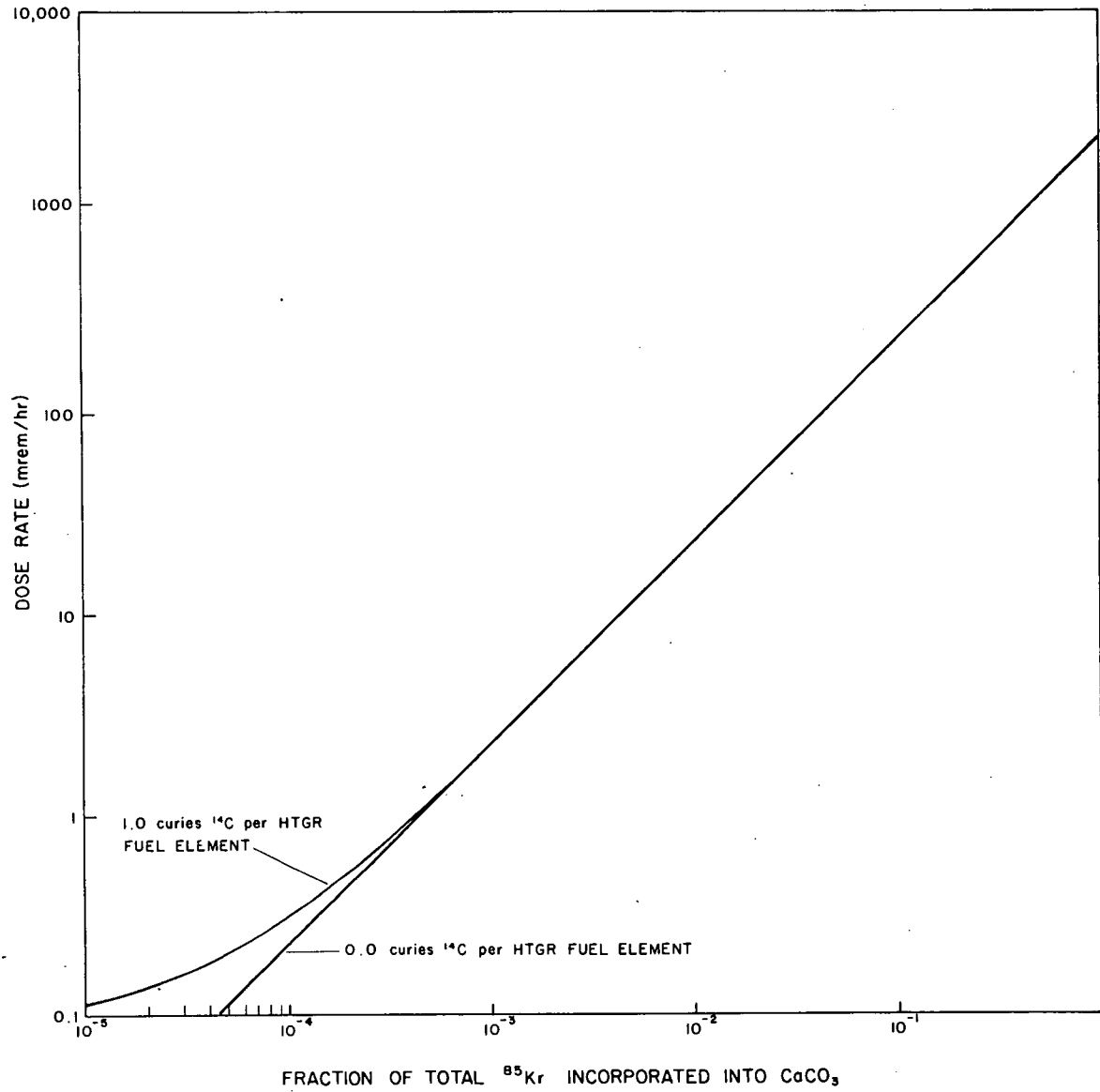


Fig. 5. Dose rate at surface of 55-gal drum containing  $\text{CaCO}_3$  product with  $^{14}\text{C}$  and  $^{85}\text{Kr}$ .

5. The wet solid is counted for gamma content, and the portion of  $^{85}\text{Kr}$  in the solid is obtained by accounting for the activity in the water in the wet solid.

This procedure yields an excellent balance for the  $^{85}\text{Kr}$  in the liquid and solid portions of the slurry.

The major disadvantage of gamma counting is the high level of radiotracer which must be used to achieve the statistics necessary to properly analyze the krypton distribution.

The number of decay events for beta emissions is  $\sim 250$  times greater than the gamma decay events; hence, for equal detection efficiencies for each emission, the detectable count rate for beta is 250 times greater than that for the gamma emission. In general, then, if krypton analysis is by beta counting instead of gamma counting, the effective level of  $^{85}\text{Kr}$  required in simulated HTGR feed gas can be reduced for standard semibatch (and continuous) operating conditions in the 20.3-cm contactor. Analysis of  $^{85}\text{Kr}$  by beta counting is complicated by the inability to count the solids portion of the slurry by standard beta scintillation techniques.

Additional details concerning the comparison of beta and gamma counting and the standardization of the beta counting method are given in Appendix A. The definitions for the DFs describing the distribution of krypton in these experiments are also given in Appendix A.

The primary DF for krypton was established during tests with a single contactor in continuous or semibatch contactor operation, or with two contactors in series in continuous-flow operation. All effluent ports on the contactor were closed upon termination of the experiment so that there would be no slow evolution of krypton from the slurry to the circulating air above the liquid in the contactor. After the contactor ports were closed, the slurry was immediately sampled upon termination of the run because of possible adjustments in the krypton distribution between slurry and the gas phase trapped over the slurry.

## 2.4 Feed Gas Analysis

In order to adequately determine the DFs for the KALC process, Levins et al.<sup>14</sup> developed an in-line beta scintillation counter (for gases) that was capable of accurately measuring DFs of  $10^3$  for  $^{85}\text{Kr}$  concentrations in feed gas as low as 60 ppb. The off-gas from HTGR fuel reprocessing would generally discharge  $\sim 2 \times 10^7$  Ci krypton/year for a 450-MTHM plant with a flow rate of 900 scfm (21°C, 1 atm). The krypton concentration in this off-gas would be  $\sim 1.6 \times 10^{-3}\%$  total,<sup>1</sup> of which  $1.2 \times 10^{-4}\%$  would be radioactive. Thus, the actual feed gas to KALC would contain  $\sim 1.8$  mCi/std liter, at a  $^{85}\text{Kr}$  concentration of  $1.2 \times 10^{-4}\%$  (1200 ppb).

### 2.4.1 Determination of $^{85}\text{Kr}$ content in the feed gases

Feed gases were obtained commercially or were blended in our laboratory. The amount of  $^{85}\text{Kr}$  in the feed gases was determined with the flow-through beta-emission detector designed by Levins.<sup>14</sup> The efficiency of our beta-sensitive radiation detector [utilizing a  $\text{CaF}_2(\text{Eu})$  scintillation disc] was established by counting a standard gas mixture, obtained from Matheson, which contained 0.017 mCi/liter. This efficiency, 13.6%, was used to calculate the actual disintegrations per minute (dpm) of  $^{85}\text{Kr}$  in unknown feed-gas mixtures.

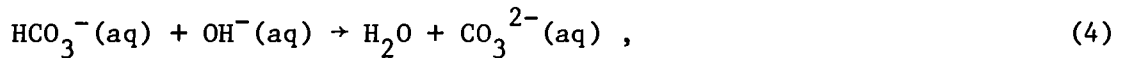
### 2.4.2 Determination of $\text{CO}_2$ and total krypton in the feed gases

A Tracor gas chromatograph with a thermal conductivity detector was used to analyze the feed gas and effluent gas compositions. The detection limit for krypton and  $\text{CO}_2$  was  $\sim 10^{-3}\%$ . In general, the accuracy of detection varied directly with the  $\text{CO}_2$  concentration in the sample gas.

## 3. THEORY OF CARBONATION OF LIME SLURRIES

Juvekar and Sharma<sup>15</sup> have extensively discussed the mechanism for the absorption of  $\text{CO}_2$  into a suspension of  $\text{Ca}(\text{OH})_2$  in both bubble columns

and mechanically agitated contactors. It was suggested that the overall mechanism for the carbonation of lime could be described by



Because Eqs. (4) and (5) are instantaneous, the controlling mechanism is in Eqs. (1), (2), or (3). The gas-phase diffusional resistance is significant only for gases containing very low concentrations of  $\text{CO}_2$ . After consideration of the rate equation for the transport of  $\text{CO}_2$  through the gas film, for the rate of dissolution of  $\text{Ca(OH)}_2$ , and for the rate of transport of  $\text{CO}_2$  into the liquid and the reaction of  $\text{CO}_2$  with hydroxyl ions, Juvekar derived the expression

$$Ra = \frac{\alpha H p_{cd} [D_{cd} k_2 (\text{OH}_s^{-}) + k_L^2]^{0.5}}{1 + \frac{\alpha H [D_{cd} k_2 (\text{OH}_s^{-}) + k_L^2]^{0.5}}{k_G \alpha}} , \quad (6)$$

where

R = specific rate of absorption of  $\text{CO}_2$ , g-mole/(sec-cm<sup>2</sup> of dispersion);

$\alpha$  = gas-liquid interfacial area, cm<sup>2</sup>/cm<sup>3</sup> dispersion;

H = Henry's coefficient of solubility for  $\text{CO}_2$ , g-moles/(cm<sup>3</sup>-atm);

$p_{cd}$  = partial pressure of  $\text{CO}_2$  in the bulk gas, atm;

$D_{cd}$  = diffusivity of  $\text{CO}_2$  in aqueous solution, cm<sup>2</sup>/sec;

$k_2$  = rate constant for the reaction between  $\text{CO}_2$  and  $\text{OH}^{-}$  ions, cm<sup>3</sup>/g-mole-sec;

$(\text{OH}_s^{-})$  = saturation concentration of  $\text{OH}^{-}$  ions in aqueous solutions in equilibrium with solid  $\text{Ca(OH)}_2$ , g-ion/cm<sup>3</sup>;

$k_L$  = liquid-side mass transfer coefficient in the absence of chemical reaction, cm/sec; and

$k_G\alpha$  = gas-side mass transfer coefficient, g-mole/(cm<sup>3</sup> dispersion-sec-atm).

This expression should apply, for semibatch operation of the mechanically agitated contactor, to ~80% of the reaction time (called the "constant-rate period"), wherein the hydroxyl concentration remains constant. It also applies to continuous slurry flow which provides for OH<sup>-</sup> stabilization when total Ca(OH)<sub>2</sub> concentration is maintained at >0.1 M

The applicability of the mechanism described by Eq. (6) is discussed in further detail in Sect. 5 on modeling. Particular discussion will be focused on methods in which the interfacial area can be estimated. Models would be useful for affording reasonable empirical estimates of scaled-up tank dimensions or of DFs which could be obtained for various tank dimensions. Previous analyses of the model<sup>16</sup> have been presented for describing CO<sub>2</sub> fixation from dilute CO<sub>2</sub> air feeds.

#### 4. DISCUSSION OF RESULTS

##### 4.1 Determination of the Distribution of Krypton from the Feed Gas to the Product CaCO<sub>3</sub> Slurry

The distribution of krypton during the fixation of CO<sub>2</sub> in Ca(OH)<sub>2</sub> slurries was obtained in a single contactor with semibatch and continuous slurry operation and also in two stirred contactors in series with continuous slurry flow. Parametric studies included effects of temperature, feed CO<sub>2</sub> concentration, feed krypton concentration, and superficial gas velocity. The results of these experiments are presented in Tables A.1, A.2, and A.3 in Appendix A.

The distribution of krypton from the feed gas to the CaCO<sub>3</sub> slurry was determined by counting beta emissions in the liquid phase of the slurry and gamma emissions in both liquid and solid portions of the slurry. Details of these counting procedures are discussed in Appendix A.

In general, DFs ranged from  $\sim 100$  to 200 for primary processes in which  $\text{CO}_2$  was removed from the simulated HTGR fuel reprocessing off-gas in continuous or semibatch operation of a single agitated gas-slurry contactor. However, initial studies quickly showed that when the product slurry was exposed to gases containing none or smaller-than-equilibrium concentrations of krypton, a very large overall DF could be achieved for krypton in a  $\text{CaCO}_3$  slurry.

In the primary tests conducted, the distribution of the krypton between liquid and solid phases of the slurry was found to be independent of operating conditions. However, no analyses were made of the 2.0 M slurry products; hence, the effects of increasing slurry concentration were not studied. Thus, there may be combinations of operating conditions, involving variations in such parameters as impeller speed, slurry density, temperature, or gas flow rate, which would result in changes in  $\text{CaCO}_3$  nucleation and particle growth, thus affecting the distribution of krypton to the solid phase.

However, it was determined, for a very wide range of operating conditions, that the krypton included in the slurry after the primary  $\text{CO}_2$  removal process in the agitated contactor could be relatively easily removed by a combined treatment of mechanical agitation and application of a vacuum, with minimal sparging.

The effects of various treatments on the krypton content of the slurries produced in primary  $\text{CO}_2$  removal are shown in Table A.5. In most of the quantitative cases, determination of krypton after treatment was based on counting of beta emissions because the gamma emission level was not significantly above background after the add-on process to allow for statistically meaningful results. Application of absolute pressures of  $\sim 9$  in. Hg for a holding time of  $\sim 5$  min resulted in add-on DFs for krypton of 10 to 20 [add-on DF is equal to  $\text{dpm } ^{85}\text{Kr}$  per liter of slurry before treatment/ $\text{dpm } ^{85}\text{Kr}$  per liter of slurry after treatment]. Add-on DFs  $\geq 10^2$  could be achieved for vacuum treatment at pressures of 7 to 9 in. Hg (absolute) for  $\geq 10$  min. The add-on DFs that could be obtained by applying a vacuum to the product slurry did not appear to be a function of conditions under which the product slurry was formed.

In some cases, the product slurries from the primary CO<sub>2</sub> removal process were sparged with pure O<sub>2</sub>, air, or feed gas (>90% CO<sub>2</sub>, 10% O<sub>2</sub>, and N<sub>2</sub>, etc.). For examples of such experiments, see runs TR14, TR16, or TR18 in Table A.5. Decontamination factors ranged from 10 to 50 for sparge times of ~10 min (with agitation) using O<sub>2</sub>. Add-on DFs were also 10 to 50 for sparging with feed gas; however, flow rates of O<sub>2</sub> or air required to achieve these add-on DFs would bear the penalty of greatly increasing the off-gas from the primary processes. Such increases in product gas (i.e., krypton passing through or later stripped from the slurry, plus carrier gases) from the CO<sub>2</sub> removal process would necessitate the enlargement of the subsequent process equipment in which krypton would be concentrated for final storage. The promising results obtained for slurry stripping with feed gas led to further experiments with the operation of contactors in series. These experiments resulted in enhanced CO<sub>2</sub> removal while simultaneously minimizing the included krypton in the slurry.

For equal treatment times, the highest add-on DFs were obtained for vacuum treatment. An additional advantage of the vacuum treatment is that the krypton received from the CaCO<sub>3</sub> product would be in a relatively small volume of gas. As part of the overall process, this stripped krypton would be added back to the krypton-rich product stream, which would then be treated for final krypton removal. If the stripped krypton is contained in a small volume, the size and cost of the krypton removal equipment will be minimized.

Thus, the extensive reduction obtained for the amount of krypton included in the slurry (both liquid and solid portions) alleviated some of the concern about the amount of krypton which is present in the 10% of slurry that is solid. At the conclusion of a run, it is likely that there will be a readjustment of krypton distribution between the gas-liquid-solid phases in the agitated slurry contactor. This readjustment is particularly expected if the gas phase over the slurry and the slurry are not in equilibrium with respect to krypton. The readjustment would be a function of gas and slurry volumes and of the dynamic distribution initially operative in the system prior to run termination. In one treatment process (TR17, Table A.5), the contactor was sealed off and

agitation was continued. After a period of agitation, there was a detectable increase in the quantity of krypton in the slurry. This increase was consistent with the observed trend for all runs that the slurry was not in equilibrium with the effluent krypton-gas concentration during the runs. The krypton concentration in equilibrium with the slurry was some intermediate or average value between inlet and effluent concentrations because of the large amount of shrinkage in the feed-gas stream (resulting in an increasing partial pressure of krypton) during the passage of feed through the agitated  $\text{Ca}(\text{OH})_2$  slurry. This effect is discussed further in Sect. 4.2.5.

Following a similar primary  $\text{CO}_2$  removal process, the slurry was stirred in a vessel exposed to the atmosphere, not in the closed contactor. The loss of krypton from the stirred slurry to the open air (no sparging) is shown in Fig. 6. The krypton content of the slurry was determined by counting 5.0-ml slurry samples in the Searle gamma counter. The rapid loss of krypton to the atmosphere shown in these experiments emphasizes that (1) krypton is easily removed from the slurry (both liquid and solid portions) and (2) care must be exercised during analysis of a slurry following a primary  $\text{CO}_2$  removal process.

#### 4.2 Dependency of DFs for $\text{CO}_2$ and Krypton on Operating Parameters

The objective of this study was to determine if, during the treatment of HTGR fuel reprocessing off-gas, the  $\text{CO}_2$  removal process could be conducted before krypton removal. Thus, operating conditions had to be established that provided for both a high removal efficiency for  $\text{CO}_2$  and a very low inclusion of krypton in the  $\text{CO}_2$ -fixation product ( $\text{CaCO}_3$ ). The ranges of operating parameters for which acceptable DFs for both  $\text{CO}_2$  and krypton could be obtained would then define an operating window.

Based on the general applicability of Eq. (6), the DF for  $\text{CO}_2$  is dependent on the hydrodynamic conditions (gas flow rate,  $U_s$ ; contactor geometry; slurry density,  $\rho_s$ ; impeller speed,  $n$ ; impeller design,  $d_i$ ; and slurry surface tension,  $\sigma$ ) and the physicochemical properties

ORNL DWG 78-17864

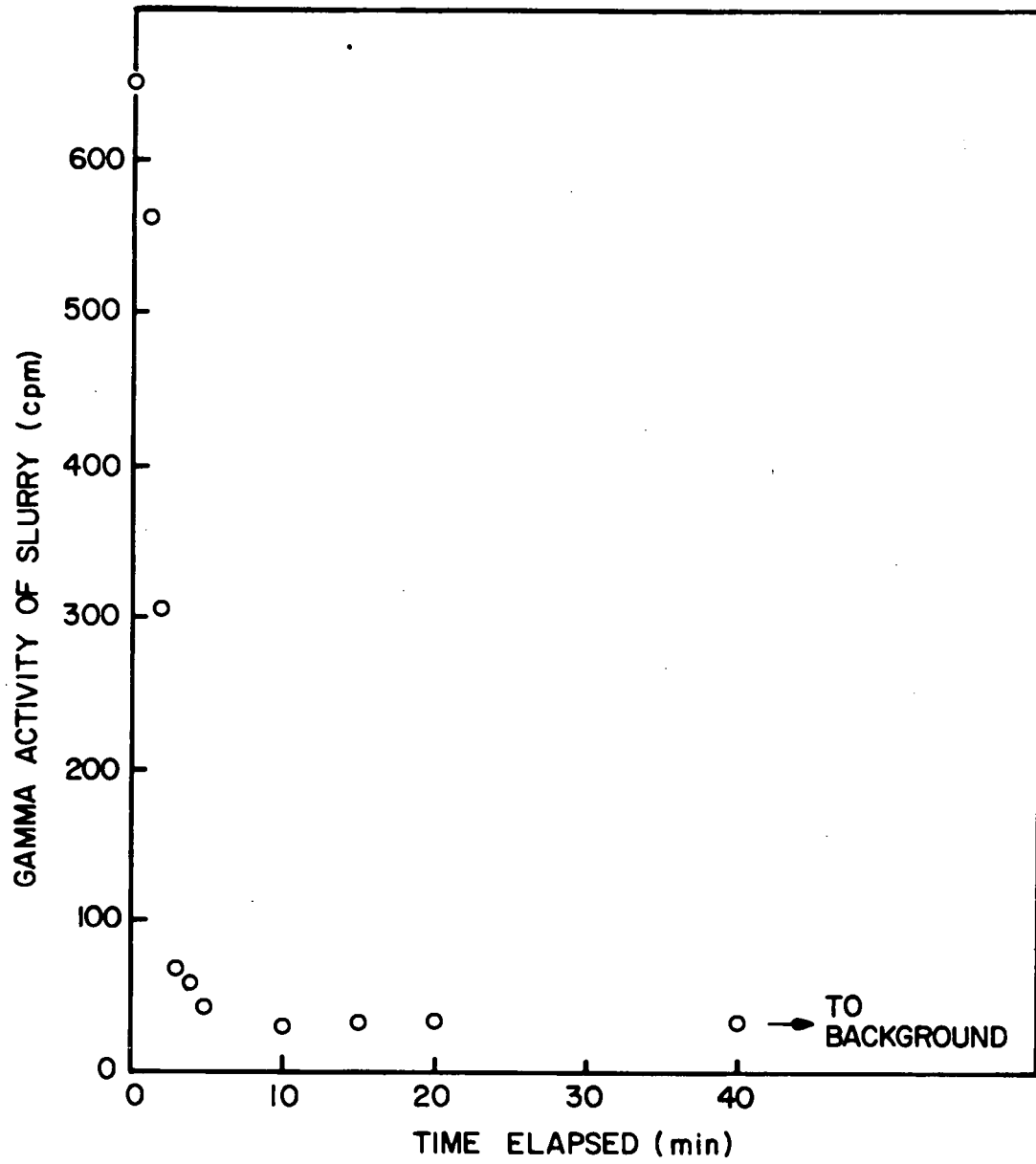


Fig. 6. Rate of  $^{85}\text{Kr}$  dispersion into air while stirring.

(solubility of  $\text{CO}_2$  in the slurry,  $H$ ; diffusivity of dissolved  $\text{CO}_2$  and reactants in the slurry,  $D_{\text{cd}}$  and  $D_{\text{OH}}$ ; and kinetics of the carbonation reaction,  $k_2$ ). The hydrodynamic factors can usually be represented by two quantities:  $k_L$  (the liquid-film coefficient for absorption without reaction) and  $a$  (the effective gas-liquid interfacial area). However, these dependent parameters are best represented by the independent variables upon which they are based in order to obtain the most general model. The following discussions are the results of tests to experimentally ascertain the nature of the dependency of DFs for  $\text{CO}_2$  and krypton on some of these parameters.

#### 4.2.1 Types of contactor operation

Shown in Fig. 7 are DF curves obtained for removing  $\text{CO}_2$  from 70%  $\text{CO}_2$ -air and ~90%  $\text{CO}_2$ -air feeds in semibatch and continuous operation modes. The semibatch mode here refers to operation of the agitated contactor using various batches of  $\text{Ca}(\text{OH})_2$  slurry with continuous sparging by the feed gas. The continuous mode refers to the operation of the agitated contactor with both feed gas and  $\text{Ca}(\text{OH})_2$  slurry in continuous flow. Slightly higher DFs were generally obtained for all feed gas concentrations in the continuous mode than in the semibatch mode. The more efficient operation in the continuous mode was attributed to the relatively larger dispersed phase (~10 to 15% in height), which was normally maintained in continuous operation.

It should be stressed that the DF for  $\text{CO}_2$  is defined differently from the DF for krypton:

$$\text{DF for } \text{CO}_2 = \frac{\text{moles } \text{CO}_2 \text{ into contactor in feed gas}}{\text{moles } \text{CO}_2 \text{ in effluent gas}}, \quad (7)$$

$$\text{DF for krypton} = \frac{\text{moles krypton into contactor in feed gas}}{\text{moles krypton remaining in slurry}}. \quad (8)$$

#### 4.2.2 Dependency of DFs for $\text{CO}_2$ and krypton on gas superficial velocity

As shown in Figs. 7 and 8, experimentally, the DF for  $\text{CO}_2$  varied inversely with  $U_s$ , whereas there was a slight direct dependency of  $\text{DF}_k$  on  $U_s$  up to flow rates of ~60 cm/min.

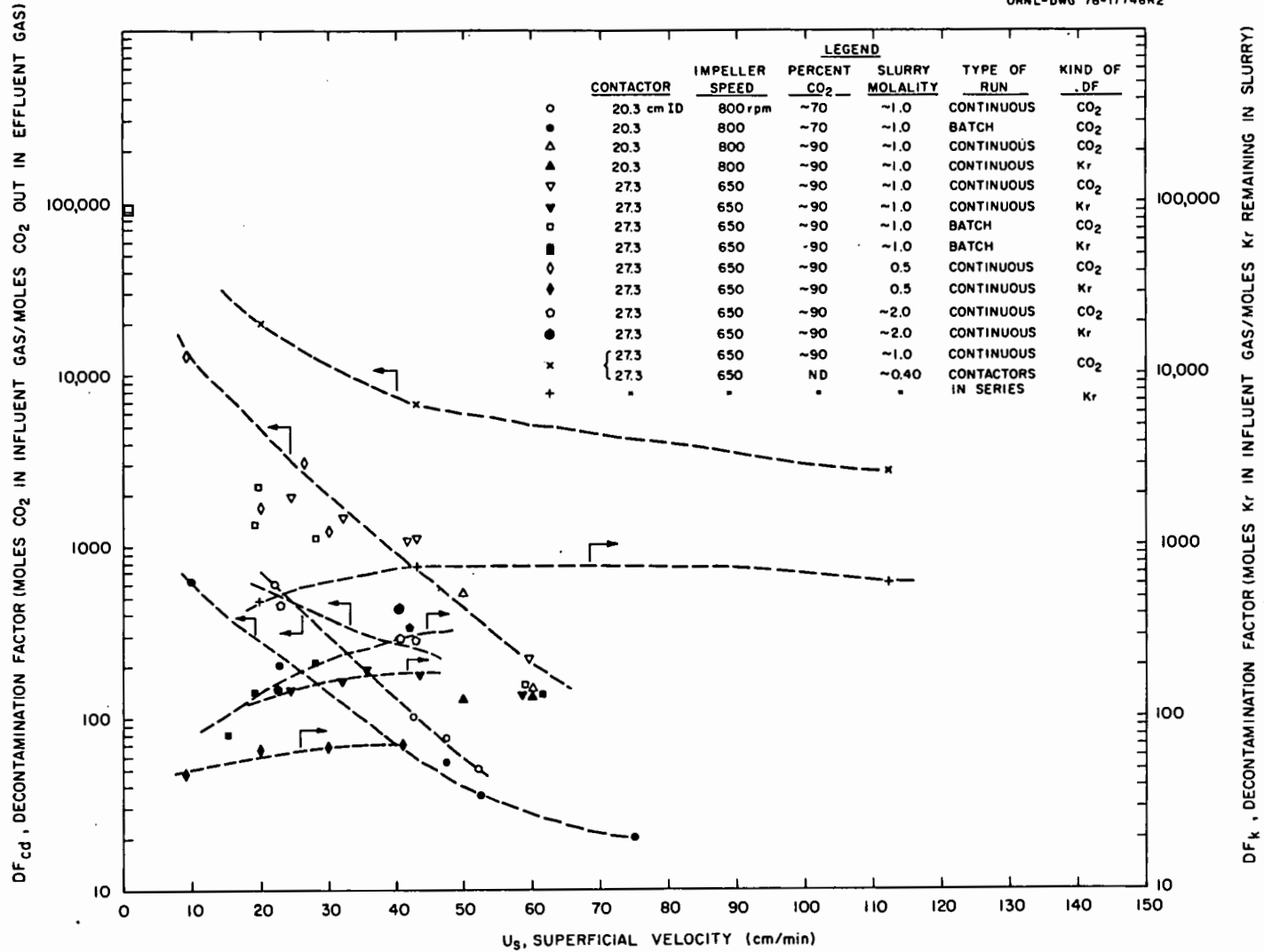


Fig. 7. Decontamination factors for removal of both krypton and CO<sub>2</sub> from simulated HTGR fuel reprocessing off-gas.

ORNL-DWG 78-17747R

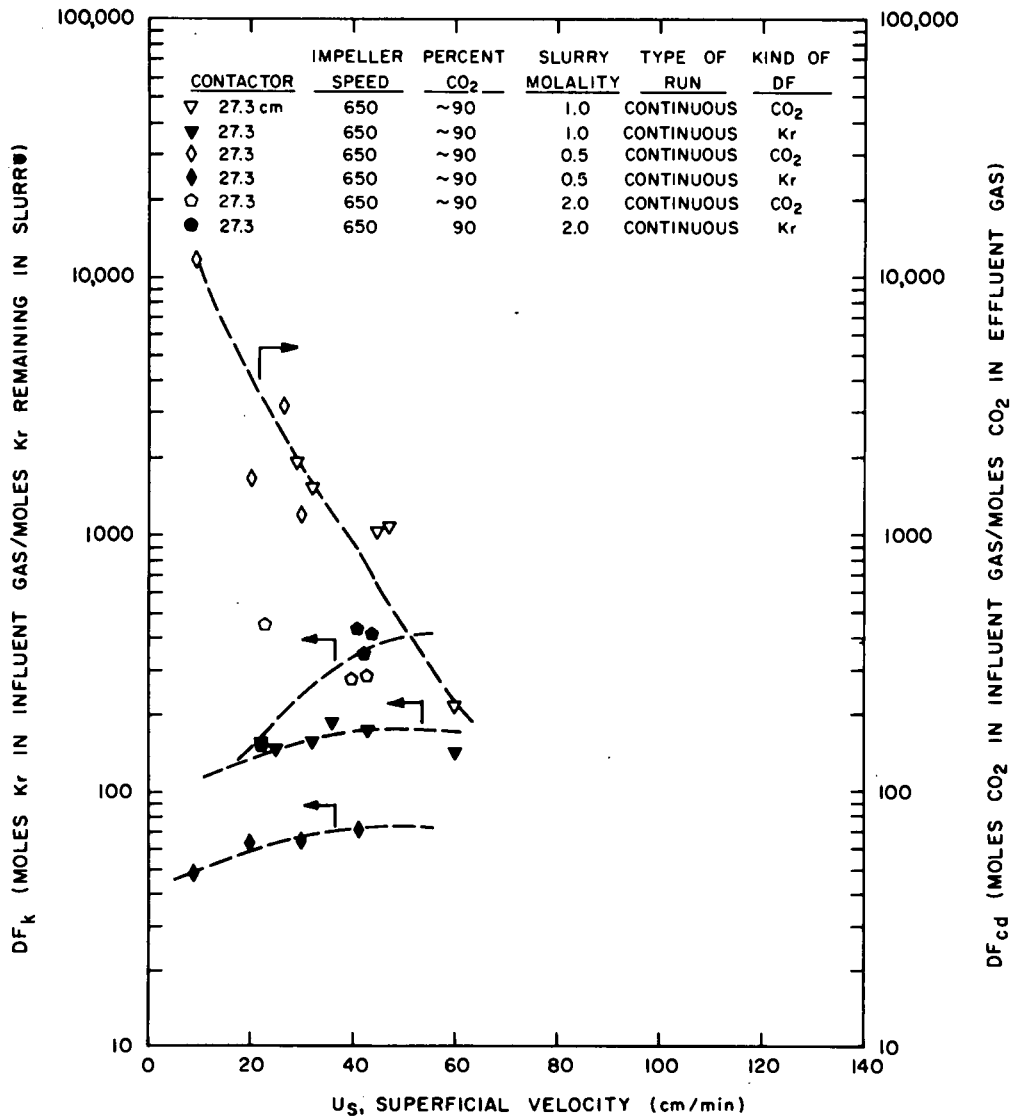


Fig. 8. Variation in DFs for krypton and CO<sub>2</sub> as a function of slurry concentration.

For continuous-flow operation of a single agitated contactor, Forsberg<sup>13</sup> has suggested the following estimate (see Appendix B) for DFs of krypton ( $DF_k$ ):

$$DF_k = \frac{K(1 - F_r) + F_r C}{F_r C}, \quad (9)$$

where

$K$  = distribution coefficient for krypton,  $K = y_k/x_k$ ;

$y_k$  = mole fraction of krypton in gas;

$x_k$  = mole fraction of krypton in the liquid phase;

$F_r = (F_{t,i} - F_{t,o})/F_{t,i}$ ;

$F_t$  = total molar gas-flow rate ( $i = \text{in}$ ,  $o = \text{out}$ ); and

$C$  = moles of  $H_2O$  out of reactor per mole of  $CO_2$  reacted, determined primarily by gas flow rate and slurry molality.

The DFs of  $CO_2$  for all  $CO_2$  feed gas concentrations that have been studied<sup>11,16</sup> for the removal of  $CO_2$  from fuel reprocessing off-gas in agitated  $Ca(OH)_2$  slurries varied inversely with gas superficial velocity. For the model given in Eq. (6), with no gas-phase control and the pressure driving force in the log-mean form, the DF for  $CO_2$  ( $DF_{cd}$ ) can be estimated by (see Appendix C-2):

$$[\ln DF_{cd} + \ln(1 - p_{cd,i})]Ra \cong aH(p_{cd,i} - p_{cd,o}) \chi [D_{cd} k_2(OH_s^-) + k_L^2]^{0.5}. \quad (10)$$

$DF_{cd}$  is predicted to vary inversely with  $U_s$  when physicochemical properties and hydrodynamic conditions are fixed because  $R$  is directly proportional to  $U_s$  and  $p_{cd,i} - p_{cd,o}$  is essentially constant ( $p_{cd,o} \ll p_{cd,i}$ ).

Based on the increase in krypton partial pressure in the effluent gas which accompanies an increase in the fraction of  $CO_2$  removed from the feed gas, there would be an increase in the krypton in the slurry

and thus a decrease in  $DF_k$ . Mathematically,  $F_r$  and  $DF_{cd}$  are related by (see Appendix B):

$$F_r = 1 - \frac{y_{cd,i}}{DF_{cd} y_{cd,o}}, \quad (11)$$

where

$$DF_{cd} = \frac{y_{cd,i} (1 - y_{cd,o})}{y_{cd,o} (1 - y_{cd,i})}. \quad (12)$$

Equations (9), (11), and (12) can be utilized to calculate the dependency of  $DF_k$  on  $DF_{cd}$ . A few calculations are listed in Table 1. The direct variation of  $DF_k$  with  $U_s$  is also implied by Fig. 9, where a decreasing value of  $DF_k$  corresponds to an increasing  $F_r$ .

Table 1. Decontamination factor for krypton as a function of the DF for  $CO_2$

$F_r$	$DF_{cd}$	$y_{cd,i}$	$y_{cd,o}$	$DF_k$	$U_s$ (cm/min)
0.899	891	0.9	0.01	62	40
0.892	103	0.9	0.08	68	80
0.875	36	0.9	0.20	80	120

#### 4.2.3 Krypton distribution in dynamic contactor operation

The curves in Fig. 9 were calculated using a distribution coefficient for krypton ( $K$ ) value of  $3.11 \times 10^4$ . This value is normally calculated from

$$K = \frac{22414}{18\alpha P_t}, \quad (13)$$

where

$$\alpha = V_o / Vp_k;$$

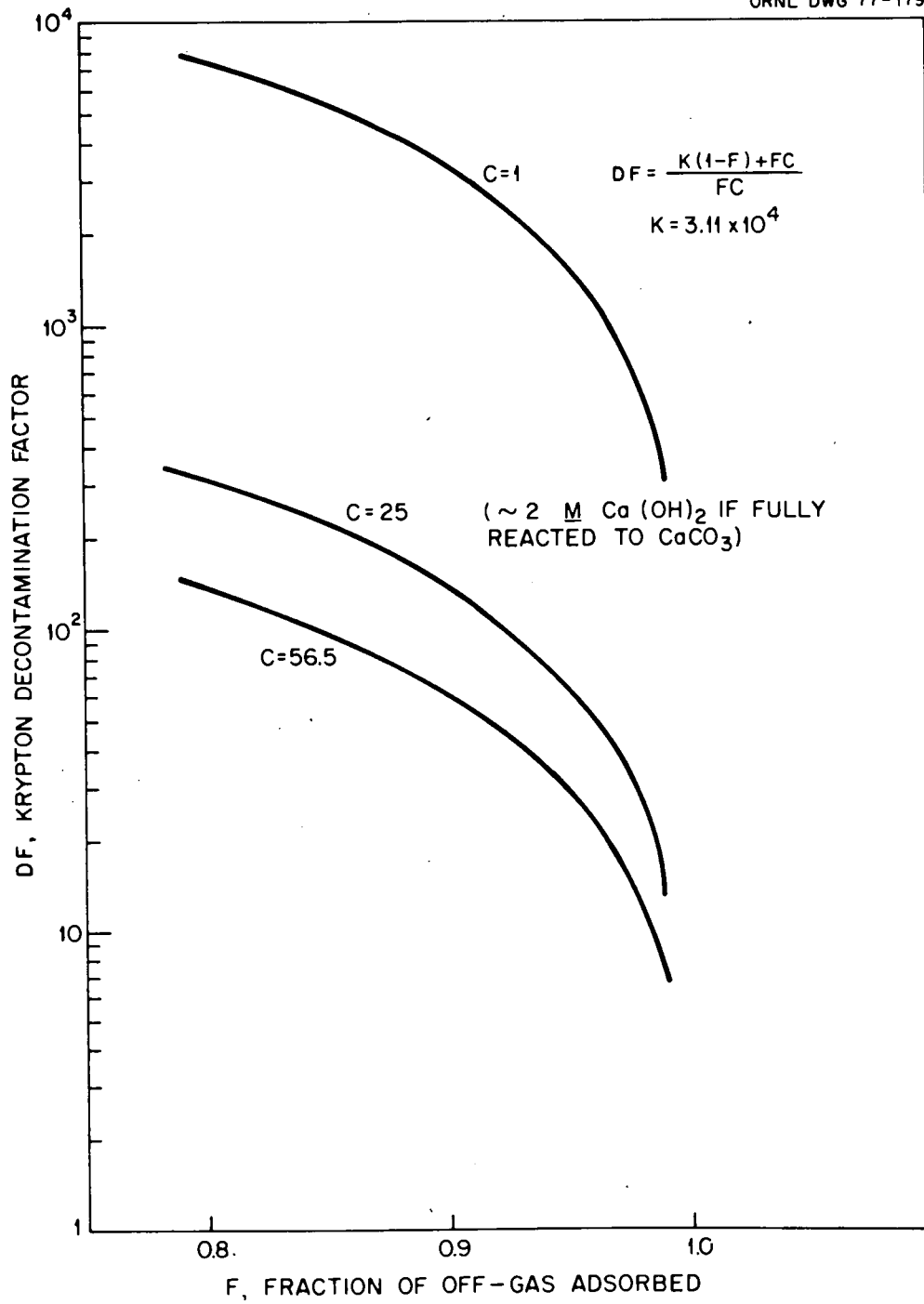


Fig. 9. Krypton decontamination factor for stirred-tank reactors vs fraction of off-gas adsorbed.

$$\begin{aligned}
 V_o &= \text{volume of krypton absorbed at STP in water} \\
 &= (\text{moles of water}) \left( x_k \right) \left( \frac{22414 \text{ cm}^3 \text{ gas}}{\text{mole of krypton}} \right); \\
 V &= \text{volume of liquid} = (\text{moles of water}) \left( \frac{18 \text{ g}}{\text{mole of water}} \right) \\
 &\quad \left( \frac{1 \text{ cm}^3}{\text{g of water}} \right); \text{ and} \\
 p_k &= \text{partial pressure of krypton, atm.}
 \end{aligned}$$

To obtain a tractable and accurate form for Eq. (9), a relationship between  $x_{k,o}$  and  $y_{k,o}$  is required (see Appendix B). The  $y_k = Kx_k$  expression may actually be applicable when the standard K values are used. However, the proper  $y_k$  value to use is unknown because of extensive stream shrinkage during the removal and fixation of  $\text{CO}_2$  for high  $\text{CO}_2$  concentrations. (Note that in processing a feed gas with a  $\text{CO}_2$  concentration  $<1\%$ , for example, the krypton partial pressure would be virtually the same for influent and effluent gases.)

The DFs calculated for krypton by Eq. (9) with standard K values ( $\text{DF}_k$  in Table 2) were too low by more than a factor of 2 (compare predicted  $\text{DF}_k$  in Table 1 and actual  $\text{DF}_k$  in Table 2). Thus, to accurately represent the actual  $y_k = Kx_k$  relationship obtained in dynamic operation and thus provide accurate K values for Eq. (9), K values were calculated from the experimental data for the following three assumed cases of equilibrium distribution of krypton: (1) between influent gas and effluent slurry concentrations; (2) between effluent gas and effluent slurry concentrations; (3) between the log-mean of influent and effluent gas krypton concentration and the effluent slurry concentration. Based on the calculated K values shown in Table 2, for a 1.0-M slurry, a range for K of  $6 \times 10^4$  to  $8 \times 10^4$  (for the  $y_{k,o} = Kx_{k,o}$  assumption) would appear to adequately predict the distribution of krypton during the standard primary processes for  $\text{CO}_2$  removal. If the molality of the slurry were increased to the range of 1.5 to 2.0 M, a higher value of K would be required ( $\sim 10 \times 10^4$  to  $12 \times 10^4$ ) to accurately estimate the DF for krypton. More information on the prediction of primary and add-on DFs for krypton is given in Sect. 5 on modeling.

Table 2. Experimental and theoretical distributions of krypton between the feed gas and the reactant  $\text{CaCO}_3$  slurry

Run	Total inlet krypton conc. (ppm)	Gas inlet $^{85}\text{Kr}$ conc. (dpm/liter)	Effluent krypton conc. (ppm)	$^{85}\text{Kr}$ remaining in slurry (dpm/liter)	Actual krypton distribution ( $\frac{\text{liter krypton}}{\text{liter slurry}}$ )	K value for theor. equil. with feed gas	K value for theor. equil. with effluent gas	K value calculated for log-mean model	Actual DF for krypton	Slurry molality ( $M$ )
CF-10	33	$2.4 \times 10^7$	270	$3.0 \times 10^6$	$4.2 \times 10^{-6}$	$1.0 \times 10^4$	$8.0 \times 10^4$	$3.5 \times 10^4$	138	0.99
BR-10	33	$2.4 \times 10^7$	270	$3.7 \times 10^6$	$5.2 \times 10^{-6}$	$0.8 \times 10^4$	$6.5 \times 10^4$	$2.7 \times 10^4$	132	0.99
BR-11	33	$2.4 \times 10^7$	270	$2.2 \times 10^6$	$3.0 \times 10^{-6}$	$1.3 \times 10^4$	$11.2 \times 10^4$	$4.7 \times 10^4$	213	0.99
BR-12	33	$2.4 \times 10^7$	270	$2.7 \times 10^6$	$3.7 \times 10^{-6}$	$1.1 \times 10^4$	$9.0 \times 10^4$	$3.8 \times 10^4$	142	0.99
CF-11	18	$3.4 \times 10^6$	180	$3.8 \times 10^5$	$2.0 \times 10^{-6}$	$1.1 \times 10^4$	$11.0 \times 10^4$	$4.3 \times 10^4$	47	0.50
CF-12	18	$3.4 \times 10^6$	180	$5.7 \times 10^5$	$3.1 \times 10^{-6}$	$0.7 \times 10^4$	$7.3 \times 10^4$	$2.9 \times 10^4$	63	0.50
CF-13	18	$3.4 \times 10^6$	180	$6.1 \times 10^5$	$3.3 \times 10^{-6}$	$0.7 \times 10^4$	$6.8 \times 10^4$	$2.7 \times 10^4$	64	0.50
CF-14	18	$3.4 \times 10^6$	180	$2.9 \times 10^5$	$1.6 \times 10^{-6}$	$1.5 \times 10^4$	$14.5 \times 10^4$	$5.7 \times 10^4$	477	2.00
CF-15	18	$3.4 \times 10^6$	180	$4.1 \times 10^5$	$2.2 \times 10^{-6}$	$1.0 \times 10^4$	$10.2 \times 10^4$	$4.0 \times 10^4$	336	2.00
CF-18	172	$5.9 \times 10^7$	1720	$1.1 \times 10^7$	$3.1 \times 10^{-5}$	$0.7 \times 10^4$	$6.8 \times 10^4$	$2.7 \times 10^4$	145	1.95
CF-19	172	$5.9 \times 10^7$	1720	$5.3 \times 10^6$	$1.5 \times 10^{-5}$	$1.4 \times 10^4$	$14.0 \times 10^4$	$5.5 \times 10^4$	443	1.97

#### 4.2.4 Dependency of DFs for krypton and CO<sub>2</sub> on slurry molality

Based on the results shown in Table A.1 for runs CF-3, CF-4, CF-11, CF-12, and CF-13 for 0.5 m Ca(OH)<sub>2</sub> slurries and runs CF-14 through CF-19 for 2.0 m Ca(OH)<sub>2</sub> slurries, the following dependencies of DF<sub>k</sub> and DF<sub>cd</sub> on Ca(OH)<sub>2</sub> concentration were noted. The DFs for CO<sub>2</sub> removal did not vary significantly for slurry concentrations ≤1.0 m. However, the DFs for CO<sub>2</sub> varied inversely with Ca(OH)<sub>2</sub> concentrations in the range of 1.0 to 2.0 m. This variation was considerable, amounting to a reduction in DF for CO<sub>2</sub> by a factor of at least 3 or 4 when molality was increased from 1.0 m to 2.0 m while all other operating conditions were maintained. This reduction in DF<sub>cd</sub> at high Ca(OH)<sub>2</sub> molalities had been previously observed during semibatch operation of the Ca(OH)<sub>2</sub> slurry contactor.<sup>11</sup> However, previous determinations were made with 100% CO<sub>2</sub> feeds so that the variation in DF<sub>cd</sub> could not be as easily established as with 90% CO<sub>2</sub> feeds. The magnitude of the DF<sub>cd</sub> reduction for 90% CO<sub>2</sub> feeds was somewhat unexpected for the continuous mode of operation. It is suspected that the reduction may be due to an effect of the increased solids concentration on the bubble size and the gas-liquid interfacial area  $a$  for mass transfer.

As was normally observed for experiments which produced significant variations in the DF for CO<sub>2</sub>, there was a corresponding variation in the DF for krypton; that is, the DF for krypton varied directly with slurry molality. However, most of the variation in DF<sub>k</sub> was due primarily to the definition of that factor. As shown in Eq. (A-2), the slurry flow rate was included in the denominator. When a higher molality was used for a fixed gas flow rate, the slurry flow rate could be decreased and, thus, the DF<sub>k</sub> values increased.

#### 4.2.5 Dependency of DFs for krypton and CO<sub>2</sub> on the CO<sub>2</sub> concentration in the feed

In one run, the CO<sub>2</sub> mole fraction (m.f.) in the feed gas was 0.97 (CF-1B, Table A.1). The DFs for CO<sub>2</sub> and krypton obtained for this run could be compared with DFs for CO<sub>2</sub> and krypton measured for a run of

similar superficial velocity but different feed  $\text{CO}_2$  m.f. (run CF-10). The DFs for  $\text{CO}_2$  are seen to vary directly with the feed  $\text{CO}_2$  m.f., while the DFs for krypton are seen to vary inversely with  $\text{CO}_2$  m.f. The direct variation of  $\text{DF}_{\text{cd}}$  with the  $\text{CO}_2$  m.f. in the feed has been shown previously<sup>11</sup> and is also evident from a comparison of  $\text{DF}_{\text{cd}}$  data for feed gases containing 70%  $\text{CO}_2$  and 90%  $\text{CO}_2$  (Fig. 7).

Theoretically, the direct variation of  $\text{DF}_{\text{cd}}$  with  $\text{CO}_2$  m.f. in the feed gas ( $y_{\text{cd},i} P_t = p_{\text{cd},i}$ ) is apparent from Eq. (10). Finally, the inverse variation of  $\text{DF}_k$  with the  $\text{CO}_2$  m.f. in the feed gas can be argued from a physical viewpoint as follows. An increase in the  $\text{CO}_2$  m.f. resulted in a higher DF for  $\text{CO}_2$ . The gas stream shrinkage factor then increased from  $\sim 10$  for 90%  $\text{CO}_2$  feeds to  $\sim 30$  for a 97%  $\text{CO}_2$  feed. As a result, the krypton partial pressure increased by a factor of  $\sim 30$ , as compared to  $\sim 10$  for 90%  $\text{CO}_2$  feeds. This higher partial pressure (or krypton mole fraction) resulted in more krypton being included in the slurry according to the relationship

$$x_k = y_k / K .$$

#### 4.2.6 Dependency of DFs for krypton and $\text{CO}_2$ on temperature

Based on comparison of runs CF-17, CF-19, CF-21, and CF-22 in Table A.1, for the temperature operating range of 28 to 61°C, there was no significant variation in the DFs for  $\text{CO}_2$ . According to the model given by Eq. (C-11) for the limited temperature range of 28 to 45°C, essentially no increase was predicted. It thus follows that, in the case of temperature, the DFs for  $\text{CO}_2$  predicted by Eq. (C-11) agree with the experimental results for a limited temperature range (see Sect. C-3 in Appendix C for a sample calculation).

Over the range of temperatures studied (28 to 61°C), there was no significant variation in the DFs for krypton. The solubility of krypton in water<sup>\*</sup> is slightly affected by temperatures in this range, as shown in Fig. 10. Apparently the krypton-slurry interaction behaved similarly to the krypton-water system in terms of dependence on temperature.

---

\* Solubility =  $\sim 0.4$  ml/ml.

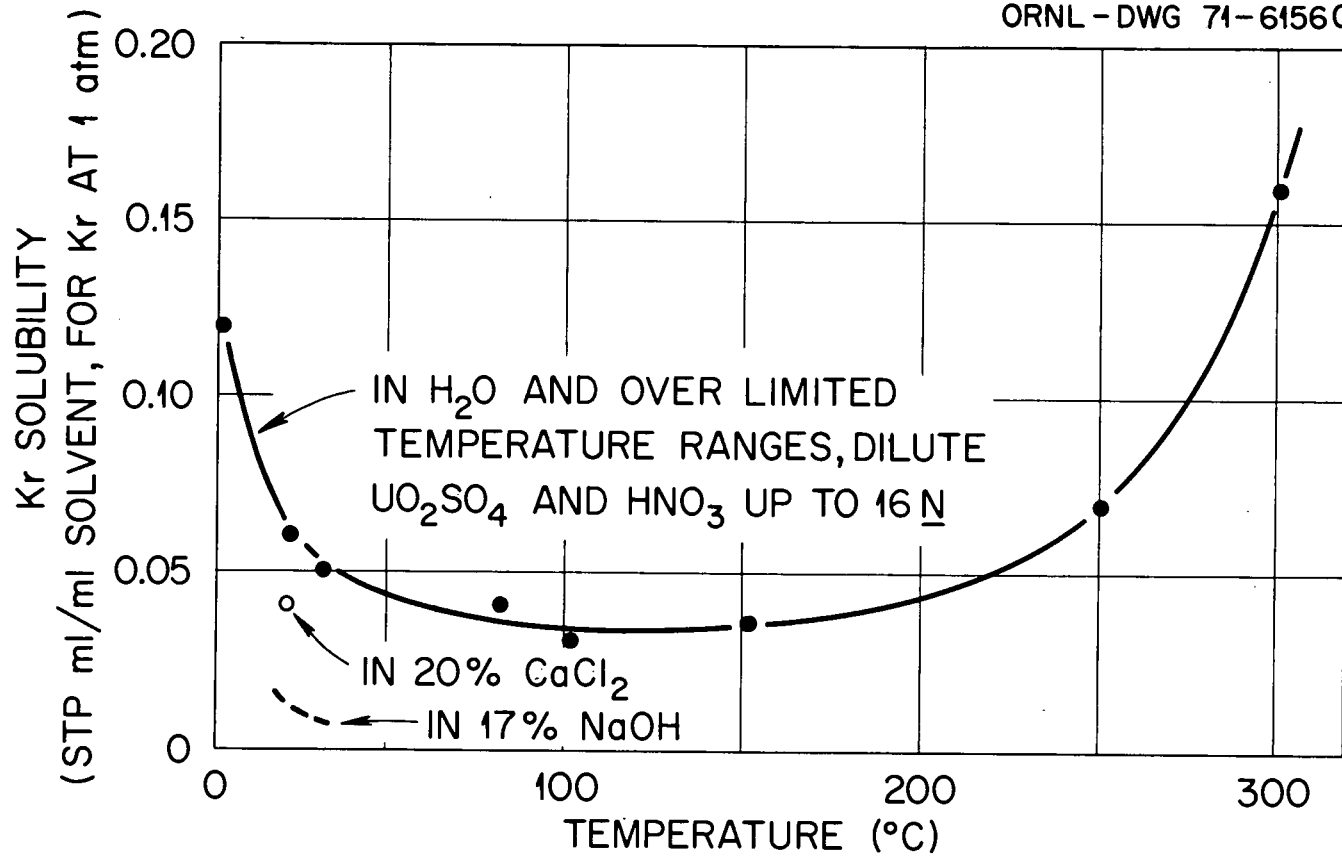


Fig. 10. The solubility of krypton in H<sub>2</sub>O.

#### 4.2.7 Dependency of DFs for krypton and CO<sub>2</sub> on impeller speed

During this study, no tests were conducted to determine the effect of varying impeller speed on DFs for CO<sub>2</sub> and krypton during treatment of simulated HTGR fuel reprocessing off-gas in an agitated Ca(OH)<sub>2</sub> slurry. It has been shown<sup>11,16</sup> that when all other operating variables were fixed ( $U_s$ ,  $D_{cd}$ ,  $P_{cd,i}$ ,  $d_t$ ,  $\rho_s$ ,  $H$ ,  $OH_s^-$ ,  $\sigma$ ,  $\mu$ , and  $T$ ), the DFs for CO<sub>2</sub> varied directly and significantly with impeller speed ( $n$ ). The magnitude of the variation was not exactly established, but when the impeller speed was doubled, DFs for removing CO<sub>2</sub> from both 90% CO<sub>2</sub>-air feeds<sup>11</sup> and 1 to 3% CO<sub>2</sub>-air feeds<sup>16</sup> were determined to increase by a factor of 3 to 4. The factor by which the DFs for CO<sub>2</sub> increased when  $n$  was doubled was, to some degree, a function of gas flow rate.

In Eq. (C-11), there is no explicit relationship between interfacial area and impeller speed. Various relationships have been developed in the literature which are used to predict interfacial area  $a$  as a function of hydrodynamic operating parameters. The variation in  $a$  predicted by these correlations could be used to represent the effects of hydrodynamic variables in Eq. (C-11). For example, Miller<sup>17</sup> has expanded on Calderbank's<sup>18</sup> original work and developed the following correlation for interfacial area:

$$a = 1.44 \left( \frac{(P_e/V_L)^{0.4} \rho_s^{0.2}}{\sigma^{0.6}} \right) \left( \frac{U_s}{U_s + U_t} \right)^{0.5}, \quad (14)$$

where

$P_e$  = effective power input, kg-m<sup>2</sup>/sec<sup>3</sup>;

$V_L$  = clear liquid volume, m<sup>3</sup>;

$\rho_s$  = slurry density, kg/m<sup>3</sup>;

$\sigma$  = surface tension, kg/sec<sup>2</sup>;

$U_s$  = gas superficial velocity, m/sec; and

$U_t$  = bubble terminal velocity of rise, m/sec.

Effective power input can be estimated in a sparged, mechanically agitated system by

$$P_m/V_L = \frac{0.706}{V_L} \left[ \frac{f^{2.7} n^{13} d_i^2 \rho_s}{Q^{0.56}} \right]^{0.45}, \quad (15)$$

where the power factor  $f$  is defined by Rushton et al.<sup>19</sup> Assuming that effective power input is essentially equal to mechanical power input,  $P_m$  can be replaced by  $P_e$  (true for the range of gas velocities used in this study). Equations (14) and (15) can be combined to yield an expression for  $\alpha$ :

$$\alpha = 1.44 \frac{0.870}{V_L^{0.4}} \left[ \frac{f^{0.36} n^{1.26} d_i^{2.34} \rho_s^{0.56}}{Q_t^{0.101} \sigma^{0.6}} \right] \left[ \frac{U_s}{U_s + U_t} \right]^{0.5}. \quad (16)$$

This equation for  $\alpha$  is valid in the kg-m-sec system. Calculated values of  $\alpha$  for 20.3-cm-ID and 27.3-cm-ID contactors for different values of  $Q_t$  are listed in Table 3. Also listed in Table 3 are effective power values estimated by Eq. (15). In later sections on modeling, the  $\alpha$  values estimated by Eq. (16) will be compared with those calculated by a form of Eq. (C-11). Thus, the feasibility of estimating  $\alpha$  by a correlation of hydrodynamic parameters, as shown in Eq. (16), can be tested.

No data were obtained to elucidate the variation of DF for krypton with  $n$ . However, based on the inverse relationship that was previously established for  $DF_k$  and  $DF_{cd}$ ,  $DF_k$  values should vary slightly inversely with  $n$  (because of the direct variation of  $DF_{cd}$  with  $n$ ).

#### 4.2.8 Dependency of DFs for krypton and CO<sub>2</sub> on multiple contactor operation

Theoretically, DFs for CO<sub>2</sub> should be increased significantly when the feed gas is processed through two contactors in series. This enhancement in DF is particularly noticeable for feeds rich in CO<sub>2</sub> because of the effect that a reduction in superficial gas velocity has on  $DF_{cd}$  in the second tank. In previous experimental studies,<sup>11</sup> the

Table 3. Interfacial areas and power consumption in the 20.3- and 27.3-cm-ID contactors

Volumetric flow rate, $Q_t$ (slm) <sup>a</sup>	20.3-cm-ID contactor				27.3-cm-ID contactor				Interpolated DFs for CO <sub>2</sub>
	Superficial velocity (cm/min)	Interfacial area, $a$ (cm <sup>2</sup> /cm <sup>3</sup> )	Effective power consumption (hp/ft <sup>3</sup> ) (kW/m <sup>3</sup> )		Superficial velocity (cm/min)	Interfacial area, $a$ (cm <sup>2</sup> /cm <sup>3</sup> )	Effective power consumption (hp/ft <sup>3</sup> ) (kW/m <sup>3</sup> )		
10	30.9	1.95	0.47	12.4	17.1	1.54	0.60	15.8	6000
20	61.8	2.47	0.40	10.5	34.2	2.02	0.49	12.9	1500
25	77.2	2.68	0.38	1.0	42.7	2.19	0.46	12.1	750
30	92.7	2.86	0.37	9.8	51.3	2.35	0.44	11.6	400
35	108.0	3.02	0.35	9.2	59.8	2.50	0.42	11.1	200
40	123.5	3.18	0.34	9.0	68.4	2.62	0.41	10.8	150
50	154.3	3.43	0.32	8.4	85.5	2.86	0.39	10.3	70
60	185.2	3.66	0.31	8.2	102.6	3.05	—	—	45

<sup>a</sup>slm = standard liters per minute.

range of DFs for carbon dioxide which could be easily obtained for two agitated gas-slurry contactors in series was  $\geq 10^4$  ( $\geq 10^2$  for each stage). For CIS countercurrent operation (the contactor-in-series process), the "first" contactor was the one into which the slurry flowed first.

In general, for comparable experiments with the same fraction of feed conversion maintained in each contactor, the cumulative DFs for  $\text{CO}_2$  were directly dependent on the superficial velocity at tank 2. That is, for the same flow rate, the  $\text{DF}_{\text{cd}}$  will vary directly with the diameter of tank 2. (This is not to imply, however, that the process is to be scaled precisely according to the tank diameter.) The variation of  $\text{DF}_{\text{cd}}$  values with residence time is shown for runs CIS-5 and CIS-6 in Table A.2. The cumulative DF for CIS-6 at a superficial velocity of  $\sim 18$  cm/min was  $\sim 10,000$ ; the  $\text{DF}_{\text{cd}}$  for CIS-5 at a superficial velocity of  $\sim 42$  cm/min was  $\sim 2400$ .

Another key factor which affects DFs for both  $\text{CO}_2$  and krypton during processing with contactors in series is the fraction of total conversion of  $\text{CO}_2$  which occurs in each tank (that is, if  $F_r$  is the fraction of conversion in tank 1, then  $1 - F_r$  is the fraction of conversion in tank 2). This effect was shown by runs CIS-2 and CIS-6 in Table A.2. When slurry flow rate and the degree of initial concentration of  $\text{Ca(OH)}_2$  in tanks 1 and 2 were properly controlled, the fractions of  $\text{CO}_2$  conversion in tanks 1 and 2 could be adjusted. When the fraction of  $\text{CO}_2$  conversion in tank 2 was allowed to increase, the gas flow rate to tank 1 was decreased. The net effect was then twofold: (1) the  $\text{DF}_{\text{cd}}$  for tank 1 (and thus the cumulative two-tank  $\text{DF}_{\text{cd}}$ ) increased because of the reduction in flow rate to tank 1; (2) the DFs for krypton in both tanks (and then the cumulative  $\text{DF}_k$ ) decreased.

For the extreme case of maximizing  $\text{CO}_2$  conversion in tank 2, the operating conditions could be arranged so that DFs  $> 10^3$  for  $\text{CO}_2$  could be obtained. Essentially all of the  $\text{CO}_2$  would then be removed, and  $\sim 90\%$  of the slurry would be converted in tank 2. Thus, very little  $\text{CO}_2$  would be processed in tank 1, but the total DF for  $\text{CO}_2$  would be high. For tank 1, the amount of krypton included in the slurry would be

determined by a dynamic operating equilibrium that is dependent on a krypton partial pressure about ten times greater than that of the feed gas. Because the effective pressure of krypton in tank 2 would be lower than that in tank 1, less krypton would be included in the slurry of tank 2. In effect, tank 2 would be operating as a single contactor.

In the other extreme case in which  $\text{CO}_2$  conversion was maximized in tank 1, the feed gas to tank 2 served essentially as a sparge gas with a partial pressure for krypton which was about equal to the initial concentration, and approximately ten times less (for 90%  $\text{CO}_2$  feeds) than that in tank 1. A DF for  $\text{CO}_2$  of  $\geq 10^3$  and a DF for krypton of  $\geq 10^3$  were easily obtained. The DFs for krypton in tank 1 for a wide range of gas flow rates and DFs for  $\text{CO}_2$  were equal to  $\sim 100$  to 200. An additional  $\text{DF}_k$  of 10 was obtained by the sparging action of the feed gas to tank 2. For the ideal case in which the molar slurry feed rate equalled the  $\text{CO}_2$  gas feed rate,  $\sim 90\%$  of the  $\text{Ca}(\text{OH})_2$  would be reacted in tank 1, leaving  $\sim 10\%$  of the  $\text{Ca}(\text{OH})_2$  to react with 10% of the  $\text{CO}_2$  feed in tank 2. Thus, a DF for  $\text{CO}_2$  of only 1.11 would be obtained in tank 2.

#### 4.2.9 Dependency of DFs for krypton and $\text{CO}_2$ on $d_i$ , $\text{OH}_s^-$ , $H$ , $D_{cd}$ , $k_2$ , $\sigma$ , and $\mu$ and correlations for those parameters

The parameters  $\text{OH}_s^-$ ,  $D_{cd}$ ,  $H$ , and  $k_2$ , for similar compositions of alkaline-earth slurries [ $\text{Ca}(\text{OH})_2$ ,  $\text{Ba}(\text{OH})_2$ , etc.], are primarily functions of temperature.

The relationships given in Sect. C.3, Appendix C, were used to explain the effect of temperature on  $k_2$ ,  $H$ , and  $D_{cd}$  and on DFs for  $\text{CO}_2$  in Sect. 4.2.6. The variation of  $\text{Ca}(\text{OH})_2$  solubility with temperature is discussed in Sect. C.3. Hydroxyl ion concentration can also be varied by substituting another alkaline-earth metal hydroxide such as  $\text{Ba}(\text{OH})_2$  in the gas-slurry contactor. However, no tests with  $\text{Ba}(\text{OH})_2$  were conducted in these experiments.

Tests were performed with only one value of  $d_i$ . It would appear, however, that for a model based on Eq. (16), interfacial area  $a$  is a very strong function of  $d_i$ . Because DF is generally strongly affected by  $a$ , it would be expected that  $\text{DF}_{cd}$  would be a strong function of  $d_i$ .

Interfacial area and therefore DFs for  $\text{CO}_2$  removal are also predicted by Eq. (16) to be a function of surface tension. No variations in surface tension ( $\sigma$ ) or viscosity ( $\mu$ ) were tested in this study.

This review of the parameters which are most likely to affect DFs for  $\text{CO}_2$  and krypton during gas-slurry reaction provides information on the variables useful for scale-up considerations. As noted, only the most critical parameters were varied. Other critical parameters such as  $d_i$  and  $n$  were not extensively studied because they could be further constrained by such conditions as maintenance of geometric similarity, equal power consumption, etc.

In general, however, it would be desirable to have the most general model which would allow for straightforward design of an agitated contactor where the following conditions would be known: (1) a set gas composition; (2) desired DFs for  $\text{CO}_2$  and krypton; (3) flow rate; and (4) a certain kind of slurry (this would fix  $D_{cd}$ ,  $\text{OH}_S^-$ ,  $k_2$ ,  $k_L$ ,  $H$ , and  $\mu$ ). It would be desirable to have a correlation which could predict the size of contactors needed to achieve the required DFs, or DFs that could be achieved for a given contactor size.

The derivation of such correlations is discussed in the following section on modeling.

##### 5. DEVELOPMENT OF MODELS TO DESCRIBE THE DFs FOR SIMULTANEOUS $\text{CO}_2$ and KRYPTON DISTRIBUTION TO A $\text{Ca}(\text{OH})_2$ SLURRY

The general approach to modeling gas-liquid reactions in agitated tanks is to develop two independent descriptions of the process. A first expression is obtained to describe the mass transfer mechanism in the gas-liquid dispersion, leading to a method of estimating the overall mass transfer rate,  $Ra$ . The overall mass transfer rate is not explicitly expressed as a function of the geometry, power input, and mixing characteristics of the contactor. The explicit dependence of  $Ra$  on these parameters must be defined in a second more or less independent expression. In this section, discussions are presented of two related derivations of expressions which may be used to link, in one equation, the hydrodynamics

and geometrical design of the mixing equipment to the mass transfer kinetics of the process in order to provide general models for description and design of the total operation. A recent review<sup>20</sup> of design considerations for scaling up agitated contactors included descriptions for all basic operational criteria and parameters such as impeller design (geometry and material); drive-train selection; design of shafts and seals; power input; geometric, dynamic, and kinematic similarity; etc.

### 5.1 Rate Expression for Carbonation of Lime Slurries and Models for Process Scale-Up

#### 5.1.1 Possible rate expressions

Juvekar and Sharma<sup>15</sup> proposed two rate expressions for describing the carbonation of lime slurries. The applicability of each rate expression is dependent primarily on the location of the reaction between dissolved  $\text{CO}_2$  and the hydroxyl ions. The conditions that must be satisfied before either expression is adequate to describe the carbonation reaction are discussed in detail in Appendix C. The two candidate rate expressions are

$$Ra = \frac{aH p_{cd} [D_{cd} k_2 (\text{OH}_s^-) + k_L^2]^{0.5}}{1 + \frac{aH [D_{cd} k_2 (\text{OH}_s^-) + k_L^2]^{0.5}}{k_G a}} \quad (6)$$

and

$$Ra = \frac{aH p_{cd} k_L \phi}{1 + \frac{aH k_L \phi}{k_G a}} \quad (17)$$

where

$$\phi = \frac{[D_{cd} k_2 (\text{OH}_s^-)]^{0.5}}{k_L} \left[ \frac{1 + \frac{(\text{OH}_s^-) D_{OH}}{zA^* D_{cd}} - \phi}{\frac{(\text{OH}_s^-) D_{OH}}{zA^* D_{cd}}} \right]^{0.5} \quad (18)$$

It is shown in Sect. C.4 (Appendix C) that for the conditions of this study [90% CO<sub>2</sub> reacted with Ca(OH)<sub>2</sub> slurries], gas-side mass transfer resistance is negligible. Thus, the two rate expressions become

$$Ra = aHp_{cd} [D_{cd}k_2(OH_s^-) + k_L^2]^{0.5} \quad (19)$$

and

$$Ra = aHp_{cd} k_2 \phi . \quad (20)$$

Based on the standard tests applied to these equations (Sect. C.5, Appendix C), it was concluded that the 90% CO<sub>2</sub>-Ca(OH)<sub>2</sub> reaction could be described by either model. However, for simplicity and brevity of arguments, only Eq. (19) was utilized for later efforts to develop methods of estimating interfacial area, which could then be used to construct a general expression for estimating scaled-up operation dimensions. The possibilities for the form of the pressure driving force ( $p_{df}$ ) term are also discussed in Appendix C.

To show the general applicability of either expression, interfacial areas were calculated for the experimental data by utilizing overall mass transfer rates,  $N_{cd}$  (moles CO<sub>2</sub> sorbed/time,  $N_{cd} = RaV_d$ ) and appropriate values of hydrodynamic and physicochemical variables. These values of interfacial area, along with the calculations using Eq. (16) from the hydrodynamic model, are shown in Fig. 11. The agreement of interfacial areas calculated by Eqs. (19) or Eq. (D-6) and (20) should be expected because of the overlap of the two models. The interfacial area predicted by Eq. (16) continued to increase past a velocity of ~2 cm/sec. This behavior is contrary to the general leveling off of interfacial areas at velocities past 2 cm/sec reported by Juvekar and Sharma. It should be noted that the superficial velocity shown in Fig. 11 is based on the inlet gas velocity. Since the stream shrinks by about a factor of 10 for 90% CO<sub>2</sub> feeds, a direct comparison of the behavior of interfacial area between this work and that of Juvekar and Sharma's is not possible. However, their results have been confirmed by Holladay and Haag<sup>16</sup> in studies of removing CO<sub>2</sub> from dilute-in-CO<sub>2</sub> feed gases in a gas-Ca(OH)<sub>2</sub> slurry contactor, where influent and effluent gas rates are essentially equal.

ORNL DWG 78-17863R3

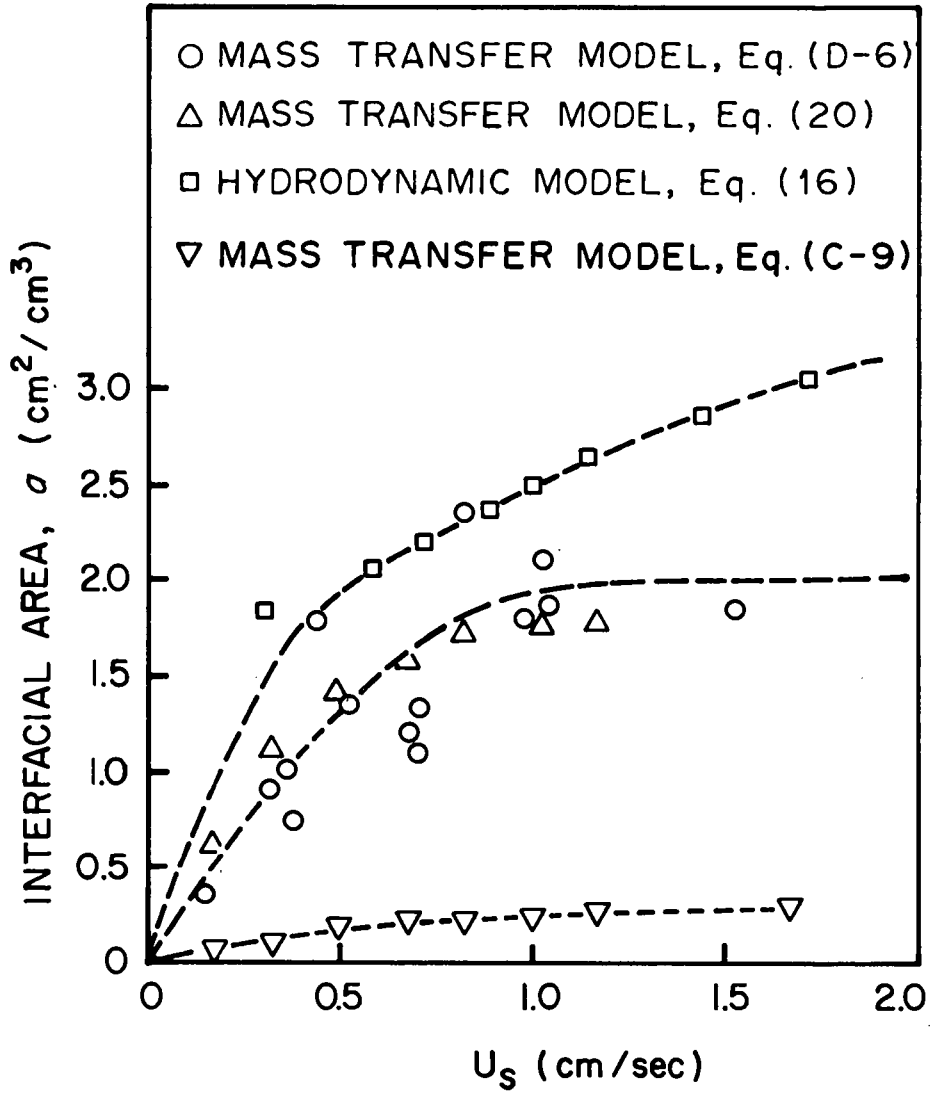


Fig. 11. Comparison of experimental and theoretical values of interfacial area.

When Eq. (19) or Eq. D-6 is used to describe the rate of carbonation of lime slurries, there is a question about the appropriate form for the pressure driving force term. It was concluded from arguments shown in Appendix C that the rate expression in the form of

$$Ra = \frac{\alpha H(p_{cd,i} - p_{cd,o})}{\ln \frac{p_{cd,i}}{p_{cd,o}}} [D_{cd} k_2 (\text{OH}_s^-) + k_L^2]^{0.5} \quad (21)$$

was sufficient to describe removal of  $\text{CO}_2$  from a 90%  $\text{CO}_2$ -air feed stream in an agitated  $\text{Ca}(\text{OH})_2$  slurry. Other forms of Eq. (21) can be utilized to calculate interfacial area. Because of the shrinkages of the gas stream, it is not clear exactly which method is the best for calculating interfacial area.

It can be seen in Fig. 11 that interfacial areas calculated from Eq. (C-9) seem to be much smaller than those calculated for Eq. (D-6). However, the  $U_s$  values plotted in Fig. 11 are influent superficial velocities, while Eq. (C-9) takes into account stream shrinkage. Thus, if interfacial areas from Eq. (C-9) are plotted vs effluent superficial velocity, they fall on the curve of  $\alpha$ 's for Eq. (D-6) and Eq. (20) if the values of  $U_s$  are corrected for the gas stream shrinkage factor.

### 5.1.2 Forms of models used for calculating scale-up contactor dimensions

Regardless of the form for calculating  $\alpha$ , the standard procedure used here for developing a model for predicting contactor scale-up included the following steps:

1. The mass-transfer rate expression was rearranged in terms of  $DF_{cd}$ , the other operating parameters, and interfacial area.
2. An expression predicting interfacial area was developed and inserted into the general mass transfer expression for the  $\text{CO}_2$ - $\text{Ca}(\text{OH})_2$  reaction.

3. For a given temperature and operating values of  $H$ ,  $D_{cd}$ ,  $k_2$ ,  $OH_S^-$ ,  $k_L$ ,  $n$ ,  $DF_{cd}$ , and gas feed and composition, the tank diameter could be calculated.
4. For the same conditions in 3, but with a specified value of  $d_t$ ,  $DF_{cd}$  could be calculated.

Scaled-up tank dimensions were calculated with Eq. (D-6) and two different methods of estimating interfacial area (Appendix D). The results are given in Tables D.1 and D.2. Finally, a general modeling approach was attempted by simply obtaining a multiple regression fit (based on the SAS Program) for the data on hand but with no pre-determined rate expression. Results obtained for the general fit were used to predict DF curves for standard operating conditions. Also, the DFs predicted by Eq. (D-10) are included in a plot in which predicted DFs are compared with experimental DFs (Fig. D.2).

The best model for predicting DFs and scaled-up dimensions seems to be the one based on Eq. (D-10), using an empirical fit for  $a$  as a function of experimental small-scale DFs. It is suggested that further refinement of the general model approach would be useful if more data from properly designed factorial experiments were available.

### 5.1.3 Expressions for predicting DFs for krypton

In these derivations for empirical expressions of DFs for  $CO_2$  and krypton, emphasis was placed first on developing expressions for predicting DFs for  $CO_2$  because of the dependency of the DF for krypton on the DF for  $CO_2$ . Thus, models are presented in Appendix D that provide for DF estimates which could be obtained for  $CO_2$  in tanks of known dimensions for known hydrodynamic and physicochemical properties. For a desired DF and known hydrodynamic and physicochemical properties, the tank dimensions required to process any flow rate can also be estimated.

However, for a tractable process, it is necessary not only that the DF for  $CO_2$  be satisfactory, but also that the amount of krypton included in the  $CaCO_3$  product formed by  $CO_2$  fixation be kept to a minimum. Thus,

equations are presented which are capable of estimating DFs for krypton in a single continuous-slurry-flow gas-Ca(OH)<sub>2</sub> slurry contactor. As was discussed in Sect. 4.1, the primary DF for krypton is generally in the 100 to 200 range. However, this DF<sub>k</sub> can be greatly increased by provision of an add-on process (evacuation with slurry agitation was the best add-on treatment) following primary contactor treatment. No empirical fit was finalized for the experimental data obtained from the add-on reductions in krypton contained in the slurry. However, an expression is suggested in Appendix D which should adequately describe add-on DFs for krypton. Forsberg's<sup>13</sup> ideal-case calculations provide a basic form for an empirical expression which is adequate, with appropriate experimentally determined values for Henry's constant K, to describe the DFs for krypton obtained for two agitated contactors in series. The total DF for krypton during gas processing in two contactors in series then consists of primary and add-on DFs. The add-on DF can be described by the same type of expression utilized for the treatment following a single Ca(OH)<sub>2</sub> slurry contactor.

## 6. SUMMARY AND CONCLUSIONS

Experiments were conducted to determine the distribution of krypton during the fixation of CO<sub>2</sub> from simulated HTGR reprocessing off-gas in a mechanically agitated Ca(OH)<sub>2</sub> slurry. The DFs for CO<sub>2</sub> in the 10<sup>2</sup> to 10<sup>3</sup> range were feasible for CO<sub>2</sub> removal in single-stage contactors, and DFs for CO<sub>2</sub> of 10<sup>3</sup> to 10<sup>4</sup> were feasible for two-stage contactor operation. DFs for krypton were 100 to 200 for the primary contactor operation, and add-on DFs for krypton of 10<sup>2</sup> could be readily obtained by applying a vacuum to the stirred product slurry. DFs for krypton of 10<sup>3</sup> could easily be obtained for gas treatment with two contactors in series. Thus, total DFs for krypton of 10<sup>4</sup> to 10<sup>5</sup> could be obtained by using a combination of primary processes and add-on treatments. Best DFs for krypton were obtained for add-on treatment following operation of two contactors in series. It is important to note the definition of DFs for CO<sub>2</sub> and krypton:

$$\text{DF for CO}_2 = \frac{\text{moles of CO}_2 \text{ into contactor in feed gas}}{\text{moles of CO}_2 \text{ out in effluent gas}},$$

$$\text{DF for krypton} = \frac{\text{moles of krypton into contactor in feed gas}}{\text{moles of krypton in the slurry}}.$$

The following parametric relationships were experimentally established (relationships 1 through 4 were observed for CO<sub>2</sub> sorption in a single agitated slurry contactor):

1. For a 1.0 *m* Ca(OH)<sub>2</sub> slurry, the DFs for CO<sub>2</sub> varied inversely with gas superficial velocity, whereas the DFs for krypton had a slight direct variation with superficial velocity.
2. The DFs for CO<sub>2</sub> varied inversely with slurry molality in semibatch and continuous operation. The DFs for krypton varied directly with slurry molality for continuous contactor operation.
3. The DFs for CO<sub>2</sub> did not have a significant dependency on temperature for the range of 28 to 61°C. The dependency of DFs for krypton on temperature in the 28 to 61°C range also could not be accurately established.
4. The DFs for CO<sub>2</sub> vary directly with impeller speed. The DFs for krypton should vary slightly inversely with impeller speed, but this dependency was not established in these experiments.
5. For the gas-slurry interaction with two contactors in series, the overall DFs for CO<sub>2</sub> varied directly with the extent of the conversion of CO<sub>2</sub> that occurred in tank 2. For contactors-in-series operation, the overall DFs for krypton varied inversely with the extent of CO<sub>2</sub> conversion in tank 2.
6. The DFs for CO<sub>2</sub> varied directly with CO<sub>2</sub> concentration in the feed gas. The DFs for krypton varied inversely with CO<sub>2</sub> concentration in the feed gas.

7. Dependencies on process variables that were not established but could be inferred from literature models and correlations were as follows: the direct variation of DFs for  $\text{CO}_2$  with impeller diameter, soluble hydroxyl ion concentration, diffusivity of  $\text{CO}_2$  in the slurry, the liquid-side mass transfer coefficient, and the solubility of  $\text{CO}_2$  in the slurry.

The development of the most useful models for prediction of DFs for  $\text{CO}_2$  and krypton and for scaled-up contactor dimensions was dependent on expressions for the interfacial area. Interfacial area could be estimated either from a general hydrodynamic correlation or from an expression constructed from the experimental data of the bench-scale contactors of this study. For the latter case, the removal of  $\text{CO}_2$  in the agitated  $\text{Ca}(\text{OH})_2$  slurry could be adequately described by the following model:

$$\frac{1}{\text{DF}_{\text{cd}}} = 1 - \frac{\text{func}(\text{DF}_{\text{cd}}) H (\pi d_t^3 / 4) P_{\text{df}} [D_{\text{cd}} k_2 (\text{OH}_s^-) + k_L^2]^{0.5}}{y_{\text{cd},1} Q_t / (24.12) (60)}, \quad (22)$$

where

$$\text{func}(\text{DF}_{\text{cd}}) = a = 6.18 \text{DF}_{\text{cd}}^{-0.128}.$$

This model could be useful for predicting process DFs when the characteristics of the slurry [ $D_{\text{cd}}$ ,  $k_2$ ,  $U_t$ ,  $(\text{OH}_s^-)$ ,  $H$ ], the flow and feed conditions ( $Q_t$ ,  $k_L$ ,  $y_{\text{cd},1}$ ), and the tank size ( $d_1$  and  $d_t$ ) are known. It is perhaps more useful for predicting the dimensions of the contactor necessary to achieve a given DF for a specified gas flow rate and feed and slurry conditions.

If the expression in Eq. (22) is to be generally applicable for scale-up calculations, it is necessary that the functional relationship between  $a$  and  $\text{DF}_{\text{cd}}$  remain valid. That is, for a constant superficial velocity, the geometry and power input would have to be selected so that the interfacial area and the DF for  $\text{CO}_2$  in the larger contactor would be equal to those values measured in the experimental small contactor. For a treatment of the off-gas in a single contactor, the

DF for krypton is estimated by the expression

$$DF_k = \frac{K(1 - F_r) + F_r C}{F_r C}, \quad (9)$$

where K and C are known parameters of krypton-slurry interaction and  $F_r$  is related to  $DF_{cd}$  predicted by the model according to

$$F_r = 1 - \frac{y_{cd,i}}{DF_{cd} y_{cd,o}}. \quad (11)$$

For a combination of the primary  $CO_2$  removal process in stirred tanks followed by an add-on process to further reduce the krypton included in the product slurry, the following expressions appeared applicable.

The total DF for krypton using a single contactor is:

$$DF_{kt,1} = \frac{[K(1 - F_r) + F_r C]}{F_r C} C_1 t^{-C_2}. \quad (23)$$

The total DF for krypton using contactors in series is:

$$DF_{kt,2} = 1 + \frac{K^2}{F_r C} \left[ \frac{(1 - F_r)(1 - F_r + R_1 C)}{F_r C + L(1 - F_r)} \right] C_1 t^{-C_2}. \quad (24)$$

APPENDIX A: METHODS OF ANALYZING THE DISTRIBUTION OF  
 KRYPTON BETWEEN THE FEED GAS AND THE SOLID AND  
 LIQUID PHASES OF THE  $\text{CaCO}_3$  SLURRY

A.1 General Comments on Beta and Gamma Counting

The advantages of analyzing the krypton content by gamma counting have been summarized in Sect. 2.3. The major restriction on the use of gamma detection in this study was the quantity of  $^{85}\text{Kr}$  radiotracer required for runs with extended operation time. Regulations for ORNL Type C laboratories required that the amount of  $^{85}\text{Kr}$  used for each run be restricted to  $\sim 10$  mCi. A balance had to be maintained between total  $^{85}\text{Kr}$  activity, operating flow rate, and, thus, total feed-gas volume and resultant  $^{85}\text{Kr}$  concentration. Examples of possible operating conditions and radiotracer concentrations are as follows.

If 100 mCi of  $^{85}\text{Kr}$  were fed at a rate of 10 liters/min for 10 min to 15 liters of 1.0 *m*  $\text{Ca}(\text{OH})_2$  slurry in the 27.3-cm-ID contactor, and only 0.1% of the krypton was sorbed in that time, then 0.1 mCi of  $^{85}\text{Kr}$  would be contained in 15,000 ml of slurry. The resulting slurry concentration would be  $0.15 \times 10^5$  dpm/ml. Because the gamma emissions are only 0.4% of all the decay events, the maximum number of gamma counts, based on 50% efficiency in the gamma counter, would be

$$1.5 \times 10^4 \times 4 \times 10^{-3} \times 0.5 = 30 \text{ counts/min/ml},$$

or 150 counts/min for the 5-ml samples normally counted in the Searle gamma counter. For a total feed content of 10 mCi  $^{85}\text{Kr}$ , and 0.1% of the krypton included in the slurry, the approximate counting level would be 15 gamma counts/min for a 5.0-ml sample; for the same run and feed conditions, the beta count rate would be 750 counts/min/ml. For a 0.4-ml sample normally used in the beta counting technique, the count rate would be 300 counts/min.

Background for the Searle gamma counter was 25 counts/min. The standard deviation about this mean was  $\sim 4$ . The mean count rate for the beta counter was 225, with a standard deviation of  $\sim 15$ . Count rates were

not considered significant unless they exceeded the background by two standard deviations.

Based on these arguments, DFs of  $\sim 10^3$  could be measured for experiments in which the feed gas contained a total of 10 mCi of  $^{85}\text{Kr}$  by counting gamma emissions (the product would be  $\sim 15$  gamma counts/min above background). For the counting of beta emissions, a DF of  $\sim 10^3$  could be determined based on a count rate of 300 counts/min. However, because the beta counts could be reliably detected at the 30-counts/min level (above a background of  $\sim 225$ ), another DF factor of 10 could be measured for krypton. The total DF measurable with beta counting then became  $10^4$ .

Since the method of adding  $^{85}\text{Kr}$  to the feed gases was not exact, the  $^{85}\text{Kr}$  content generally ranged from  $10^7$  to  $10^8$  dpm (0.01 to 0.1 mCi) per liter (Table A.1).

Some DFs calculated for krypton for contactor-in-series operation using gamma counting were accurate up to  $2 \times 10^3$  because of an increase in gamma counting efficiency achieved during these studies (Table A.2).

## A.2 Procedure for Obtaining Beta and Gamma Counts

To obtain a balance for krypton based on beta emissions during a semibatch operation, the total dpm of krypton in the feed gas could be very accurately determined by quantitative counting in the calibrated in-line Levins<sup>14</sup> beta cell. The quantity of  $^{85}\text{Kr}$  included in the liquid portion of this slurry could be determined by counting portions of the liquid samples in a beta scintillation cocktail, after careful separation of the solids from the liquid. However, the efficiency of counting samples of  $^{85}\text{Kr}$  in the organic liquid scintillation system had to be determined.

In general, the addition of an aqueous solution to the standard beta detection scintillation cocktail\* results in spurious counting

---

\*The standard cocktail was prepared as follows: 6.0 g POPOP [1,4-bis-2-(5-phenyloxazolyl)-benzene], 0.15 g DPO (2,5-diphenyloxazole), 1005 ml toluene, and 445 ml Triton X-100.

Table A.1. Experimental results for krypton and CO<sub>2</sub> distributions during CO<sub>2</sub> fixation in semibatch and continuous agitated contactor operation

Run No.	Volumetric gas flow rates (std liters/min)	Inlet CO <sub>2</sub> mole fraction	Inlet Kr concentration (ppm)	Inlet <sup>85</sup> Kr concentration (dpm/liter)	Molality of Ca(OH) <sub>2</sub> slurry (g-mole/1000 g H <sub>2</sub> O)	Slurry flow rate (liters/min)	Slurry conversion (%)	Steady-state pH	Average temperature (°C)	Effluent CO <sub>2</sub> concentration (mole fraction)	Effluent Kr concentration (ppm)	DF <sub>cd</sub> , moles CO <sub>2</sub> in / moles CO <sub>2</sub> out	DF <sub>k</sub> , moles Kr in / moles Kr in slurry	DF <sub>k</sub> , moles Kr in / moles Kr in solids	<sup>85</sup> Kr remaining in slurry (dpm/liter)	<sup>85</sup> Kr in slurry flow (dpm/min of flow)
BR-2 <sup>a,b</sup>	9.2	0.91	88	1.4 x 10 <sup>9</sup>	1.00	-	>90	12.3	34	ND <sup>c</sup>	ND <sup>c</sup>	ND <sup>c</sup>	284 <sup>d</sup>	1022	1.2 x 10 <sup>8</sup>	-
BR-3 <sup>a,b</sup>	19.2	0.91	88	1.1 x 10 <sup>7</sup>	1.01	-	95 <sup>e</sup>	12.2	34	0.2100	960	38 <sup>e</sup>	409 <sup>d</sup>	ND	8.5 x 10 <sup>7</sup>	-
BR-4 <sup>a,b</sup>	34.3	0.92	44	2.1 x 10 <sup>8</sup>	1.00	-	98 <sup>e</sup>	12.2	34	0.5700	500	9 <sup>e</sup>	414 <sup>d</sup>	ND	2.0 x 10 <sup>7</sup>	-
CF-4 <sup>a</sup>	8.6	0.91	85	5.2 x 10 <sup>8</sup>	0.50	0.95	78	12.1	46	0.0030	ND	3,230	29 <sup>d</sup>	104	1.7 x 10 <sup>8</sup>	1.6 x 10 <sup>8</sup>
CF-5 <sup>a</sup>	13.2	0.90	ND <sup>(~80)</sup>	2.9 x 10 <sup>8</sup>	0.50	0.90	95 <sup>e</sup>	11.8	46	ND	ND	ND	70 <sup>d</sup>	ND	5.7 x 10 <sup>7</sup>	5.1 x 10 <sup>7</sup>
CF-6 <sup>a</sup>	16.0	0.91	50	2.4 x 10 <sup>8</sup>	1.00	0.80	86	12.0	46	0.0186	595	535	128 <sup>d</sup>	ND	3.9 x 10 <sup>7</sup>	3.2 x 10 <sup>7</sup>
CF-5 <sup>a</sup>	19.2	0.91	72	2.7 x 10 <sup>8</sup>	1.06	1.00	78	12.1	46	0.0590	ND	143	130 <sup>d</sup>	ND	4.5 x 10 <sup>7</sup>	4.5 x 10 <sup>6</sup>
CF-1B <sup>f</sup>	34.2	0.97	38	4.3 x 10 <sup>7</sup>	0.94	2.00	71	12.0	46	0.0320	378	946	24	ND	3.0 x 10 <sup>6</sup>	6.1 x 10 <sup>6</sup>
BR-1C <sup>b,f</sup>	11.4	0.91	47	3.4 x 10 <sup>7</sup>	1.00	-	91	12.3	40	0.0046	882	2,200	185	ND	6.8 x 10 <sup>6</sup>	-
CF-10 <sup>f</sup>	35.1	0.88	33	2.4 x 10 <sup>7</sup>	0.99	2.00	72	12.1	45	0.0320	250	215	138	ND	3.0 x 10 <sup>6</sup>	6.1 x 10 <sup>6</sup>
BR-10 <sup>f,b</sup>	35.1	0.88	33	2.4 x 10 <sup>7</sup>	0.99	-	82	12.2	33	0.0430	250	158	132	ND	3.7 x 10 <sup>6</sup>	-
BR-11 <sup>f,b</sup>	16.4	0.88	33	2.4 x 10 <sup>7</sup>	0.99	-	74	12.2	32	0.0060	260	1,096	213	745	2.2 x 10 <sup>6</sup>	-
BR-12 <sup>f,b</sup>	10.9	0.88	23	2.4 x 10 <sup>7</sup>	0.99	-	65	12.3	33	0.0050	199	1,315	142	497	2.7 x 10 <sup>6</sup>	-
BR-13 <sup>f,b</sup>	8.7	0.88	23	2.4 x 10 <sup>7</sup>	0.73	-	64	12.3	33	ND	ND	ND	78	ND	3.9 x 10 <sup>5</sup>	-
CF-11 <sup>f</sup>	5.4	0.90	18	3.4 x 10 <sup>6</sup>	0.49	1.00	33	12.5	28	0.0007	161	12,772	47	ND	3.8 x 10 <sup>5</sup>	3.8 x 10 <sup>5</sup>
CF-12 <sup>f</sup>	11.7	0.90	18	3.4 x 10 <sup>6</sup>	0.49	1.10	79	12.3	35	0.0056	177	1,638	63	ND	6.3 x 10 <sup>5</sup>	6.3 x 10 <sup>5</sup>
CF-13 <sup>f</sup>	17.5	0.90	18	3.4 x 10 <sup>6</sup>	0.49	1.50	83	12.4	35	0.0077	161	1,188	64	ND	6.1 x 10 <sup>5</sup>	9.2 x 10 <sup>5</sup>
CF-14 <sup>f</sup>	24.6	0.90	18	3.4 x 10 <sup>6</sup>	1.94	0.60	80	11.8	57	ND	179	ND	477	ND	2.9 x 10 <sup>5</sup>	1.7 x 10 <sup>5</sup>
CF-15 <sup>f</sup>	24.8	0.90	18	3.4 x 10 <sup>6</sup>	1.94	0.60	97 <sup>e</sup>	10.5	38	0.1470	175	53 <sup>e</sup>	337	ND	4.1 x 10 <sup>5</sup>	2.5 x 10 <sup>5</sup>
CF-17 <sup>f</sup>	25.1	0.90	172 <sup>g</sup>	5.9 x 10 <sup>7</sup>	1.95	0.60	89	12.3	34	0.0300	1,846	280	ND	ND	ND	ND
CF-18 <sup>f</sup>	13.2	0.90	172 <sup>g</sup>	5.9 x 10 <sup>7</sup>	1.95	0.50	75	12.5	30	0.0190	1,906	444	145	ND	1.1 x 10 <sup>6</sup>	5.4 x 10 <sup>6</sup>
CF-19 <sup>f</sup>	23.7	0.90	172 <sup>g</sup>	5.9 x 10 <sup>7</sup>	1.97	0.60	85	11.9	61	0.0300	1,756	282	443	ND	5.3 x 10 <sup>6</sup>	3.2 x 10 <sup>6</sup>
CF-20 <sup>f</sup>	14.4	0.91	180 <sup>g</sup>	6.2 x 10 <sup>7</sup>	1.03	0.70	79	12.1	43	0.0055	1,836	1,840	144	ND	8.9 x 10 <sup>6</sup>	6.3 x 10 <sup>6</sup>
CF-21 <sup>f</sup>	25.4	0.91	180 <sup>g</sup>	6.2 x 10 <sup>7</sup>	1.02	1.10	81	12.0	46	0.0096	1,902	1,053	172	ND	8.4 x 10 <sup>6</sup>	9.2 x 10 <sup>7</sup>
CF-22 <sup>f</sup>	24.3	0.91	180 <sup>g</sup>	6.2 x 10 <sup>7</sup>	1.02	1.10	87	12.1	28	0.0099	1,960	1,018	102	311	1.4 x 10 <sup>7</sup>	1.5 x 10 <sup>7</sup>
CF-23 <sup>f</sup>	18.6	0.93	18	3.4 x 10 <sup>8</sup>	0.97	0.80	90	12.1	44	0.0052	177	1,471	158	437	5.0 x 10 <sup>7</sup>	4.0 x 10 <sup>7</sup>
CF-24 <sup>f</sup>	20.8	0.88	18	3.4 x 10 <sup>8</sup>	1.02	0.80	91 <sup>e</sup>	11.9	46	0.0120	ND	640 <sup>e</sup>	189	576	4.7 x 10 <sup>7</sup>	3.8 x 10 <sup>7</sup>

<sup>a</sup>20.3-cm-ID contactor.<sup>b</sup>Indicates semibatch operation; all other operations with continuous slurry flow.<sup>c</sup>Not determined.<sup>d</sup>DFs for <sup>85</sup>Kr determined by analysis of gamma counting; otherwise, <sup>85</sup>Kr was determined from beta counts.<sup>e</sup>Low DF<sub>cd</sub> because of excessive slurry conversion (>90%).<sup>f</sup>27.3-cm-ID contactor.<sup>g</sup>Commercial gas mixture (all others blended in-house). Also, contained 60 ppm xenon, 7% O<sub>2</sub>, and 2% N<sub>2</sub>.

Table A.2. Experimental results for krypton and CO<sub>2</sub> distributions during CO<sub>2</sub> fixation with contactors in series<sup>a</sup>

Contactor ID (cm)	Run No.	Volumetric gas flow rates (std liters/min)	Inlet CO <sub>2</sub> mole fraction	Inlet Kr concentration (ppm)	Molality of Ca(OH) <sub>2</sub> slurry (g-mole/1000 g H <sub>2</sub> O)	Slurry flow rate (liters/min)	Slurry conversion (%)	Steady-state pH	Average temperature (°C)	DF <sub>cd</sub> , moles CO <sub>2</sub> in / moles CO <sub>2</sub> out	DF <sub>k</sub> <sup>b</sup> , moles Kr in / moles Kr in slurry	DF <sub>ks</sub> , moles Kr in / moles Kr in solids
1-27.3	C1S-1	ND <sup>c</sup>	ND <sup>c</sup>	ND <sup>c</sup>	0.99	1.10	86	11.95	38	ND <sup>c</sup>	138	276
2-20.3	C1S-1	24.3	0.92	54	ND	1.10	100	6.6	38	ND	9.2/1267	2,534
1-27.3	C1S-1	ND	ND	ND	1.02	1.0	60	12.3	38	6,577	158	ND
2-27.3	C1S-1	25.3	0.91	180 <sup>d</sup>	ND	1.0	100	6.1	38	ND	5/793	ND
1-27.3	C1S-2	ND	ND	ND <sup>d</sup>	1.00	0.6	62	12.5	38	20,000	111	ND
2-27.3	C1S-2	11.4	0.91	180 <sup>d</sup>	ND	0.6	100	6.7	38	ND	4.3/475	ND
1-27.3	C1S-3	ND	ND	ND <sup>d</sup>	1.00	1.6	60	12.3	29	2,658	140	ND
2-20.3	C1S-3	36.4	0.92	142 <sup>d</sup>	ND	1.6	100	6.7	29	ND	4.1/578	ND
1-27.3	C1S-4	ND	ND	ND <sup>d</sup>	0.95	1.75	74	12.2	37	1,405	100	ND
2-20.3	C1S-4	34.7	0.93	142 <sup>d</sup>	ND	1.75	100	6.1	37	ND	13.8/1386	ND
1-27.3	C1S-5	ND	ND	ND <sup>d</sup>	0.94	1.75	65	12.3	39	2,418	103	ND
2-20.3	C1S-5	13.6	0.90	185 <sup>d</sup>	ND	1.75	100	5.9	39	ND	7.9/817	ND
1-27.3	C1S-6	ND	ND	ND <sup>d</sup>	0.97	0.7	69	12.25	43	10,168	118	ND
2-27.3	C1S-6	10.7	0.90	185 <sup>d</sup>	ND	0.7	100	5.9	43	ND	7.8/925	ND

<sup>a</sup>Inlet <sup>85</sup>Kr concentrations varied from  $6.1 \times 10^7$  to  $2.6 \times 10^8$  dpm/liter.

<sup>b</sup>Based on beta counts.

<sup>c</sup>Not determined.

<sup>d</sup>Commercial gas mixture. Also, contained 60 ppm xenon, 7% O<sub>2</sub>, and 2% N<sub>2</sub>.

effects. The efficiency for detection of  $^{85}\text{Kr}$  by beta counting in the scintillation cocktail was established as follows. The efficiency of the Searle gamma counter (Series 1185, Searle Analytic, Inc., Des Plaines, Illinois) for measuring gamma emissions from  $^{85}\text{Kr}$  was established by counting known quantities of  $^{85}\text{Kr}$  which were contained in sealed glass ampules. These standard  $^{85}\text{Kr}$  samples (4.2, 11.4, and 12.9  $\mu\text{Ci}$ ) had been prepared for the KALC campaign.<sup>21</sup> Prior to analysis in the Searle counter, the  $^{85}\text{Kr}$  content was corrected for decay time since preparation. Once the efficiency of the gamma counter for counting  $^{85}\text{Kr}$  was established (31% for most of these studies), identical samples of slurry were analyzed for their beta and gamma emission content as follows.

At the end of a typical experiment, samples (in triplicate) to be analyzed for beta emissions were transferred immediately to screw-capped vials (vials were essentially completely filled). The vials were capped and spun in a tabletop centrifuge at  $\sim 6000$  rpm (Model CL, International Clinical Centrifuge, International Equipment Co., Needham Hts., Mass.). The vials were then opened, and a 0.4-ml sample of the clear liquid supernatant (solid  $\text{CaCO}_3$  collected as a precipitate in the vial bottom) was added to 10 ml of standard liquid scintillation cocktail. The beta counts were then determined in the New England Nuclear beta emission counter. Five milliliter samples (in triplicate) of the same slurry were transferred to the appropriate vials and placed in the Searle gamma counter for analysis. Once the true amount of  $^{85}\text{Kr}$  in 5.0 ml of slurry was established with the calibrated Searle gamma counter, a factor for correcting the number of counts per minute in the beta counter for 0.4 ml liquid was obtained; hence, the actual disintegrations per minute in the 5.0-ml slurry sample could be calculated. Thus, in some tests, when residual krypton was too low for gamma counting and the beta counts were determined for the supernatant of centrifuged samples, the correction factor could be supplied to predict the actual disintegrations per minute of  $^{85}\text{Kr}$  in the product slurry. For example, when the beta liquid scintillation

results for 0.4 ml of supernatant from the  $\text{CaCO}_3$  product slurry were 4100 counts/min, the total counts were

$$\frac{4100 \text{ counts/min}}{0.4 \text{ ml}} \times \frac{1000 \text{ ml}}{\text{liter}} = 10.25 \times 10^6 \text{ beta counts/min per liter of}$$

liquid. Gamma liquid scintillation counts for 5 ml of the same slurry (including krypton in both liquid and solid phases) were 105 counts/min. The total dpm were:

$$\frac{21 \text{ counts/min}}{\text{ml}} \times \frac{1000 \text{ ml}}{\text{liter}} \times \frac{\text{gamma dpm}}{0.31 \text{ counts/min}} \times \frac{\text{total dpm}}{0.0041 \text{ gamma dpm}} =$$

$$1.65 \times 10^7 \frac{\text{dpm}}{\text{liter of slurry}}$$

$$\text{Correction factor} = \frac{10.25 \times 10^6 \text{ counts/min of beta/liter of liquid}}{16.5 \times 10^6 \frac{\text{dpm of krypton}}{\text{liter of slurry}}} = 0.62.$$

The aqueous samples were allowed to cool in the refrigerated counter and were then shaken immediately prior to assay in order to attain consistent counting of the samples in the liquid scintillation system. The major assumption in this technique is that the relative amounts of krypton in the liquid and solid portions of the slurry were about the same, regardless of operating conditions (different slurry molarities, slurry temperature, gas flow rate, etc.). The reasonableness of this assumption is shown in Table A.3.

As shown in Table A.4, the residual krypton in the product slurry in many of the runs was sufficiently large to be determined by both beta and gamma counting. In general, the DFs for krypton obtained by analysis of beta emissions (using the correction factor) were in excellent agreement with those obtained by counting of gamma emissions, for a wide range of operating conditions.

Thus, in those runs where the residual  $^{85}\text{Kr}$  was too low to be detected by gamma counting (Table A.1), there was confidence in those DFs for krypton that were estimated by the beta counting technique.

The distributions determined by gamma counting were usually slightly higher than those obtained by beta counting (Table A.4). One possible

Table A.3. Experimental results for the distribution of  $^{85}\text{Kr}$  between solid and liquid phases of the  $\text{CaCO}_3$  slurry

Gas feed rate, $Q_t$ (std liters/min)	Contactore diameter, $d_t$ (cm)	Impeller speed, $n$ (rpm)	Temp. ( $^{\circ}\text{C}$ )	Gamma counts for 5 ml of liquid	Gamma counts for 0.5 g of solids plus 0.5 g of included water	Gamma counts per ml of liquid	Gamma counts of recoverable wet solids in 1 liter of slurry	Gamma counts in the liquid portion of 1 liter of slurry	Total gamma counts per liter of slurry	DF for discharge or recycle of $\sim 800$ ml of free water
10.0	20.3	800	46	7100	2200	1420	$4.4 \times 10^5$	$11.40 \times 10^5$	$15.8 \times 10^5$	3.59
9.5	20.3	800	46	4600	2000	920	$4.0 \times 10^5$	$7.36 \times 10^5$	$11.36 \times 10^5$	2.84
25.0	27.3	650	46	160	50	32	$1.0 \times 10^4$	$2.56 \times 10^4$	$3.56 \times 10^4$	3.56
20.8	27.3	650	46	475	185	95	$3.7 \times 10^4$	$7.60 \times 10^4$	$11.30 \times 10^4$	3.05

Table A.4. Comparison of experimental methods for  
detection of  $^{85}\text{Kr}^a$   
(beta count determination vs gamma count determination)

Run No.	Gas flow rate (std liters/min)	Superficial velocity (cm/min)	DF calculated with beta counts	DF calculated with gamma counts
BR-2	9.2	28	--	284
CF-3	13.2	41	--	70
CF-5	19.2	59	--	130
CF-6	16.0	49	--	128
BR-10	35.1	60	132	157
BR-12	10.9	19	142	205
CF-20	14.4	25	144	--
CF-21	25.4	43	172	--
CF-22	25	42	102	--
CF-23	18.6	32	158	171
CF-24	20.8	36	189	243
C1S-1	25.3	43	793	1000
C1S-2	11.4	20	475	548
C1S-3	36.4	112	526	630
C1S-4	34.7	107	1386	1920
C1S-5	13.6	42	816	820
C1S-6	10.7	18	925	820

<sup>a</sup>Slurry molality  $\approx 1.0$  m.

reason for this trend was that the absolute gamma counts were lower relative to background; thus, there was more uncertainty in actual net gamma counts. Regardless of the causes of the slight deviations in krypton distribution calculated by the two analyses, the deviations were considered to be insignificant in view of the ease with which the krypton included in the product slurry could be removed in subsequent add-on processes, or by simple exposure to the atmosphere.

### A.3 Distribution of Krypton in the Solid and Liquid Phases of the Slurry

After primary processes in which  $\text{CO}_2$  was removed from the simulated HTGR fuel reprocessing off-gas during continuous operation of the agitated contactor, the DFs for krypton were  $\sim 1.5 \times 10^2$ . The amount of krypton in the slurry was essentially controlled by the equilibrium relationship for krypton based on its concentration in the slurry and an average concentration in the gas phase. The concentration must be expressed as an average because of the shrinkage in the gas flow while in transit through the contactor by a factor of  $\sim 10$  (for 90%  $\text{CO}_2$  feeds). The krypton remained in the slurry as long as there was krypton in the gas phase--either bubbling through the slurry or as a cover gas for the slurry. However, continued exposure of the slurry to a cover gas or sparge gas without krypton always resulted in very rapid removal of krypton from the slurry (see Fig. 6).

Thus, efforts to ascertain the distribution of the krypton between the solid and liquid phases of the slurry were always complicated by the rapid rate at which krypton was lost from either phase to the ambient air. Although this behavior complicated analytical tests for krypton, the argument that  $\text{CO}_2$  fixation could be conducted prior to krypton removal was certainly supported by the absence of any sizeable absorptive or adsorptive attraction of krypton to the  $\text{CaCO}_3$  product slurry.

The determination of krypton in the dry  $\text{CaCO}_3$  solid was not practical because any routine method used to dry the wet  $\text{CaCO}_3$  solids resulted in the complete loss of krypton to the atmosphere. Thus, a technique was

developed to count the krypton in the  $\text{CaCO}_3$  in the wet solid state. This technique, as previously outlined, was based on the separation of wet solids from the slurry by centrifugation as follows. Initial slurry samples were removed immediately at the end of a run and loaded into screw-capped vials until the vials were virtually full. It was necessary to fill the sample bottles as full as possible in order to minimize the loss of krypton from the slurry to the gas space above the slurry. After the vials were centrifuged, the free-water supernatant was removed from the vials and placed in a separate screw-capped vial for counting of gamma emissions. The remaining solid precipitate in the vial was also analyzed for gamma emissions.

For most of the cases studied, the amount of krypton in the slurry was distributed as shown in Table A.3. Because of the loss of krypton from the free-water supernatant during transfer for gamma counting, considerable scatter occurred in the data. Thus, the ratios of krypton in the supernatant to krypton in the wet solids (as can be obtained from Table A.3) should be considered conservatively low. These ratios are in the range of  $\sim 2$  or  $3$  to  $1$ . There were generally  $\sim 800$  ml of free water per liter of slurry which could be recovered either by centrifugation or filtration.

In general, then, it could be argued that the krypton level in the wet solids would have been due solely to sorption in the included water. Thus, a ratio of krypton in the supernatant to krypton in the solids would have been  $\sim 8:1$ . However, in all cases studied, the krypton in the wet centrifuged solids was higher than that expected for included water only, resulting in experimental ratios, as noted above, of  $\sim 2:1$  or  $3:1$ . It is possible that the centrifugation process itself could have resulted in some concentration by entrapping krypton into the wet solids of the sample vials. However, the alternative method of separating the solids from the free water by gravity settling was not a viable alternative because of the slow settling rate and poor phase separation. In some cases, identical samples from the same run were both centrifuged and allowed to settle by gravity. In either case, the ease with which krypton could be removed by add-on processes from the supernatant and wet solids did not

appear to be a function of the method of solid-free water separation. The level of krypton for these determinations was obtained by counting total slurry content, without attempting to separate the solids from the free water.

In summary, it appeared that there was more krypton in the solids recovered by centrifugation than was expected from simple absorption in the included water of the solids. However, the subsequent simplicity with which the krypton could be removed from 1 liter of slurry, including both solid and liquid phases, alleviated any concern about the uncertainties of the solid-liquid distribution. It should be stressed that when samples of slurry were analyzed after add-on processes, the slurry was always counted for both beta and gamma emissions. Thus, the high DFs obtained for krypton removal as shown in Table A.5 were based on: (1) accurate detection of low levels of gamma counts, (2) corroborative detection of the higher concentration of beta emissions, or (3) detection of the higher concentration of beta emissions when the gamma counts were statistically insignificant. In some cases, DFs for krypton were too high to be detected even by analysis of beta emissions, as can be seen in Table A.5.

There appeared to be  $\sim 100$  g of  $H_2O$  closely associated with the 100 g of  $CaCO_3$  [for complete conversion of a 1.0  $\underline{m}$   $Ca(OH)_2$  slurry] in 1 liter of slurry. There is a possibility that this  $H_2O$  was  $H_2O$  of hydration. Mellor<sup>22</sup> has reported that  $CaCO_3 \cdot 6H_2O$  can be produced by reaction between  $CO_2$  and  $Ca(OH)_2$  slurries at  $\sim 2^\circ C$ . Thus, it should not be stable at room temperature for any length of time. In limited tests of the stability of our wet solids product, the  $H_2O$  was removed by heating  $\sim 70^\circ C$  for 2 to 3 hr, or by drying in an open vessel overnight. No tests were designed to determine the distribution of the krypton in the solid-included water product before  $H_2O$  removal. This approach was adopted primarily because the loss of krypton from the solid product, before water removal, was extremely rapid when (1) exposed to air, (2) exposed to vacuum, or (3) heated. Thus, the crystalline form of the solid  $CaCO_3$  product and the nature of the water-solid interaction became more of academic interest than practical significance because of the results observed

Table A.5. Experimental results for add-on treatment for krypton reduction of primary process slurries

Treatment No.	Run No. for product slurry	Sparge gas flow rate (std liters/min)	Absolute pressure (in. Hg)	Absolute pressure (Pa)	Contactor ID and slurry volume	Treatment time (min)	dpm/liter before treatment, based on beta counts/min	dpm/liter after treatment, based on beta counts/min	dpm/liter before treatment, based on gamma counts/min	dpm/liter after treatment, based on gamma counts/min	Based on beta emissions			Based on gamma emissions		
											Primary DF	Add-on DF	Total DF	Primary DF	Add-on DF	Total DF
TR13	CF-5 <sup>a</sup>	0	7.9	$2.675 \times 10^4$	20.3 cm, 7 liters	10	ND <sup>b</sup>	ND <sup>b</sup>	$1.2 \times 10^7$	$3.2 \times 10^5$	ND <sup>b</sup>	ND <sup>b</sup>	ND <sup>b</sup>	130	36.5	4745
TR14	CF-6 <sup>a</sup>	O <sub>2</sub> /10.3	29.9	$1.01 \times 10^5$	20.3 cm, 7 liters	10	ND	ND	$5.1 \times 10^7$	$1.1 \times 10^6$	ND	ND	ND	128	45.4	5828
TR16	CF-7 <sup>a</sup>	CO <sub>2</sub> /3.90	29.9	$1.01 \times 10^5$	20.3 cm, 7 liters	10	ND	ND	$4.1 \times 10^7$	$1.6 \times 10^6$	ND	ND	ND	74	26	1924
TR17	BR-1D <sup>c</sup>	0	29.9	$1.01 \times 10^5$	27.3 cm, 17 liters	5	$4.2 \times 10^6$	$5.0 \times 10^6$	$3.9 \times 10^6$	$6 \times 10^6$	185	~0.8	~145	ND	ND	ND
TR16	BR-1A <sup>c</sup>	Air/20	29.9	$1.01 \times 10^5$	27.3 cm, 17 liters	3	ND	$4.4 \times 10^5$	ND	ND	ND	ND	4394	ND	ND	ND
TR22	CF-10 <sup>c</sup>	0	9.9	$2.68 \times 10^4$	27.3 cm, 17 liters	5	$3.04 \times 10^6$	$1.3 \times 10^5$	IC <sup>d</sup>	IC	138	22.6	3116	IC	IC	IC
TR23	BR-10 <sup>c</sup>	0	9.9	$2.68 \times 10^4$	27.3 cm, 17 liters	10	$3.7 \times 10^6$	$7.5 \times 10^4$	$3.1 \times 10^6$	IC	131	~50.0	~6550	157	IC	IC
TR24	BR-11 <sup>c</sup>	0	9.9	$2.68 \times 10^4$	27.3 cm, 17 liters	10	$2.1 \times 10^6$	<10 <sup>4</sup>	$2.9 \times 10^6$	IC	213	>10 <sup>2</sup>	>10 <sup>4</sup>	115	IC	IC
TR25	BR-12 <sup>c</sup>	0	9.9	$2.68 \times 10^4$	27.3 cm, 17 liters	10	$2.7 \times 10^6$	<10 <sup>4</sup>	$1.85 \times 10^6$	IC	142	>10 <sup>2</sup>	>10 <sup>4</sup>	205	IC	IC
TR26	BR-13 <sup>c</sup>	0	9.9	$2.68 \times 10^4$	27.3 cm, 17 liters	10	$3.9 \times 10^6$	<10 <sup>4</sup>	ND	ND	78	>10 <sup>2</sup>	>10 <sup>4</sup>	ND	ND	ND
TR30	CF-24 <sup>c</sup>	0	9.9	$2.68 \times 10^4$	27.3 cm, 17 liters	5	$4.7 \times 10^7$	$6.5 \times 10^6$	$4.5 \times 10^7$	$4.2 \times 10^6$	189		1380	243	10.7	2600

<sup>a</sup> Impeller speed - 800 rpm.<sup>b</sup> Not determined.<sup>c</sup> Impeller speed - 650 rpm.<sup>d</sup> Insufficient counts above background.

for the loss of krypton when the slurry products from the primary processes were treated for further krypton removal.

Finally, it should be noted that during actual process operations, the wet solids (with included water) could be separated from the free water. The free water could be stripped of the krypton and recycled back to the CO<sub>2</sub> fixation contactor. Thus, even without further removal of krypton from the wet solids (which could be easily attained), additional DFs, as indicated in the last column of Table A.3, would be achieved.

#### A.4 Definitions of DFs for Krypton

$$\text{Primary DF} = \frac{\text{dpm/min into contactor in influent gas}}{\text{dpm/min out in slurry prior to treatment}} \quad (\text{A-1})$$

Using beta emission counting in liquid scintillation cocktails,

$$\text{Primary DF} = \frac{\text{influent}}{\text{effluent}}, \text{ or}$$

$$\frac{\frac{\text{gas, beta counts/min}}{22\text{-ml flow cell}} \frac{1000 \text{ ml}}{\text{liter of gas}} (\text{gas flow, liters/min})}{\frac{\text{liquid, beta counts/min}}{0.4 \text{ ml}} \frac{1000 \text{ ml}}{\text{liter}} \frac{\text{dpm}}{0.6 \text{ counts/min}}} \times \frac{\text{dpm}}{0.136 \text{ counts/min}} \frac{1}{(\text{slurry flow rate, liters/min})} ; \quad (\text{A-2})$$

$$\text{Primary DF with gamma} = \frac{\frac{\text{gas, beta counts/min}}{22\text{-ml flow cell}} \frac{1000 \text{ ml}}{\text{liter of gas}}}{\frac{\text{gamma, counts/min}}{5\text{-ml slurry}} \frac{1000 \text{ ml}}{\text{liter of slurry}}} \times \frac{(\text{gas flow, liters/min}) \frac{\text{dpm}}{0.136 \text{ counts/min}}}{\frac{\text{dpm}}{0.31 \text{ counts/min}} (\text{slurry flow rate, liters/min})} \quad (\text{A-3})$$

$$\begin{aligned} \text{But overall DF} &= \frac{\text{dpm/min in influent gas}}{\text{dpm/min out in slurry after treatment}} \\ &= \text{primary DF} \times \text{add-on DF} , \end{aligned} \quad (\text{A-4})$$

where

$$\text{add-on DF} = \frac{\text{dpm/min in slurry before treatment}}{\text{dpm/min in slurry after treatment}} . \quad (\text{A-5})$$

$$\begin{aligned} \text{Add-on DF} &= \frac{\frac{\text{liquid, counts/min}}{0.4 \text{ ml}} \cdot \frac{1000 \text{ ml}}{\text{liter}} \cdot \frac{\text{dpm}}{0.6 \text{ counts/min}}}{\frac{\text{liquid, counts/min}}{0.4 \text{ ml}} \cdot \frac{1000 \text{ ml}}{\text{liter}} \cdot \frac{\text{dpm}}{0.6 \text{ counts/min}}} \\ \text{with beta} & \times \frac{(\text{primary tank slurry flow rate, liters/min})}{(\text{slurry flow from holding tank, liters/min})} . \end{aligned} \quad (\text{A-6})$$

$$\begin{aligned} \text{Add-on DF} &= \frac{\frac{\text{gamma, counts/min}}{5\text{-ml slurry}} \cdot \frac{1000 \text{ ml}}{\text{liter}} \cdot \frac{\text{dpm}}{0.31 \text{ counts/min}}}{\frac{\text{gamma, counts/min}}{5\text{-ml slurry}} \cdot \frac{1000 \text{ ml}}{\text{liter}} \cdot \frac{\text{dpm}}{0.31 \text{ counts/min}}} \\ \text{with gamma} & \times \frac{(\text{primary tank slurry flow rate, liters/min})}{(\text{slurry flow from holding tank, liters/min})} . \end{aligned} \quad (\text{A-7})$$

APPENDIX B: DEVELOPMENT OF THEORETICAL EQUATIONS TO CALCULATE  
DFs FOR KRYPTON ( $DF_k$ ) AND FOR  $CO_2$  ( $DF_{cd}$ ) AND TO SHOW THE  
DEPENDENCY OF  $DF_k$  ON  $DF_{cd}$

B.1 An Expression for  $DF_{cd}$

Definitions:

$F_{cd}$  =  $CO_2$  molar flow rate, g-moles/sec;

$F_{n,o}$  = inert flow out ( $O_2$ ,  $N_2$ , Xe, Kr, etc), g-moles/sec;

$F_{n,i}$  =  $F_{n,o}$  (good assumption because of the large fraction of  $O_2$  and  $N_2$   
in the inerts);

$F_r$  = fraction of incoming gas reacting with the  $Ca(OH)_2$ ;

$F_{t,i}$  = total gas flow rate in, g-moles/sec;

$F_{t,o}$  = total gas flow rate out, g-moles/sec;

$L$  = total molar liquid flow rate, g-moles/sec ( $i = in, o = out$ );

$y_{cd}$  =  $CO_2$  m.f. in the gas phase, ( $i = in, o = out$ );

$y_n$  = inert gas mole fraction ( $i = in, o = out$ );

$y_k$  = krypton m.f. in the gas phase ( $i = in, o = out$ );

$x_k$  = krypton m.f. in the liquid phase ( $i = in, o = out$ ).

The fraction of incoming gas reacting with the  $Ca(OH)_2$  slurry, assuming

$F_{n,i} = F_{n,o}$ , is

$$F_r = \frac{F_{t,i} - F_{t,o}}{F_{t,i}} = \frac{F_{cd,i} - F_{cd,o}}{F_{t,i}} \quad (B-1)$$

because

$$F_{t,o} = F_{cd,o} + F_{n,o} \quad (B-2)$$

and

$$F_{t,i} = F_{cd,i} + F_{n,i} \quad (B-3)$$

From Eq. (B-3),

$$F_{t,i} = y_{cd,i} F_{t,i} + y_{n,i} F_{t,i} \quad (B-4)$$

But

$$y_{n,i} = 1 - y_{cd,i} \quad (B-5)$$

or

$$F_{n,i} = (1 - y_{cd,i}) F_{t,i} \quad (B-6)$$

$$F_{n,o} = F_{n,i} = (1 - y_{cd,i}) F_{t,i} \quad (B-7)$$

$$F_{n,o} = (1 - y_{cd,o}) F_{t,o} \quad (B-8)$$

Also, Eqs. (B-7) and (B-8) are used to set  $F_{t,o}$  as a function of measurable quantities.

$$F_{t,o} = \frac{F_{n,o}}{(1 - y_{cd,o})} = \frac{(1 - y_{cd,i}) F_{t,i}}{(1 - y_{cd,o})} \quad (B-9)$$

Now DF for  $CO_2$  is defined as

$$DF_{cd} = \frac{F_{cd,i}}{F_{cd,o}} = \frac{\text{moles } CO_2 \text{ in}}{\text{moles } CO_2 \text{ out}} \quad (B-10)$$

Flow rates  $F_{cd,i}$  and  $F_{cd,o}$  are given by

$$F_{cd,i} = y_{cd,i} F_{t,i} \quad (B-11)$$

and

$$F_{cd,o} = y_{cd,o} F_{t,o} = y_{cd,o} \frac{(1 - y_{cd,i}) F_{t,i}}{(1 - y_{cd,o})} \quad (B-12)$$

Equations (B-10), (B-11), and (B-12) are combined to give an expression for  $DF_{cd}$ :

$$DF_{cd} = \frac{y_{cd,i} F_{t,i}}{y_{cd,o} \frac{(1 - y_{cd,i}) F_{t,i}}{(1 - y_{cd,o})}} = \frac{y_{cd,i}}{y_{cd,o} \frac{(1 - y_{cd,i})}{(1 - y_{cd,o})}} \quad (B-13)$$

Now, using Eq. (B-1) for  $F_r$  and Eq. (B-9) for  $F_{t,o}$ , we obtain

$$F_r = \frac{F_{t,i} - \frac{(1 - y_{cd,i}) F_{t,i}}{(1 - y_{cd,o})}}{F_{t,i}}, \quad (B-14)$$

which is simplified to

$$F_r = 1 - \frac{(1 - y_{cd,i})}{(1 - y_{cd,o})}. \quad (B-15)$$

Equations (B-13) and (B-15) are combined to give  $F_r$  as a function of  $DF_{cd}$ :

$$F_r = 1 - \frac{y_{cd,i}}{DF_{cd} y_{cd,o}}. \quad (B-16)$$

## B.2 Relationship Between $DF_k$ and $DF_{cd}$

Because  $F_r$  appears in the expressions for  $DF_k$ , the relationship between  $DF_k$  and  $DF_{cd}$  can be derived from Eq. (B-16) and expressions for  $DF_k$  developed in this section.

The krypton balance for a single continuous-flow contactor is

$$y_{k,i} F_{t,i} = y_{k,o} F_{t,o} + x_{k,o} L_o. \quad (B-17)$$

$DF_k$  is defined as

$$DF_k = \frac{\text{krypton into contactor in gas}}{\text{krypton out of contactor in slurry}}, \quad (B-18)$$

or

$$DF_k = \frac{y_{k,i} F_{t,i}}{x_{k,o} L_o}. \quad (B-19)$$

From Eqs. (B-17) and (B-19),

$$DF_k = \frac{y_{k,o} F_{t,o} + x_{k,o} L_o}{x_{k,o} L_o}. \quad (B-20)$$

To put this equation into a more general form, expressions are needed for  $x_{k,o}$ ,  $L_o$ , and  $F_{t,o}$ . From Eq. (B-1) we get

$$F_r F_{t,i} = F_{t,i} - F_{t,o} , \quad (B-21)$$

or

$$F_{t,o} = F_{t,i} (1 - F_r) . \quad (B-22)$$

For the major equilibrium assumptions, different expressions for  $DF_k$  can be derived with different forms for  $x_{k,o}$ :

$$y_{k,o} = Kx_{k,o}, \text{ case 1;} \quad (B-23)$$

or

$$y_{k,i} = Kx_{k,o}, \text{ case 2;} \quad (B-24)$$

or

$$x_{k,o} = \frac{\ln \text{ mean } y_k}{K} = \frac{y_{k,i} - y_{k,o}}{K \ln y_{k,i}/y_{k,o}} , \text{ case 3} . \quad (B-25)$$

Finally,  $L_o$  is defined by using an operating factor (C) as follows:

$$L_o = F_r F_{t,i} C ,$$

where

$$F_r F_{t,i} = \text{moles CO}_2 \text{ reacted, and} \quad (B-26)$$

$C = \text{moles of H}_2\text{O out of reactor per mole of CO}_2 \text{ reacted,}$   
determined primarily by gas flow rate and slurry molality.

So, generally, Eqs. (B-20), (B-22), and (B-26) are used to obtain

$$DF_k = \frac{y_{k,o} (1-F_r) F_{t,i} + x_{k,o} F_r F_{t,i} C}{x_{k,o} F_r F_{t,i} C} , \quad (B-27)$$

or

$$DF_k = \frac{y_{k,o} (1-F_r) + x_{k,o} F_r C}{x_{k,o} F_r C} . \quad (B-28)$$

Case 1:  $y_{k,o} = Kx_{k,o}$ ,

$$DF_k = \frac{K(1-F_r) + F_r C}{F_r C} \quad (B-29)$$

Case 2:  $y_{k,i} = Kx_{k,o}$ ,

$$DF_k = \frac{y_{k,o}(1-F_r) + (y_{k,i}/K) F_r C}{\frac{y_{k,i} F_r C}{K}} \quad (B-30)$$

Case 3:  $x_{k,o} = \frac{y_{k,o} - y_{k,i}}{K \ln \frac{y_{k,o}}{y_{k,i}}}$

$$DF_k = \frac{y_{k,o}(1-F_r) + \frac{y_{k,o} - y_{k,i}}{K \ln \frac{y_{k,o}}{y_{k,i}}} F_r C}{\frac{y_{k,o} - y_{k,i} F_r C}{K \ln \frac{y_{k,o}}{y_{k,i}}}} \quad (B-31)$$

Some examples of C are given below.

A 1.0 m Ca(OH)<sub>2</sub> solution will react with 1.0 mole of CO<sub>2</sub>,

$$C = \frac{1000}{18} = \frac{55.5 + 1}{1 \text{ mole CO}_2} = 56.5 .$$

For 1.0 m Ca(OH)<sub>2</sub> with 0.8 mole CO<sub>2</sub>,

$$C = \frac{55.5 + 0.8}{0.8} = 70 .$$

For 0.5 m Ca(OH)<sub>2</sub>, with 0.5 mole of CO<sub>2</sub> reacted,

$$C = \frac{55.5 + 0.5}{0.5} = 112 .$$

For 2.0 m Ca(OH)<sub>2</sub>, with 2.0 moles of CO<sub>2</sub> reacted,

$$C = \frac{55.5 + 2.0}{2.0} = 28.75 .$$

Dependency of  $DF_k$  on  $DF_{cd}$  is readily obtained by the combination of Eqs. (B-29), (B-30), or (B-31) with (B-16).

APPENDIX C: DEVELOPMENT OF MASS TRANSFER MODELS FOR DESCRIBING  
FIXATION OF CO<sub>2</sub> IN Ca(OH)<sub>2</sub> SLURRIES

C.1 Considerations of Rate Expressions

Juvekar and Sharma<sup>15</sup> developed the following rate expression for CO<sub>2</sub> absorption in an alkaline slurry:

$$Ra = \alpha H p_{cd} [D_{cd} k_2 (\text{OH}_s^-) + k_L^2]^{0.5}, \quad (\text{C-1})$$

for negligible gas-phase resistance (see Sect. C.4). There are several possible ways in which this expression can be utilized to describe the mass transfer of CO<sub>2</sub> from CO<sub>2</sub>-rich feed gases to Ca(OH)<sub>2</sub> slurries. The most rigorous approach, which may most closely represent the CO<sub>2</sub>-Ca(OH)<sub>2</sub> reaction in a stirred tank, is presented as follows.

A differential balance for a unit volume of the contactor is

$$-F_t dy_{cd} = (Ra)(A)(dh), \quad (\text{C-2})$$

where

A = cross-sectional area of contactor,

h = height in contactor.

This expression can then be integrated over the depth of the gas-slurry dispersion. However,  $F_t$  is a function of h, so it must be replaced by

$$F_n = (1 - y_{cd}) F_t. \quad (\text{C-3})$$

Equation (C-2) then becomes

$$\frac{-F_n}{1 - y_{cd}} dy_{cd} = Ra \cdot A \cdot dh. \quad (\text{C-4})$$

Substituting Eq. (C-1) into Eq. (C-4), we obtain

$$\frac{-F_n}{1 - y_{cd}} dy_{cd} = \alpha H p_{cd} [D_{cd} k_2 (\text{OH}_s^-) + k_L^2]^{0.5} A dh. \quad (\text{C-5})$$

But

$$p_{cd} = y_{cd} P_t = y_{cd} \text{ for } P_t \approx 1.0 \text{ atm},$$

as was the case in the agitated contactor. Thus, Eq. (C-5) can be integrated over the slurry depth and for  $y_{cd}$  between influent and effluent gas concentrations as follows:

$$\int_0^{\text{eff}} \frac{-F_n}{(y_{cd})(1-y_{cd})} dy_{cd} = \alpha H [D_{cd} k_2 (\text{OH}_s^-) + k_L^2]^{0.5} A \int_0^h dh. \quad (\text{C-6})$$

After integration, we obtain

$$-F_n \ln \left( \frac{y_{cd}}{1-y_{cd}} \right)_{\text{in}}^{\text{eff}} = \alpha H [D_{cd} k_2 (\text{OH}_s^-) + k_L^2]^{0.5} V_d. \quad (\text{C-7})$$

This equation can be rearranged as

$$F_n \ln \left[ \frac{y_{cd,i}}{1-y_{cd,i}} / \frac{y_{cd,o}}{1-y_{cd,o}} \right] = \alpha H [D_{cd} k_2 (\text{OH}_s^-) + k_L^2]^{0.5} V_d. \quad (\text{C-8})$$

Utilizing Eq. (B-13), we obtain

$$F_n \ln DF_{cd} = \alpha H [D_{cd} k_2 (\text{OH}_s^-) + k_L^2]^{0.5} V_d. \quad (\text{C-9})$$

Alternatively, it can be assumed that the reactor is perfectly backmixed and the reaction per volume of the single-stage contactor is homogeneous; hence, the total mass transfer rate,  $N_{cd}$  (moles  $\text{CO}_2$  removed per second) for the contactor is simply equal to  $R\alpha V_d$  ( $V_d$  is the volume of the slurry-gas dispersion). In this case, there are two pragmatic choices for  $p_{cd}$ . It can be taken to be either the effluent partial pressure of  $\text{CO}_2$  (backmix case) or the log-mean of the influent and effluent partial pressures (a type of plug-flow case).

As would be expected because of the consideration of gas-phase shrinkage, the more rigorous case predicts interfacial areas that are considerably smaller than those calculated by Eq. (C-1) with a log-mean pressure driving force:

$$R\alpha = \alpha H p_{df} [D_{cd} k_2 (\text{OH}_s^-) + k_L^2]^{0.5}, \quad (\text{C-10})$$

where

$$p_{df} = p_{cd,o} \text{ or } (p_{cd,i} - p_{cd,o}) / \ln(p_{cd,i}/p_{cd,o}).$$

The essential difference between Eqs. (C-9) and (C-10) is that they predict different interfacial areas for the process. However, either expression can be used to model the process. In this study, models were developed using Eq. (C-10). It is suggested that further consideration be given at some time to the development of models based on the more rigorous analysis given by Eq. (C-9).

## C.2 Mass Transfer Rate as a Function of Superficial Velocity

Equation (C-10) can be rewritten as follows:

$$Ra = aH \left[ \frac{p_{cd,i} - p_{cd,o}}{\ln \frac{p_{cd,i}}{p_{cd,o}}} \right] [D_{cd} k_2 (\text{OH}_s^-) + k_L^2]^{0.5} . \quad (\text{C-11})$$

From Eq. (B-13), it follows that

$$DF_{cd} = \frac{p_{cd,i}}{p_{cd,o}} \frac{(1 - p_{cd,o})}{(1 - p_{cd,i})} , \quad (\text{C-12})$$

but

$$1 - p_{cd,o} \cong 1.0 ,$$

so that

$$DF_{cd} \cong \frac{p_{cd,i}}{p_{cd,o}} \frac{1}{(1 - p_{cd,i})} . \quad (\text{C-13})$$

Then,

$$\ln DF_{cd} + \ln(1 - p_{cd,i}) \cong \ln \frac{p_{cd,i}}{p_{cd,o}} , \quad (\text{C-14})$$

and inserting Eq. (C-14) into Eq. (C-11), we obtain

$$[\ln DF_{cd} + \ln(1 - p_{cd,i})] Ra \cong aH(p_{cd,i} - p_{cd,o}) [D_{cd} k_2 (\text{OH}_s^-) + k_L^2]^{0.5} . \quad (\text{C-15})$$

### C.3 Prediction of the Effect of Temperature on the DF for CO<sub>2</sub>

Danckwerts and Sharma<sup>23</sup> have shown that for sorption of CO<sub>2</sub> into HaOH solutions, the following expressions are useful in according for temperature effects:

$$\log_{10} k_2 = 13.635 - \frac{2895}{T} \quad (T \text{ in K}) , \quad (\text{C-16})$$

$$\log_{10} H = \frac{1140}{T} - 5.30 \quad (T \text{ in K}) . \quad (\text{C-17})$$

Diffusivity can be estimated from

$$\frac{D_{cd} \mu}{T} = \text{constant} . \quad (\text{C-18})$$

The following values were calculated for H, k<sub>2</sub>, and D<sub>cd</sub> at 28 and 45°C:

$$H_{28} = 3.07 \times 10^{-5} \text{ g-mole}/(\text{cm}^3\text{-atm}),$$

$$H_{45} = 1.93 \times 10^{-5} \text{ g-mole}/(\text{cm}^3\text{-atm}),$$

$$k_{2,28} = 10400 \text{ liters}/(\text{g-mole-sec}),$$

$$k_{2,45} = 33980 \text{ liters}/(\text{g-mole-sec}), \text{ and}$$

$$D_{cd,45} \cong 1.06 D_{cd,28}, \quad D_{cd,28} = 2.09 \times 10^{-5} \text{ cm}^2/\text{sec}.$$

The solubility of Ca(OH)<sub>2</sub> as a function of temperature was taken from the critical tables.<sup>24</sup> For ease in performing calculations, an expression for the Ca(OH)<sub>2</sub> solubility (shown in Fig. C.1) was derived:

$$[\text{OH}] = 0.0480 - 7.5 \times 10^{-7} T^2 - 2.31 \times 10^{-4} T. \quad (\text{C-19})$$

This equation was used to obtain

$$(\text{OH}_{28}) = 0.041 \text{ g-mole/liter},$$

$$(\text{OH}_{45}) = 0.036 \text{ g-mole/liter}.$$

Based on the assumption that  $\alpha_{28} \cong \alpha_{45}$  and  $R\alpha_{28} = R\alpha_{45}$ , and with a value for k<sub>L</sub> of 0.06 cm/sec, the effect of temperature could be predicted with

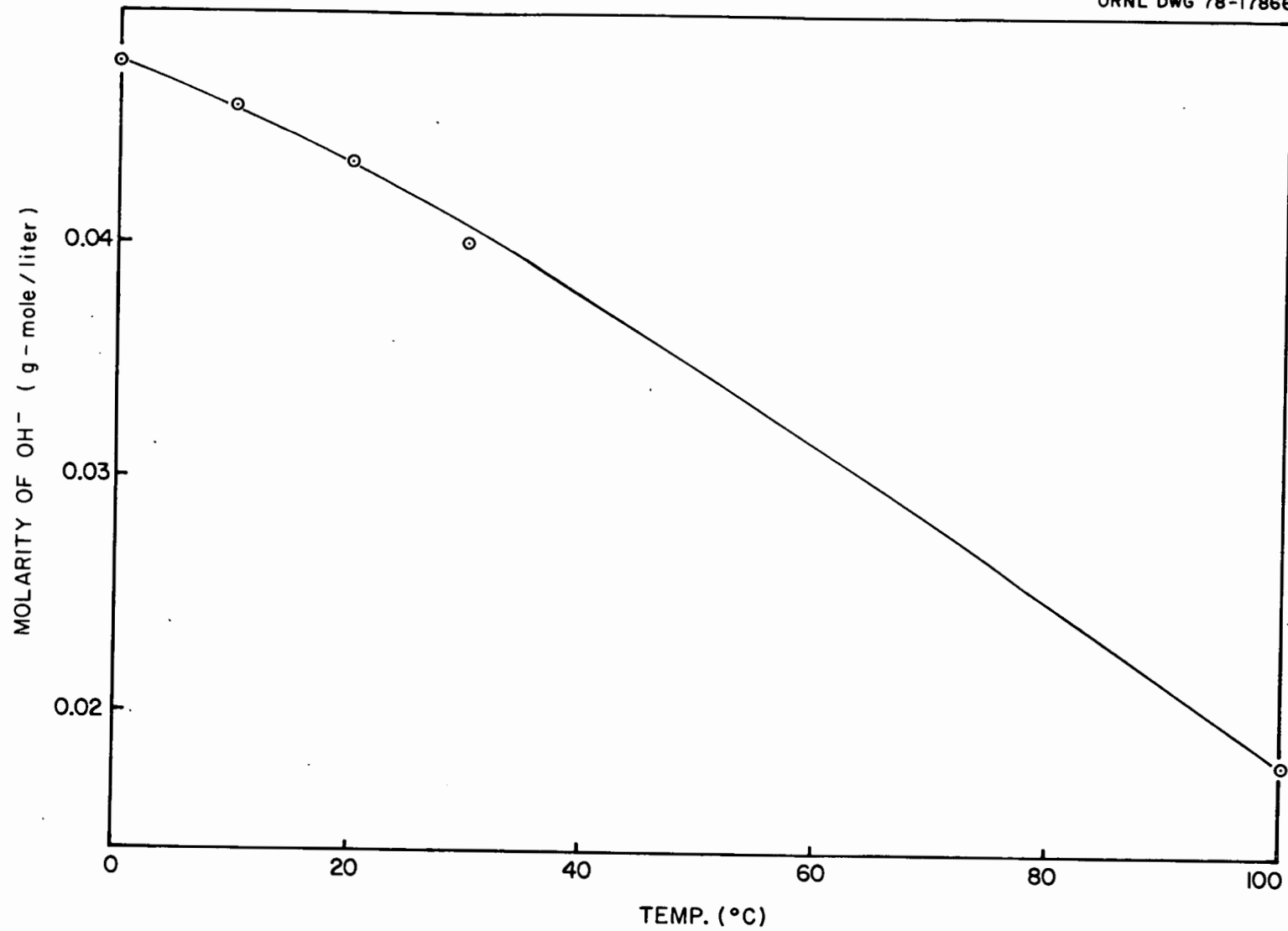


Fig. C.1. Solubility of Ca(OH)<sub>2</sub> as a function of temperature.

a version of Eq. (6), as corrected for no gas-phase control and with an appropriate pressure driving force (i.e., Eq. (C-11)).

For  $Ra_{45}/Ra_{28}$ , Eq. (C-11) predicted that

$$P_{df}(45) = P_{df}(28)/0.98 .$$

#### C.4 Gas-Side Mass Transfer Resistance

Because the contactor design and operating conditions of this study were similar to those used by Juvekar and Sharma,<sup>15</sup> we may adopt their value of  $10^{-4}$  g-mole/(cm<sup>3</sup>-sec-atm) for  $k_G\alpha$  (the value for gas-phase control in an agitated contactor). Gas-side resistance is an insignificant factor in the mass transfer if the following condition is true:

$$\frac{\alpha H_p [D_{cd} k_2 (\text{OH}_s^-) + k_L^2]^{0.5}}{k_G \alpha} \ll 1.0 . \quad (\text{C-20})$$

For a sample calculation at 30°C, the following values were used:

$$\alpha = 1.5 \text{ cm}^2/\text{cm}^3 ,$$

$$H = 2.98 \times 10^{-5} \text{ g-mole}/(\text{cm}^3\text{-atm}),$$

$$P_{df} = 0.2 \text{ atm},$$

$$D_{cd} = 2.1 \times 10^{-5} \text{ cm}^2/\text{sec},$$

$$k_2 = 12038 \text{ liters}/(\text{g-mole-sec}),$$

$$\text{OH}_s^- = 0.041 \text{ g-moles/liter},$$

$$k_L = 0.06 \text{ cm/sec}, \text{ and}$$

$$k_G \alpha = 10^{-4} \text{ g-moles}/(\text{cm}^3\text{-sec-atm}).$$

Then

$$\frac{(1.5)(2.98 \times 10^{-5})(0.2) [(2.1 \times 10^{-5})(12038)(0.04) + (0.06)^2]^{0.5}}{10^{-4}} \ll 1 ,$$

or

$$0.0104 \ll 1 ,$$

and gas-side resistance can be neglected.

### C.5 Conditions for Utilization of Rate Expressions

In order for model 1, as expressed by Eq. (C-11), to be applicable, it is necessary that certain conditions concerning the relative magnitudes of reaction rates in the gas-liquid film and in the bulk liquid be satisfied.

The two conditions that must be satisfied so that Eq. (C-11) can be used are:

$$[D_{cd}k_2(\text{OH}_s^-)]^{0.5} \cong k_L, \quad (\text{C-21})$$

$$\frac{[D_{cd}k_2(\text{OH}_s^-)]^{0.5}}{k_L} \ll \frac{(\text{OH}_s^-)}{zA^*} \left( \frac{D_{\text{OH}}}{D_{cd}} \right)^{0.5}. \quad (\text{C-22})$$

For the second condition,  $z$  is the stoichiometric coefficient for the reaction between  $\text{CO}_2$  and  $\text{OH}_s^-$  ( $= 2$ ),  $D_{\text{OH}}$  is the diffusivity of  $\text{OH}^-$  ions in aqueous solution ( $\text{cm}^2/\text{sec}$ ), and  $A^*$  is the concentration of dissolved  $\text{CO}_2$  at the liquid-gas interface which is in equilibrium with the gas (g-mole/liter). From a physical viewpoint, when condition 1 (C-21) is satisfied, it implies that part of the reaction between  $\text{CO}_2$  and  $\text{OH}^-$  occurs in the film and the rest in the bulk liquid. If condition 2 (C-22) is not satisfied, there will be depletion of  $\text{OH}^-$  ions in the liquid film. The rate of  $\text{CO}_2$  removal will then be given by model 2, Eq. (20). The enhancement factor  $\phi$  is derived from the film theory instead of the penetration theory (Juvekar and Sharma).<sup>15</sup> The difference in the predictions based on the penetration and film theories under the above conditions are, for practical purposes, insignificant.

The following sample calculations are used for testing conditions 1 and 2 in order to ascertain which of the rate expressions is most applicable for the removal of  $\text{CO}_2$  from simulated HTGR fuel reprocessing off-gas. At  $30^\circ\text{C}$ ,

$$D_{cd} = 2.1 \times 10^{-5} \text{ cm}^2/\text{sec},$$

$$H = 2.98 \times 10^{-5} \text{ g-mole}/(\text{cm}^3\text{-atm}),$$

$$\text{OH}_s^- = 0.04 \text{ g-mole/liter},$$

$$k_2 = 12038 \text{ liters}/(\text{g-mole-sec}),$$

$$(D_{\text{OH}}/D_{\text{cd}})^{0.5} = 1.42,$$

$$k_L = 0.06 \text{ cm/sec, and}$$

$$A^* = H p_i.$$

Condition 1:

$$[(2.1 \times 10^{-5})(12038)(0.04)]^{0.5} \cong 0.06 ,$$

or

$$0.1006 \cong 0.06 ,$$

In testing Eq. (C-22), there is some question as to how  $A^*$  should be estimated. The actual value should be calculated from the partial pressure of  $\text{CO}_2$  at the interface. This interfacial concentration may be estimated for our case either by the effluent partial pressure of  $\text{CO}_2$  ( $p_{\text{cd},o}$ ) or a log-mean average of  $p_{\text{cd},i}$  and  $p_{\text{cd},o}$ . A comparison of the relative magnitudes of  $p_{\text{cd},i}$ ,  $p_{\text{cd},o}$ , and  $(p_{\text{cd},i} - p_{\text{cd},o})/\ln(p_{\text{cd},i}/p_{\text{cd},o})$  for several superficial gas velocities of  $\sim 90\%$   $\text{CO}_2$  feeds is shown in Table C.1.

Table C.1. Pressure driving force for  $\text{CO}_2$  removal from 90%  $\text{CO}_2$ -air feeds

Run No.	$U_s$ (cm/min)	$P_{\text{cd},i}$ (atm)	$P_{\text{cd},o}$ (atm)	$\frac{P_{\text{cd},i} - P_{\text{cd},o}}{\ln(P_{\text{cd},i}/P_{\text{cd},o})}$	$DF_{\text{cd}}$
CF-11	9.1	0.90	0.0007	0.126	12,772
BR-12	18.6	0.88	0.0050	0.170	1,315
CF-20	24.6	0.91	0.0055	0.177	1,840
CF-23	31.8	0.88	0.0052	0.170	1,471
CF-21	43.4	0.91	0.0096	0.198	1,053
CF-6	49.4	0.91	0.0186	0.227	535
CF-10	60.0	0.88	0.032	0.256	215
BR-10	60.0	0.88	0.043	0.278	158

Based on an average value for log-mean  $p_{df}$  of 0.2, the inequality [Eq. (C-22)] at a temperature of 30°C becomes

$$\frac{0.1006}{0.06} \ll \frac{0.04}{2(0.0298)} \frac{(1.42)}{(0.2)}$$

or

$$1.6 \ll 4.77 .$$

Although condition 2 is not strictly satisfied for the log-mean pressure driving force, it is likely that in this region of overlap of the rate expression given by Eq. (C-11) with the rate expression given by Eq. (20), either expression is suitable to describe the  $\text{CO}_2\text{-Ca(OH)}_2$  slurry reaction.



## APPENDIX D: UTILIZATION OF MODELS FOR PREDICTION OF SCALE-UP

## D.1 Rearrangement of Eq. (C-10)

The model described by Eq. (C-10) can be used for scale-up calculations as follows:

$$Ra = \frac{F_{cd,i} - F_{cd,o}}{V_d}, \quad (D-1)$$

where

$F_{cd}$  = molar flow rate of  $CO_2$ , g-moles/sec;

$V_d$  = volume of total dispersion,  $cm^3$ ; and

$i,o$  = influent and effluent, respectively.

However,  $DF_{cd}$  can also be expressed by

$$F_{cd,o} = \frac{F_{cd,i}}{DF_{cd}}. \quad (D-2)$$

Also,

$$F_{cd,i} = y_{cd,i} F_{t,i}. \quad (D-3)$$

Equations (D-2) and (D-3) are used with Eq. (D-1) to give

$$Ra = (F_{cd,i} - F_{cd,o})/V_d = y_{cd,i} F_{t,i} (1 - \frac{1}{DF_{cd}})/V_d. \quad (D-4)$$

When Eq. (D-4) is inserted into Eq. (C-10), we obtain

$$y_{cd,i} F_{t,i} (1 - 1/DF_{cd}) = \alpha H p_{df} V_d [D_{cd} k_2 (OH_s^-) + k_L^2]^{0.5}. \quad (D-5)$$

Equation (D-5) can be rearranged to give

$$\frac{1}{DF_{cd}} = 1 - \frac{\alpha H p_{df} V_d}{y_{cd,i} F_{t,i}} [D_{cd} k_2 (OH_s^-) + k_L^2]^{0.5}, \quad (D-6)$$

and because  $DF$  is also given by

$$DF_{cd} = \frac{y_{cd,i} (1 - y_{cd,o})}{y_{cd,o} (1 - y_{cd,i})}, \quad (D-7)$$

we can solve for  $y_{cd,o}$  to obtain

$$y_{cd,o} = \frac{y_{cd,i}}{DF - DF y_{cd,i} + y_{cd,i}} \quad (D-8)$$

Thus, when  $y_{cd,i}$  and  $DF_{cd}$  are specified,  $y_{cd,o}$  is known and  $p_{df}$  can be calculated for use in Eq. (D-6).

## D.2 Method 1 for Estimating Interfacial Areas and Large-Scale Tank Diameters

First, before Eq. (D-6) can be used in predicting process DFs and large-scale tank diameters, some method of estimating  $\alpha$  must be developed. Both in previous studies<sup>11</sup> and in this study, values for  $\alpha$  have been calculated using either Eq. (C-11) or Eq. (D-6) for CO<sub>2</sub> removal from 90% CO<sub>2</sub>-air feed gases. The scatter in the interfacial areas calculated with Eq. (D-6) is an indirect indication of the scatter in DF values (Fig. 11). This should not be surprising in view of the uncertainty inherent in DF measurements. Values for  $\alpha$  calculated with Eq. (C-11) are very well behaved (i.e., they have less deviation from a least-squares polynomial fit) due to the averaging effect of the  $R\alpha$  term. The basic assumption of method 1 for estimating  $\alpha$  is that equal DFs are obtained for tanks of varying sizes when the superficial velocity and power per volume are maintained at a constant value (for similar slurry and feed-gas compositions). These same conditions also require that the interfacial area remain constant for contactors of different sizes. Thus,  $\alpha$  can be expressed as an empirical function of  $DF_{cd}$  (Fig. D.1). The values of  $\alpha$  shown in Fig. D.1 were obtained from Eq. (D-6), while the corresponding values of  $DF_{cd}$  were taken from the data of Table A.1. That is, if the constraint of geometric similarity is retained and the physico-chemical properties of the slurry are maintained (for example, simply by using the same slurry composition in small- and large-scale experiments), then  $\alpha$  should be reasonably estimated by a function of DF for CO<sub>2</sub>. The impeller speeds for scaled-up contactors can be estimated by utilizing both the constraints of geometric similarity and equal power

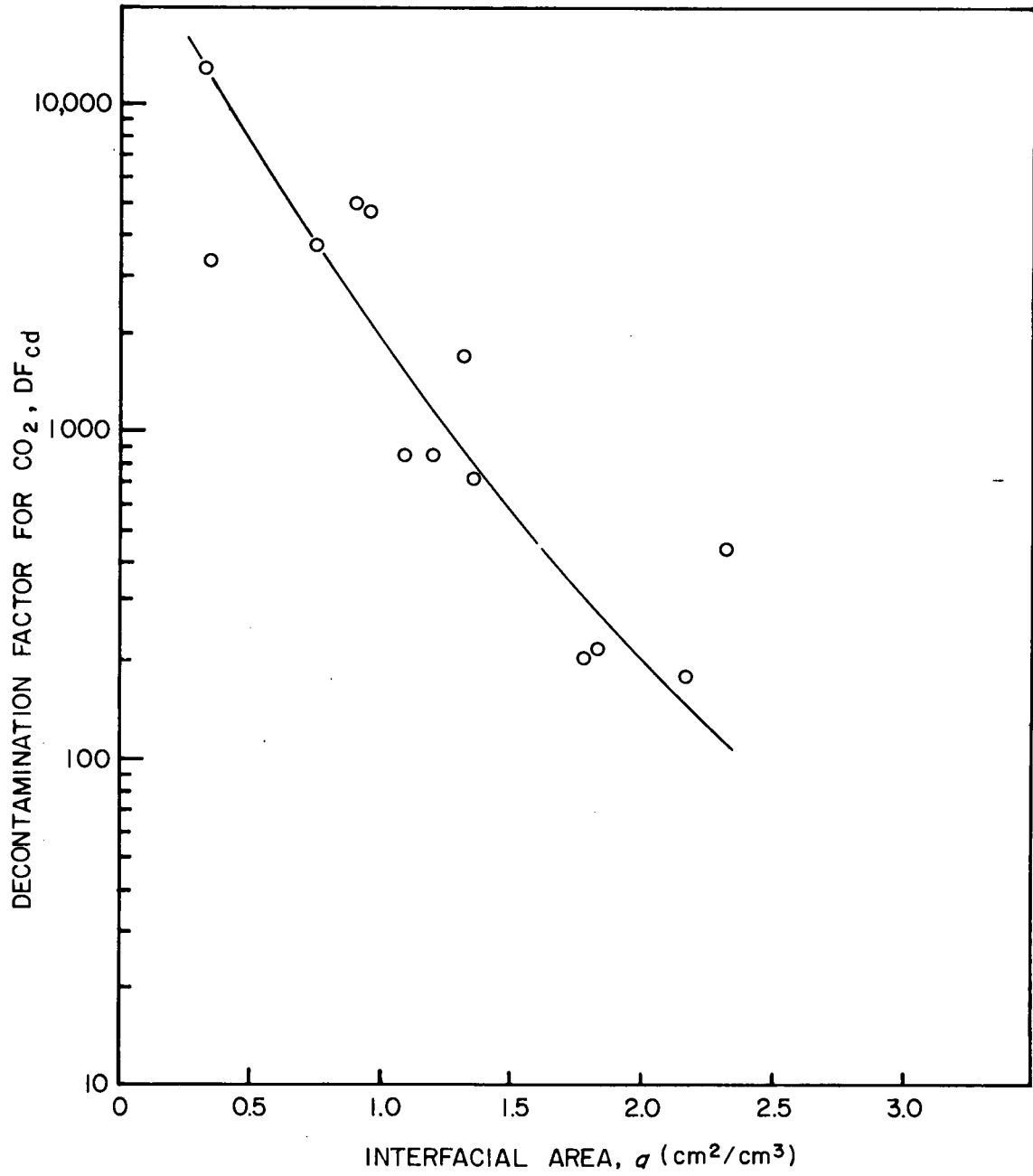


Fig. D.1. Relationship between decontamination factor for CO<sub>2</sub> and interfacial area in the contactor.

per volume of contactor.<sup>20</sup> These two conditions result in the following relationship between  $n$  and  $d_i$ :

$$n_2 = n_1 \left( \frac{d_i \text{ of small tank}}{d_i \text{ of large tank}} \right)^{2/3} \quad (D-9)$$

Thus, for a fixed tank size, known slurry composition and flow rate to be processed [ $V_d$ ,  $y_{cd,i}$ ,  $F_{t,i}$ ,  $H$ ,  $D_{cd}$ ,  $k_2$ ,  $(OH_s^-)$ , and  $k_L$  (all of which are known)] and interfacial area predicted by an empirical expression of  $DF_{cd}$ , Eq. (D-6) can be used to predict DFs for  $CO_2$  as a function of the total gas flow rate. Predictions for  $DF_{cd}$  are shown later in Sect. D.4.

A much more pragmatic and useful application of the model is the prediction of the tank size required to process a given gas composition and flow rate for a desired  $DF_{cd}$ . Thus, Eq. (D-6) can be written as

$$\frac{1}{DF_{cd}} = 1 - \frac{\text{func}(DF_{cd}) H(\pi d_t^{3/4}) p_{df}}{y_{cd,i} Q_t / (24.12)(60)} [D_{cd} k_2 (OH_s^-) + k_L^2]^{0.5} \quad (D-10)$$

In general, the calculation scheme is as follows:

1. The DF required for  $CO_2$  for a volumetric gas flow rate ( $Q_t$ ) would be set [thus,  $p_{cd,i}$  and  $p_{cd,o}$  (from Eq. (D-8)) would be available].
2. The slurry conditions would be selected, specifying  $H$ ,  $D_{cd}$ ,  $k_2$ ,  $(OH_s^-)$ , and  $k_L$ .
3. Equation (D-10) can then be used to calculate  $d_t$ .

Estimations of  $d_t$  were made for the above constraints and conditions using Eq. (D-10) and are shown in Table D.1. Equation (D-10) should also be reasonably applicable for process scale-up for different solutions and hydroxyl solubilities. Calculations were made for the following parametric values at 30°C:

$$H = 2.98 \times 10^{-5} \text{ g-mole}/(\text{cm}^3\text{-atm});$$

$$\alpha [=] \text{ cm}^2/\text{cm}^3;$$

Table D.1. Estimated tank diameters (cm) for process-sized contactors<sup>a</sup>

(Method 1 for determining  $\alpha$ )

$Q_t$ (scfm)	DF				
	100	200	300	400	500
1	20.1	22.6	24.0	25.2	26.1
2	25.3	28.5	30.4	31.7	32.8
3	29.0	32.6	34.8	36.3	37.6
4	30.8	34.6	37.0	38.6	40.0
5	34.4	38.6	41.2	43.0	44.6
100	93.3	104.8	111.9	117.0	121.0
200	117.5	132.0	140.9	147.4	152.4
300	134.5	151.2	161.3	168.7	174.5
400	143.0	160.7	171.5	179.4	185.5
500	159.5	179.2	191.3	200.0	206.9
1000	201.0	225.8	241.0	252.0	260.7
2000	253.2	284.5	303.6	317.5	328.4
3000	289.8	325.7	347.6	363.4	375.9
4000	308.1	346.3	369.5	386.4	399.7
5000	343.6	386.1	412.1	430.9	445.7

<sup>a</sup>Power required can be estimated from Table 3, for constant superficial velocities.

$y_{cd,i} \cong 0.9$ ,  $y_{cd,o}$ , calculated from DF and Eq. (D-8);

$Q_t$  = total volumetric flow, standard liters/min;

$D_{cd} = 2.1 \times 10^{-5} \text{ cm}^2/\text{sec}$ ;

$k_2 = 12038 \text{ liters}/(\text{g-mole-sec})$ ;

$(\text{OH}_s^-) = 0.041 \text{ g-mole/liter}$ ; and

$k_L = 0.06 \text{ cm/sec}$ .

Necessary relationships are

$$DF_{cd} = \frac{y_{cd,i} (1 - y_{cd,o})}{y_{cd,o} (1 - y_{cd,i})}, \quad (\text{B-13})$$

$$y_{cd,o} = \frac{y_{cd,i}}{DF_{cd} - (DF_{cd})y_{cd,i} + y_{cd,i}}, \quad (\text{D-8})$$

and for temperature variations,

$$\log_{10} k_2 = 13.635 - \frac{2895}{T^{\circ}\text{K}}, \quad (\text{C-16})$$

$$\log_{10} H = \frac{1140}{T^{\circ}\text{K}} - 5.30. \quad (\text{C-17})$$

Based on the results shown in Fig. D.1, the following expression was derived for func ( $DF_{cd}$ ):

$$\alpha = 6.18 DF_{cd}^{-0.218}. \quad (\text{D-11})$$

### D.3 Method 2 for Estimating Interfacial Areas and Scaled-Up Tank Dimensions

Numerous investigators, particularly Miller and Calderbank,<sup>17,18</sup> have studied the determination of interfacial area in sparged agitated contactors. The correlations developed for effective power input and interfacial area are given by Eqs. (15) and (16). Values for  $\alpha$  were derived from physical properties according to the expression,

$\alpha$  = fraction gas holdup/mean bubble diameter.

There is uncertainty concerning the applicability of this correlation for predicting effective interfacial areas for reactions involving both chemical reaction and the presence of solids. Also, the proper form for the gas flow rate is unknown for systems involving mass transfer with reaction-rate enhancement when there is extensive gas-phase shrinkage.

In spite of these criticisms, it was found that rather good estimates for  $a$  were obtained from Eq. (D-12) for CO<sub>2</sub> removal from 90% CO<sub>2</sub>-air feeds (where  $Q_t$  and  $U_s$  represent total inlet gas flow):

$$a = 1.44 \left[ \frac{0.870 f^{0.36} n^{1.26} d_i^{2.34} \rho_s^{0.56}}{v_d^{0.4} Q_t^{0.101} \sigma^{0.6}} \right] \left( \frac{U_s}{U_s + U_t} \right)^{0.5} \quad (D-12)$$

The values calculated for  $a$  with Eq. (D-12) can be compared with those obtained from the models for mass transfer with chemical reaction as shown in Fig. 11. The largest differences in the predictions of models given by Eq. (D-6) and Eq. (D-12) occur at high superficial velocities, where Miller's  $a$  values continue to increase while the  $a$  values of Eq. (D-6) approach a constant value (see refs. 15 and 16). Equation (D-12) can be rewritten in terms of the contactor diameter by the use of the following assumptions concerning geometric similarity and power consumption:

$$d_i = 1/2 d_t, \quad (D-13)$$

$$v_d = \pi d_t^3 / 4, \quad (D-14)$$

$$U_s = Q_t / (\pi d_t^2 / 4), \quad (D-15)$$

$$n_2 = n_1 \left( \frac{d_i \text{ of small tank}}{d_i \text{ of large tank}} \right)^{0.67} \quad (D-16)$$

The expression for  $a$  becomes

$$a = 1.44 \left( \frac{1.26 f^{0.36} \rho_s^{0.56}}{\sigma^{0.6}} \right) \left( \frac{Q_t^{0.4}}{U_t^{0.5}} \right) d_t^{-0.53} \quad (D-17)$$

(dimensionally valid in the kg-m-sec system). Equation (D-6) can then be rewritten in terms of the expression in Eq. (D-17):

$$\frac{1}{DF_{cd}} = 1 - \frac{(\text{FACTOR}/10^2) H d_t^{2.47} (p_{cd,i} - p_{cd,o}) (10^6) (\pi/4)}{p_{cd,i} F_{t,i}} \times$$

$$\frac{[D_{cd} k_2 (\text{OH}_s^-) + k_L^2]^{0.5}}{\ln(p_{cd,i}/p_{cd,o})}, \quad (\text{D-18})$$

where

$$\text{FACTOR} = \alpha/d_t^{-0.53}$$

from Eq. (D-17).

In general, the calculation scheme is:

1. The DF required for  $\text{CO}_2$  for a volumetric gas flow rate ( $Q_t$ ) would be known ( $p_{cd,i}$  and  $p_{cd,o}$  would be available).
2. The slurry conditions would be selected, thus specifying  $\rho_s$ ,  $\sigma$ ,  $U_t$ ,  $D_{cd}$ ,  $k_2$ ,  $(\text{OH}_s^-)$ ,  $H$ , and  $k_L$ .
3. Equation (D-17) can be used to calculate the hydrodynamic  $\alpha$  factor, and Eq. (D-18) can be used to calculate  $d_t$ .

Large-scale tank diameters were calculated using Eq. (D-18) and the following parametric values (at 30°C):

$$f = 6.0,$$

$$n = 10.83 \text{ rps},$$

$$\rho_s = 1040 \text{ kg/m}^3,$$

$$Q_t [=] \text{ m}^3/\text{sec},$$

$$U_t = 0.2 \text{ m/sec},$$

$$\sigma = 0.074 \text{ kg/sec}^2,$$

$$d_t [=] \text{ m},$$

$$y_{cd,i} = 0.9,$$

$$D_{cd} = 2.1 \times 10^{-5} \text{ cm}^2/\text{sec},$$

$$k_2 = 1.204 \times 10^4 \text{ liters/(g-mole-s)},$$

$$(\text{OH}_s^-) = 0.041 \text{ g-mole/liter},$$

$$k_L = 0.06 \text{ cm/sec, and}$$

$$F_{t,i} = Q_t \text{ (std liters/min)/(24.12)(60)}.$$

Calculated values are presented in Table D.2. For general scale-up applications, the expression for  $\alpha$  (Eq. D-17) is dependent on three constraints for agitated-contactor process design: constant superficial velocity, constant power input per volume, and geometric similarity.

#### D.4 A General Modeling Approach

An alternative, primarily empirical model can be constructed to describe the carbonation of lime in a stirred-tank contactor. Based on both experimental evidence and consideration of various rate expressions in the literature, it could be argued that the mass transfer of  $\text{CO}_2$  in the carbonation reaction is dependent on the following parameters: influent  $\text{CO}_2$  partial pressure, impeller speed, impeller diameter (or contactor diameter), slurry density, gas solubility, hydroxyl ion concentration, surface tension, slurry viscosity, gas diffusivity, and reaction rate constant. The general form of the equation was

$$p_{DF} \text{ or } DF_{cd} = n^1 d_i^2 (Q/V_d)^3 \rho_s^4 H^5 D^6 k_2^7 (\text{OH}_s^-)^8 y_i^9 \sigma^{10}, \quad (\text{D-19})$$

where

$$p_{DF} = p_{cd,o} \text{ or } (p_{cd,i} - p_{cd,o}) / \ln(p_{cd,i} / p_{cd,o}).$$

The general model was developed by applying the multiple regression program SAS. In order to obtain the most general model, the following gas compositions, contactor sizes, slurry compositions, and impeller speeds were studied: 87.5%  $\text{CO}_2$ --12.5%  $\text{O}_2$ , 20.3-cm-ID contactor, 1.0  $\underline{\text{m}}$   $\text{Ca}(\text{OH})_2$ ,  $n = 800$  rpm; 33.6%  $\text{CO}_2$ --66.4%  $\text{O}_2$ , 20.3-cm-ID contactor, 1.0  $\underline{\text{m}}$   $\text{Ca}(\text{OH})_2$ ,  $n = 800$  rpm; 4.74%  $\text{CO}_2$ --95.26%  $\text{O}_2$ , 20.3-cm-ID contactor, 1.0  $\underline{\text{m}}$   $\text{Ca}(\text{OH})_2$ ,  $n = 800$  rpm; 88-91%  $\text{CO}_2$ --air, 27.3-cm-ID contactor, 0.5, 1.0, and 2.0  $\underline{\text{m}}$   $\text{Ca}(\text{OH})_2$ ,  $n = 650$  rpm; 3%  $\text{CO}_2$ --air, 20.3-cm-ID contactor,

Table D.2. Estimated tank diameters (cm) for  
process-sized contactors (model 2)

$Q_t$ (scfm)	DF				
	100	200	300	400	500
1	21.1	22.7	23.8	24.5	25.0
2	24.8	26.9	28.0	28.9	29.5
3	27.4	30.0	31.0	31.9	32.6
4	28.7	31.1	32.4	33.4	35.0
5	31.0	33.6	35.0	36.0	36.9
100	65	70	73	75	77
200	76	83	86	89	91
300	84	91	95	98	100
400	90	98	102	104	104
500	95	103	108	111	113
1000	113	122	128	131	134
2000	133	145	151	155	159
3000	147	160	167	171	175
4000	154	167	174	179	183
5000	167	181	189	194	198

1.0 m Mg(OH)<sub>2</sub>, n = 800 rpm; 3% CO<sub>2</sub>-air, 27.3-cm-ID contactor,  
 1.0 m Ca(OH)<sub>2</sub>, n = 650 rpm; 3% CO<sub>2</sub>-air, 27.3-cm-ID contactor, 0.4 and  
 0.75 m Ba(OH)<sub>2</sub>·8H<sub>2</sub>O, n = 325 and 650 rpm. The data for feeds other than  
 ~90% CO<sub>2</sub> were obtained from other studies.<sup>11,16</sup> Most of the other  
 parameters were varied over somewhat limited ranges. The parameters  
 $\sigma$  and  $\mu$  were excluded from the analysis because of insufficient data.  
 Apparently there was also insufficient variation of one of the most important  
 parameters, the impeller speed (n). Thus, in the various fitting efforts  
 (dependent on the form of  $p_{DF}$ ), the parameter n was always considered  
 to be insignificant. The importance of  $d_i$  apparently outweighed the  
 contribution of n in the statistical analysis. This probably occurred  
 because no sets of data were taken for the cases in which all other  
 parameters were fixed and n was adjusted to several values.

Although the elimination of n from the empirical model would appear  
 to be an insurmountable omission, there was another constraint which  
 could provide for the specification of power input. The power conditions  
 could be delineated by previous arguments, which led to the derivation  
 of Eq. (D-16). Thus, once the appropriate n, $d_i$  relationship has been  
 established experimentally, any other n, $d_i$  combinations can be calcu-  
 lated for the restriction of  $d_i = 0.5 d_t$ .

The best statistical fits for the three types of  $p_{DF}$  terms are  
 shown in Table D.3 (exponents for  $D_{cd}$  and  $k_2$  were set at 0.5). These  
 correlations were inspected to determine whether any recognizable  
 dimensionless groups descriptive of mass transfer kinetics or turbine  
 agitation were present (e.g.,  $N_{Re} = d_i^2 n \rho_s / \mu$ ,  $N_{SC} = \mu / \rho_s D_{cd}$ ,  $N_{we} = d_i^3 n^2 \rho_s / \sigma$ ,  
 and  $N_{st} = \pi d_i n / U_s$ ). No tractable correlation for these groups was readily  
 discernible. The models should be recalculated with more extensive  
 data to fully explore the possibility of the occurrence of classical  
 dimensionless groups.

In any case, the general empirical model has some utility. The DF  
 curves as a function of gas superficial velocity could be quite accurately  
 predicted for a fixed contactor application. The effect of varying the  
 $p_{cd,i}$ , temperature, slurry composition, etc., on process DF could be

Table D.3. Empirical expressions for DFs for CO<sub>2</sub> based on the SASS program  
[exponents for Eq. (D-19)]

$P_{DF}$	$e^1(n)$	$e^2(d_i)$	$e^3$ ( $U_s$ or $Q/V_d$ )	$e^4(\rho_s)$	$e^5(H)$	$e^8(OH_s^-)$	$e^9(y_{cd,i})$	Constant
$DF_{cd}$	0.109	4.80	-0.96	-0.90	1.36	0.34	0.35	$e^{3.66}$
$\frac{P_{cd,i} - P_{cd,o}}{\ln(P_{cd,i}/P_{cd,o})}$	-0.06	-1.08	0.24	0.28	0.33	-0.09	1.04	$e^{6.84}$
$P_{cd,o}$	0.073	-4.06	0.96	1.01	-0.38	-0.40	1.27	$e^{8.61}$
$\frac{P_{cd,i} - P_{cd,o}}{\ln(P_{cd,i}/P_{cd,o})}$	0	-0.94	0.23	0.27	0.90	-0.09	1.05	$e^{12.68}$

predicted. Such a model would obviously have utility for operators of the process who must react to process perturbations. Shown in Fig. D.2 are the empirical curves predicted by the general models 1, 2, and 4 compared to experimental DFs. The large variation in the DFs predicted by the models at high superficial velocities was attributed to the differences obtained for DFs in the region for different alkaline-earth hydroxide species (see ref. 16).

Of course, the most general fit would be applicable to DFs for  $\text{CO}_2$  in any type of geometric design, range of power inputs, and slurry composition; that is, the constraints on power input and geometric design necessary to ensure constant interfacial area would not be required. Such a general model would most probably result in a different set of exponents for the critical parameters from those derived in such restricted models as Eqs. (D-10) and (D-18). An indication of this probable variation can be seen from a comparison of the exponents for  $(\text{OH}_s^-)$  in the two models [0.5 for Eq. (D-10); 0.1 to 0.35 for the more general models of Table D.3].

#### D.5 Prediction of DFs for Krypton Utilizing Empirical DFs for $\text{CO}_2$

The DFs  $\text{CO}_2$  can be predicted from such models as those given in Eq. (D-10) or Table D.3. A DF can also be specified for a given set of operating conditions so that the required contactor can be calculated from the models. Hence, the DF for krypton can be readily estimated from Eqs. (B-16) and (B-29). For example, the empirically predicted DFs for krypton (for a single contactor) based on an altered K value to correct for gas-phase shrinkage in the contactor are shown in Fig. D.2, where they can be compared with the experimental DFs for krypton. Although no specific calculations are presented here, it can also be argued that an equation similar to Eq. (B-29) but corrected for the appropriate K value could be readily derived to describe the DF for krypton during operation of two contactors in series (see Fig. 7 for DFs for krypton obtained for contactors in series). Finally, the add-on DFs achieved for krypton

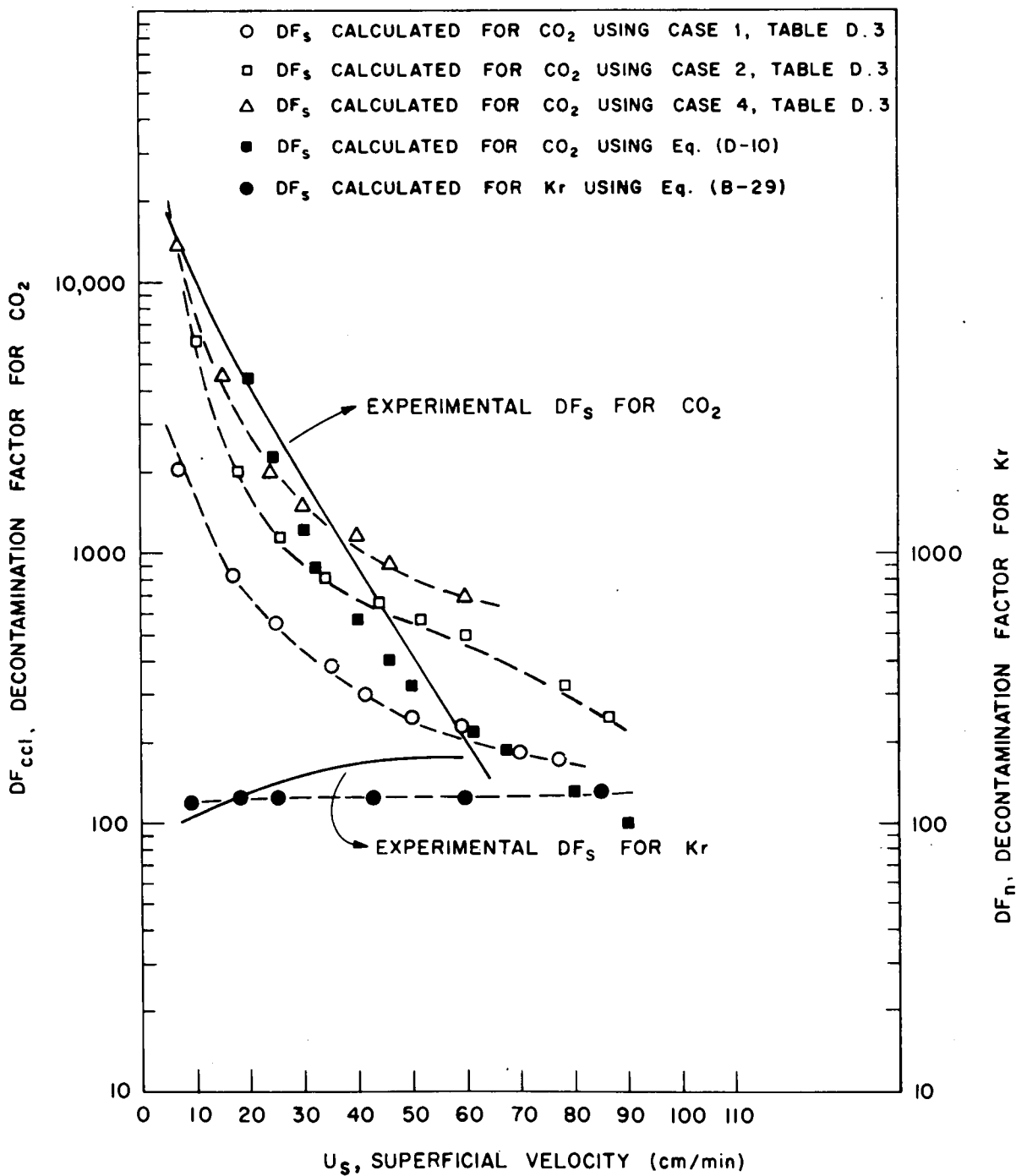


Fig. D.2. Comparison of calculated and experimental DFs for  $CO_2$  and krypton.

evolution from  $\text{CaCO}_3$  slurries during stirring and evacuation can be readily fitted by an expression such as (see Fig. 6)

$$DF_k(\text{add-on}) = C_1 t^{-C_2}, \quad (\text{D-20})$$

where

$t$  = time of evacuation.

Forsberg<sup>13</sup> has developed an expression for the DF for krypton which would be obtained for operation of two contactors in series (CIS). The terms in the expression are as previously defined for Eq. (B-29) but with the addition that  $R_1$  is the m.f. of gas feed that reacts with the slurry, which reacts in stirred tank 1. The  $DF_{k,2}$  for CIS is

$$DF_{k,2} = 1 + \frac{K^2}{F_r C} \left[ \frac{(1 - F_r)(1 - F_r + R_1 C)}{[F_r C + K(1 - F_r)]} \right]. \quad (\text{D-21})$$

This equation was based on the assumption that the krypton equilibrium in both contactors could be defined by

$$y_{k,o} = Kx_{k,o}. \quad (\text{D-22})$$

As previously discussed, this relationship is useful if an empirically derived  $K$  value can be established. Based on the data of this study, values for  $K$  of  $1 \times 10^5$  to  $2 \times 10^5$  were adequate to predict experimental results for the krypton distribution during contactor-in-series operation. Thus, the following equations are suggested for the total DF for krypton in single-contactor or contactor-in-series operation, respectively:

$$DF_{kt,1} = \left[ \frac{K(1 - F_r) + F_r C}{F_r C} \right] C_1 t^{-C_2}, \quad (\text{D-23})$$

$$DF_{kt,2} = 1 + \frac{K^2}{F_r C} \left[ \frac{(1 - F_r)(1 - F_r + R_1 C)}{F_r C + K(1 - F_r)} \right] C_1 t^{-C_2}. \quad (\text{D-24})$$

## 7. REFERENCES

1. R. W. Glass et al., HTGR Head-End Processing: A Preliminary Evaluation of Processes for Decontaminating Burner Off-Gas, ORNL/TM-3527 (July 1972).
2. W. Davis, Jr., R. E. Blanco, B. C. Finney, G. S. Hill, R. E. Moore, and J. P. Witherspoon, Correlation of Radioactive Waste Treatment Costs and the Environmental Impact of Waste Effluents in the Nuclear Fuel Cycle Reprocessing of High Temperature Gas-Cooled Reactor Fuel Containing U-233 and Thorium, ORNL/NUREG/TM-4 (1976).
3. H. Bonka et al., "Contamination of the Environment by Carbon-14 Produced in High Temperature Reactors," *Kerntech.* 15, JAHRGANG 7, 297-300 (1973).
4. A. G. Croff, An Evaluation of Options Relative to the Fixation and Disposal of  $^{14}\text{C}$ -Contaminated  $\text{CO}_2$  as  $\text{CaCO}_3$ , ORNL/TM-5171 (April 1976).
5. W. Davis, Jr., Carbon-14 Production in Nuclear Reactors, ORNL/NUREG/TM-12 (1977).
6. P. J. Magno, C. B. Nelson, and W. H. Ellett, "A Consideration of the Significance of Carbon-14 Discharges from the Nuclear Power Industry," p. 1047 in Proceedings of the Thirteenth AEC Air Cleaning Conference, CONF-740807, San Francisco, Calif., Aug. 12-15, 1974.
7. L. Machta, "Prediction of  $\text{CO}_2$  in the Atmosphere," in Carbon and the Biosphere, ed. by G. M. Woodwell and E. V. Pecon, Technical Information Center, Office of Information Services, U.S. Atomic Energy Commission, August 1973.
8. G. G. Killough et al., Progress Report on Evaluation of Potential Impact of  $^{14}\text{C}$  Releases from an HTGR Reprocessing Facility, ORNL/TM-5284 (April 1976).
9. G. G. Killough, A Diffusion-Type Model of the Global Carbon Cycle for the Estimation of Dose to the World Population from Releases of Carbon-14 to the Atmosphere, ORNL/TM-5269 (1977).
10. J. W. Snider and S. V. Kaye, "Process Behavior and Environmental Assessment of  $^{14}\text{C}$  Releases from an HTGR Fuel Reprocessing Facility," in Proceedings of the ANS-AIChE Topical Meeting, Sun Valley, Idaho, Aug. 5-6, 1976.
11. D. W. Holladay, Experiments with a Lime Slurry in a Stirred Tank for the Fixation of Carbon-14-Contaminated  $\text{CO}_2$  from Simulated HTGR Fuel Reprocessing Off-Gas, ORNL/TM-5757 (March 1978).
12. C. W. Forsberg, Separation of Radioactive Krypton from Carbon Dioxide and Oxygen with Molecular Sieves, ORNL/TM-5826 (1977).

13. C. W. Forsberg, Theoretical Analysis and Preliminary Experiments on the Feasibility of Removing CO<sub>2</sub> Containing <sup>14</sup>C Selectively with a Ca(OH)<sub>2</sub> Slurry from a <sup>85</sup>Kr-Contaminated HTGR Reprocessing Plant Off-Gas Stream, ORNL/TM-5825 (October 1977).
14. D. M. Levins, R. W. Glass, M. M. Chiles, and D. J. Inman, Monitoring and Analysis of Process Streams in a Krypton-85 Off-Gas Decontamination System, ORNL/TM-4923 (July 1976).
15. V. A. Juvekar and M. M. Sharma, "Absorption of CO<sub>2</sub> in a Suspension of Lime," Chem. Eng. Sci. 28, 825 (1973).
16. D. W. Holladay and G. L. Haag, "Removal of <sup>14</sup>C-Contaminated CO<sub>2</sub> from Simulated LWR Fuel Reprocessing Off-Gas by Utilizing the Reaction Between CO<sub>2</sub> and Alkaline Hydroxides in Either Slurry or Solid Form, pp. 546-69 in Proceedings of the DOE Nuclear Air Cleaning Conference, CONF-780819, Vol. 1 (February 1979).
17. D. N. Miller, "Scale-up of Agitated Vessels Gas-Liquid Mass Transfer," AIChE J. 20, 445 (1974).
18. P. H. Calderbank, "Physical Rate Processes in Industrial Fermentation," Trans. Inst. Chem. Eng. 36, 443 (1958):
19. J. H. Rushton, E. W. Costich, and H. J. Everett, "Power Characteristics of Mixing Impellers, Parts 1 and 2," Chem. Eng. Prog. 46 (1950).
20. R. W. Hicks and D. S. Dickey, "Application Analysis for Turbine Agitators," Chem. Eng. 83, p. 127 (Nov. 8, 1976). Other articles in the CE Refresher Series: Part 1, 82, p. 110, Dec. 8, 1975; Part 2, 83, p. 139, Jan. 5, 1976; Part 3, 83, p. 93, Feb. 2, 1976; Part 4, 83, p. 102, Apr. 26, 1976; Part 5, 83, p. 144, May 24, 1975; Part 6, 83, p. 141, July 19, 1976; Part 7, 83, p. 89, Aug. 2, 1976; Part 8, 83, p. 101, Aug. 30, 1976; Part 9, 83, p. 109, Sept. 27, 1976; Part 10, 83, p. 119, Oct. 25, 1976.
21. D. J. Inman, ORNL, personal communication to author, February 1978.
22. J. A. Mellor, A Comprehensive Treatise on Inorganic and Theoretical Chemistry, Vol. 3, Longmans, Green, and Co., London, 1923.
23. P. V. Danckwerts and M. M. Sharma, "The Absorption of Carbon Dioxide into Solutions of Alkali and Amines," Chem. Eng. (London) 202, 244 (1966).
24. International Critical Tables, Vol. 4, p. 229, McGraw-Hill, New York, 1928.



## INTERNAL DISTRIBUTION

1. J. A. Carpenter, Jr.
2. W. L. Carter
3. C. W. Forsberg
4. T. M. Gilliam
5. R. W. Glass
6. W. S. Groenier
7. G. L. Haag
- 8-12. D. W. Holladay
- 13-22. P. R. Kasten
23. W. J. Lackey
- 24-25. R. E. Leuze
26. K. H. Lin
27. J. McNair
28. K. J. Notz
- 29-30. W. W. Pitt, Jr.
31. T. H. Row
32. J. W. Snider
33. M. J. Stephenson
- 34-35. Central Research Library
36. Document Reference Section
- 37-38. Laboratory Records
39. Laboratory Records, RC
40. ORNL Patent Office

## EXTERNAL DISTRIBUTION

41. C. Bartlett, Chief, Fuel Cycle Research Branch, Division of Fuel Cycle and Environmental Research, U.S. Nuclear Regulatory Commission, Mail Stop SS 1130, Washington, D.C. 20555
42. S. J. Beard, Fuel Reprocessing Engineering, Exxon Nuclear Co., Inc., 777 106th Avenue, NE, Bellevue, Washington 98009
43. W. P. Bishop, Assistant Director for Waste Management, Division of Fuel Cycle and Material Safety, U.S. Nuclear Regulatory Commission, Washington, D.C. 20555
44. W. F. Bonner, Pacific Northwest Laboratories, Battelle Boulevard, Richland, Washington 99352
45. J. A. Buckham, Allied-General Nuclear Services, P. O. Box 847, Barnwell, S.C. 29812
46. A. B. Carson, FBR Department, Energy R and T Division, General Electric Company, 175 Curtner Avenue, San Jose, California 95100
47. R. N. Case, Allied Chemical, 550 2nd St., Idaho Falls, Idaho 83401
48. J. P. Duckworth, Nuclear Fuel Services, Inc., P. O. Box 124, West Valley, New York 14171
49. Harry Groh, E. I. du Pont de Nemours Co., Inc., Savannah River Plant, Aiken, S.C. 29801
50. C. Heath, Director, Division of Waste Isolation, Office of Nuclear Waste Management, U.S. Department of Energy, 400 First Street, N.W., Washington, D.C. 20545

51. L. R. Hill, Supervisor, Nuclear Waste Technology Division, Sandia Laboratories, Mail Drop 5311, Sandia, New Mexico 87115
52. E. R. Irish, Pacific Northwest Laboratories, Battelle Boulevard, Richland, Washington 99352
53. L. Jardine, Argonne National Laboratory, Chemical Engineering Division, Argonne, Illinois 60439
54. J. H. Jarrett, Pacific Northwest Laboratories, Battelle Boulevard, Richland, Washington 99352
55. D. E. Large, U. S. Department of Energy, Oak Ridge Operations, P. O. Box E, Oak Ridge, Tennessee 37830
56. Office of Assistant Manager, Energy Research and Development, P. O. Box E, Oak Ridge, Tennessee 37830
57. W. H. Lewis, Vice President, Nuclear Fuel Services, Inc., 6000 Executive Blvd., Rockville, Maryland 20852
58. J. E. Mendel, Pacific Northwest Laboratories, Battelle Blvd., Richland, Washington 99352
59. L. H. Meyer, Savannah River Laboratory, E. I. du Pont de Nemours and Co., Inc., Aiken, S.C. 29801
60. J. L. McElroy, Pacific Northwest Laboratories, Battelle Boulevard, Richland, Washington 99352
61. A. D. Miller, EPRI, 3412 Hillview Ave., P. O. Box 10412, Palo Alto, California 94303
62. M. A. Molecke, Nuclear Waste Technology Division, Sandia Laboratories, Sandia, New Mexico 87115
- 63-64. G. Oertel, Director, Division of Waste Products, Office of Nuclear Waste Management, U.S. Department of Energy, Washington, D.C. 20545
65. D. A. Orth, Savannah River Plant, E. I. du Pont de Nemours and Co., Inc., Aiken, S.C. 29801
66. A. M. Platt, Pacific Northwest Laboratory, P. O. Box 999, Richland, Washington 99352
67. R. Roy, Materials Research Laboratory, Pennsylvania State Univ., University Park, Pennsylvania 16802
68. A. R. Sattler, Nuclear Waste Technology Division, Sandia Laboratories, Sandia, New Mexico 87115
69. L. W. Scully, Nuclear Waste Technology Division, Sandia Laboratories, Sandia, New Mexico 87115
70. J. J. Shefcik, General Atomic Company, P. O. Box 81608, San Diego, California 92138
71. M. T. Steindler, Argonne National Laboratory, 9700 South Cass Avenue, Argonne, Illinois 60439
72. J. L. Swanson, Pacific Northwest Laboratory, P. O. Box 999, Richland, Washington 99352
73. R. E. Tomlinson, Manager, Exxon Nuclear Company, Inc., 2101 Horn Rapids Road, Richland, Washington 99352
74. J. B. Whitsett, Chief of Radioactive Waste Programs, DOE, IDO, 550 2nd St., Idaho Falls, Idaho 83401
- 75-222. Given distribution as shown in TIC-4500 under Gas Cooled Reactor Technology category.